

VISUALLY-GUIDED TIMING AND ITS NEURAL REPRESENTATION

by

Joshua Levy

A dissertation submitted to Johns Hopkins University in conformity with the
requirements for the degree of Doctor of Philosophy

Baltimore, Maryland

February, 2017

© 2017 Joshua Levy

All Rights Reserved

Abstract

Stimulus-driven timing is a fundamental aspect of human and animal behavior. This type of timing can be subdivided into three principal axes: interval generation, storage, and evaluation. In this thesis, we present results related to each of these axes and describe their implications for how we understand timed behavior. In Chapter 2, we address interval generation, which is the process of creating an internal representation of an ongoing temporal interval. While several studies have found evidence for neural oscillators which may subserve this function, it has remained an open question whether such a mechanism can be useful for timing at even the lowest level of cortex. To address this question, we analyze electrophysiological data collected from rats performing a timing task and find evidence that, indeed, timed reward-seeking behavior tracks oscillatory states in primary visual cortex. This kind of finding raises an important question: how is this temporal information stored after the interval has been generated? This process is called interval storage, and we address the sources of noise that might corrupt it in Chapter 3. Specifically, we devise a novel timing task for humans (BiCaP) to address whether memory biases can account for performance on a classification task, in which a subject must decide whether a test interval is more similar to one or another reference interval. We find that they do, and argue that these sources of noise must be accounted for in theories of timing. In Chapter 4, we deal with interval evaluation which is the process of using this stored temporal information to make valuation decisions. We study this process through the lens of foraging behavior. Specifically, we develop and test a framework that rationalizes observed spatial search patterns of wild animals and humans by accounting for the temporal

information they gather about their environment, and how they discount delayed rewards (temporal discounting). Lastly, in Chapter 5, we discuss how these processes are integrated and the implications of these findings for theories of timing.

Thesis Readers

Marshall G Hussain Shuler, Ph.D., (Advisor), Assistant Professor, Dept. of Neuroscience,
Johns Hopkins University

Geoffrey Schoenbaum, M.D., Ph.D, Senior Investigator, Intramural Research Program,
National Institute of Drug Abuse

Preface

First and foremost, I would like to thank my thesis advisor, Marshall G Hussain Shuler, without whom I am sure this thesis would not be half what it is. Marshall has not only been a great advisor to me, but also a great friend. His door was always open and I will fondly remember the long conversations we had in his office (and out) about science (and not about science).

I also thank the other members of my committee: Jim Knierim, Dan O'Connor, and Geoff Schoenbaum. Their insights and encouragement greatly improved this thesis and my development as a scientist. I would especially like to thank Jim for chairing my committee and giving me the opportunity to rotate in his lab, and Geoff for being the second reader of this thesis.

I am also indebted to the various lab mates I have had throughout my graduate studies. I would especially like to thank Vijay Namboodiri, who has been not only a wonderful collaborator but also a great friend, roommate, racquetball partner, and the list goes on. Another friend that deserves special thanks is Tanya Marton, who has been with me throughout my journey. As everyone who has met her knows, Tanya is a brilliant and compassionate person, and I have greatly benefited from our conversations and friendship. Thanks also goes out to Emma Roach, Cheng-Hang Liu, and Camila Zold, a collaborator, who were mentors to me as a junior in the lab. In addition, I would like to thank Kevin Monk and Simon Allard who are great people, scientists, and friends. I will miss my daily conversations with them. I would also like to thank Girija Hariprasad who helped with electrophysiological recordings as an undergraduate at Johns Hopkins. Finally, I would

like to thank all the colleagues and friends who are too numerous to name, but who have made these past years wonderful.

Next, I want to thank my family, which has grown considerably during the course of my graduate studies. In particular, I would like to thank my parents, Daniel and April, who have supported me throughout this endeavor, and throughout my life. I am forever indebted to them. I also thank my brothers, Aaron and Morris, my sister-in-law Daniela, and my adorable nephew and niece, Isaac and Anna, who bring everyone immense joy. I also want to thank my newly acquired family on my wife's side, who are too numerous to name individually, but who have provided love and support throughout these years. My oldest nephew, William, was born at the beginning of my graduate studies and is a joyful reminder that some things develop much faster than theses. Sadly, with all these gains come loss; I want to thank my grandmother, Yvette Levy, whose memory will continue to be an inspiration to keep learning and growing.

Finally, I thank my wife, Colleen McCullough, whom I met at the beginning of graduate school and whom I married in the thick of it. It is impossible to overstate her importance to me, and it would be trivializing to thank her for helping me complete this thesis. I thank her, instead, for being my partner in all things.

Chapters 3 and 4 describe our previously published work ((1) and (2), respectively). As such, they are reproduced with some modification from their published form. The work presented in Chapter 2 has not yet been published at the time of writing, but forms the basis for work that is currently in submission. Author contributions for these chapters are noted at the end of each section.

Table of Contents

Abstract	ii
Preface	iv
Chapter 1. Introduction.....	1
1.1 Generating temporal intervals.....	2
1.2 Storing temporal intervals.....	8
1.3 Evaluating temporal intervals	14
Chapter 2. Interval generation and oscillations in primary visual cortex	19
2.1 Introduction	20
2.2 Results: Oscillatory states appear in V1 during a visually-cued timing task.....	22
2.3 Results: Lick timing precision and accuracy improve during theta oscillation states	28
2.4 Results: Timed reward-seeking action tracks oscillation duration on a per-trial basis	35
2.5 Results: Cue-evoked single unit oscillations are predictive of timing performance....	41
2.6 Results: The likelihood of evoking an oscillation covaries with the recently experienced reward rate	47
2.7 Materials and Methods.....	51
2.7.1 Behavioral task and neural recordings	51
2.7.2 Local field potential processing.....	52
2.7.3 Oscillation detection and duration.....	52
2.7.4 Oscillation states.....	53
2.7.5 Visually-evoked potential correlation.....	54
2.7.6 Spike-LFP phase locking	55

2.7.7 Spike train analysis	55
2.7.8 Oscillation prevalence modeling	56
2.7.9 Assessing the acute effect of licking	56
2.8 Discussion.....	58
Chapter 3. Interval storage and memory bias effects	64
3.1 Introduction	66
3.2 Results: Performance on the BiCaP Task.....	71
3.3 Results: The location of the bisection point covaries with memory biases.....	76
3.4 Results: The bias-corrected bisection point exhibits the referent ratio effect	80
3.5 Material and Methods	84
3.5.1 Subjects	84
3.5.2 Apparatus.....	84
3.5.3 Task	84
3.5.4 Analysis of classification	88
3.6 Discussion.....	91
Chapter 4. Interval evaluation and spatial foraging patterns	98
4.1 Introduction	100
4.2 Results: Optimal foraging under temporal constraints.....	103
4.3 Results: Human exploratory task.....	109
4.4 Results: Path length distributions of wild animals are well-fit by a hyperbolic model	112
4.5 Results: Optimal exploration with noisy temporal representations	117
4.6 Materials and Methods.....	121
4.6.1 Experimental Design	121

4.6.2 Animal foraging data	123
4.6.3 Procedure to fit data	123
4.7 Discussion	127
Chapter 5. General discussion	131
Appendix	140
Bibliography	167
Curriculum Vitae	197

List of Tables

Table 1 <i>Results of fitting truncated power law (pl), truncated hyperbolic (hyp) and truncated exponential models to data previously collected from individual marine animals</i>	116
---	-----

List of Figures

Figure 1 <i>Oscillatory states are present in V1 during a visually-guided timing task</i>	24
Figure 2 <i>Trial-by-trial local field potential signals appear bimodal</i>	26
Figure 3 <i>Lick time precision is higher during oscillatory states</i>	31
Figure 4 <i>Trial and session statistics do not account for differences in lick precision between oscillatory and non-oscillatory trials</i>	33
Figure 5 <i>Lick time correlates with oscillation duration in trained animals</i>	37
Figure 6 <i>Lick time correlates with oscillation duration across a wide range of metrics and parameters</i>	39
Figure 7 <i>Neural oscillations occur during LFP oscillations</i>	44
Figure 8 <i>Neurons spike at a consistent phase of the oscillations in the local field potential</i>	45
Figure 9 <i>Timed lick behavior tracks single unit spike coherence</i>	46
Figure 10 <i>Reward rate is related to oscillation likelihood</i>	49
Figure 11 <i>Performance on the BiCaP Task</i>	74
Figure 12 <i>Memory bias in production and classification</i>	78
Figure 13 <i>Within-subject analysis of memory bias in production</i>	79
Figure 14 <i>The effect of referent ratio on the bisection point location</i>	82
Figure 15 <i>Optimal search of a bounded area containing reward by a forager with spatial memory</i>	102
Figure 16 <i>Model for adaptive benefits of apparent Lévy walks</i>	106
Figure 17 <i>Prey truncation leads to exponential path lengths when the density of food is high</i>	108
Figure 18 <i>Human spatial exploration task with and without temporal costs</i>	111

Figure 19 *Previously collected data from wild animals is well-fit by a hyperbolic model than a power law model* 114

Figure 20 *Optimal exploration when temporal representations are noisy.* 119

Chapter 1. Introduction

In order to survive, animals must execute precise responses to environmental stimuli. Doing so requires knowledge of what a stimulus means: both in terms of what it predicts and when. In this thesis, we focus on the temporal dimension and investigate the neural mechanisms underlying timed behaviors. In particular, we concentrate on visually-guided timed behaviors.

In studying timing, there are a variety of temporal ranges to choose from. At one extreme, animals can respond subconsciously in the millisecond range, such as when walking is perturbed by an unexpected stimulus but balance is maintained. At another extreme, biological processes across a wide range of organisms follow circadian rhythms which take hours or days to adapt to an environmental change (3). Neither of these processes occurs at a conscious level. Timing at the hundreds of milliseconds to seconds level, on the other hand, often involves conscious decision-making and voluntary actions (4, 5) and is generally thought to engage distinct neural mechanisms (6). Here, we are interested in the cognitive aspect of timing, and thus focus on interval timing in the seconds range.

Even within this temporal range, several distinct neural processes are engaged during timed behaviors (7–10). With respect to stimulus-driven behaviors, internally generating temporal intervals following a visual stimulus is critical. Note that generation of a temporal interval at the neural level may occur even in the presence or absence of an overt behavior. For instance, an animal may be instructed to produce or withhold a lever press for a certain duration following a stimulus; in either case, the animal must be able to internally generate

the interval. In some cases, interval generation would not suffice to accomplish the task at hand. Imagine, for instance, that an animal must compare the duration of an ongoing, cued interval to a remembered interval. In that case, the animal has to store that previous temporal interval in memory to be able to make a comparison to the current interval (which would also have to be translated into some common currency). This process is interval storage, and in many real-world behaviors it must be used in combination with interval generation to successfully accomplish a timed behavior. Finally, successful decision-making often relies on incorporating temporal information, even if the decision ultimately does not occur on a temporal axis. For instance, choosing between an option A and an option B may not actually require a direct temporal comparison—but information about temporal intervals associated with A and B (e.g. I will receive reward sooner if I choose option A) can play a role in the decision. We define this axis of timing as “evaluation”. In sum, we will address how cognitively-complex animals are able to generate, store, and evaluate temporal intervals in the seconds range during visually-guided decisions.

1.1 Generating temporal intervals

Several behavioral tasks have been brought to bear to better understand the neural processes underlying interval generation in humans. One advantage of using human subjects, rather than animals, is that they can be explicitly directed to produce an interval of a certain length. This sometimes occurs via verbal instruction (e.g. produce a 4 second interval) but more commonly occurs by comparison to a reference interval (e.g. produce

an interval that closely matches the interval just shown). Such non-verbal instruction is generally preferred as it eliminates the noise that may arise due to translation from a verbally-specified quantity. This may be particularly important, as time and quantity processing may rely on highly overlapping mechanisms (11). In many cases, interval production involves pressing a keypad to start and/or stop a temporal interval (start/stop task), or pressing and holding a key/lever throughout the interval. In other instances, subjects may be asked to produce rhythmic taps (where the time and variability between taps is measured), though this type of task is generally not stimulus-guided and, thus, is not of primary concern here.

Repetitive actions of a different variety are, however, one of the primary methods of assessing interval production in animals. In rodents, for example, the fixed- and peak-interval procedure are commonly used tasks (12). In the fixed-interval procedure, a stimulus is turned on at the start of a trial, and the animal can turn it off and receive a reward by performing some action (e.g. pressing a lever or poking into a reward port) after a certain amount of time has passed. If the animal performs this action during the fixed interval, nothing happens, and the animal can try again. Thus, the rate at which the action is performed throughout the trial provides a measurement for the internally generated interval. Similarly, the peak-interval procedure contains fixed-interval trials, but also interleaves probe trials in which the action neither terminates the stimulus nor results in reward. In this task, the time during which level-pressing is highest is considered to correspond to the peak of reward expectation, whereas presses around this time offer a sense of the variability associated with this estimate. While useful, these tasks do not require precise timing: the action can occur any time following the stimulus. To address

this, penalties for poor timing (e.g. performing an action well before or after a certain interval) may be imposed (13). Such a task is described in Chapter 2.

In order to generate these timed behaviors, some form of prolonged neural activity is required. For decades, the predominant view was that timing behaviors were subserved by a single centralized clock (14). Lots of experimental evidence in the last decade, however, has pointed to the involvement of many distinct brain regions. This changing perspective applies to stimulus-driven timing in particular; whereas associative areas are commonly implicated in complex tasks, mounting evidence suggests that motor and sensory regions may play key roles in timing as well.

One neural signature that has been observed in these brain regions is ramping (or step-wise) changes in firing rate. Within motor areas, the most anterior region of the supplementary motor area (pre-SMA) has been shown to represent time in this way. Specifically, distinct subsets of neurons show exponential buildup or decay in firing rates as they anticipate a change in the color of a visual stimulus after 2,4, or 8 (15). This supports an earlier finding that ramping in pre-SMA is more gradual when the temporal interval is more variable (16). This type of ramping activity has also been observed in premotor cortex. In one study, ramping was only observed for a long delayed stimulus change, but not a short delayed or variable stimulus change (17), perhaps because it would not be behaviorally useful in these cases. Outside of motor cortex, ramping activity has been observed in associative areas. Following studies showing that inactivation of PFC impairs timing (18, 19), subsequent recordings from single units with medial PFC showed ramping activity whose slope decreased as the duration to be timed increased (20, 21).

Within lateral intraparietal cortex (LIP), ramping has been observed for proactively-timed (i.e. anticipating a cue change) but not reactive (i.e. responding to a cue change) movements (22), and has been shown to track the hazard rate of receiving a visual “go” cue (which is a complex, non-linear function) (23). Interestingly, this differential response to proactively-timed and reactive movements has been found in subcortical regions, such as the putamen (24) and primate motor thalamus (25). In addition, rodents performing the peak-interval procedure exhibit peaks in activity around the targets durations (of 10 and 40 seconds) in the striatum (26).

Perhaps most surprisingly of all, interval generation has even been found in sensory cortex. Unlike the aforementioned areas, evidence suggests that sensory cortex processes temporal information in a modality-specific manner (27). For instance, disruption of the posterior parietal cortex (through rTMS) interfered with timing in the auditory as well as visual domain whereas disruption of area MT/V5 during the same task interfered with timing in the visual domain only (28). Given our emphasis on visually-guided behaviors, we will therefore focus on visual cortex. (Interestingly, supramodal timing has been found in primary auditory (but not visual) cortex through a similar TMS disruption procedure (27), suggesting that auditory cortex may take on a more diverse role in timing).

Like in parietal cortex, ramping activity has been found to track the hazard rate of a cue change in visual cortex. This has been observed in fMRI studies in primary visual cortex (V1) and V2/V3 (29) and has also been confirmed at the single neuron level within V1 (where the difference in firing rate between an unattended and attended stimulus closely tracked the hazard rate of cue disappearance) (30). This phenomenon has also been

reported in V4 neurons as monkeys anticipated an orientation change (31). Thus, it seems that tracking stimulus anticipation is a general feature of the early visual pathway.

Still more surprising is that visual cortex has been shown to carry temporal information about upcoming non-sensory events (32). Single unit recordings have revealed that neurons in V1 can represent the delay between a visual stimulus and a reward with ramping or step-wise changes in firing rate (33–35). Crucially, the duration of these changes depended on the expected duration of the delay period, which was knowable based on which of two monocular cues was presented. In these studies, there is no specific timing requirement for the animal; in fact, the fastest way to achieve reward is to lick as quickly as possible at the reward port following the visual stimulus. However, a recent study imposed a timing requirement and found that this ongoing activity is behaviorally relevant (36). Specifically, the amount of water available at the reward port was changed to be dependent on the amount of time waited to lick post-stimulus, according to a ramp-like structure (where reward increases gradually and then drops abruptly to zero). Recordings from V1 during this task showed firing rate modulations during the period between the stimulus and the action, whose optogenetic perturbation shifted behavioral timing. Together, these findings support the view that sensory cortex, and visual cortex in particular, is involved in interval generation. Thus, neural activity related to interval generation seems to be exhibited in many brain regions during visually-cued behaviors.

In addition to sustained neural activity, oscillatory activity has been linked to timing. While there are fewer studies showing a strong association between this type of activity and timing, it has nevertheless been observed in diverse brain regions. Indeed, oscillations in

motor cortex (37) and in prefrontal areas (38) have been linked to temporal prediction of visual cues. As with ramping activity, oscillatory activity in the central midline areas of cortex has been found to track the hazard rate of visual cue-change expectation (39). Within subcortical regions, oscillatory activity in the putamen has been linked to the inter-tap duration on rhythmic tapping tasks (40) and start/stop tasks (41).

Within visual cortex, oscillatory responses in the local field potential (V1) have been known about for some time (42, 43), but have only recently have been implicated in timing. (Again, it is important to keep in mind the distinction between millisecond and seconds-range timing; high-frequency oscillations in visual cortex have been strongly implicated in facilitating stimulus prediction (44, 45) and feature binding (46, 47)). As with ramping activity, oscillations have been implicated in spanning delay intervals between stimulus events (e.g. a cue change); a recent study found that gamma oscillatory power in the local field potential (LFP) increased as temporal expectation for a visual fixation point change increased (48).

Also like ramping activity, oscillations in sensory cortex have also been implicated in interval generation for non-sensory outcomes. Recently, LFP theta oscillations from V1 were analyzed in rats performing a similar task to that described earlier for reward timing (49). Whereas early in training the duration of the theta oscillations correlated with only the intensity of the stimulus, late in training it correlated strongly with the average delay to reward on a given session. Overall, these studies point to a role for oscillations in timing in primary visual cortex. It is still unclear, however, whether oscillatory activity in V1 is behaviorally meaningful as the tasks used to investigate it do not have an explicit timing

requirement; the action to achieve reward was either directly cued (48) or was atemporal in nature (i.e. ballistic licking) (49).

In sum, multiple signals have been implicated in stimulus-driven generation of temporal intervals. These signals exist in many brain regions, from motor cortex to the basal ganglia. Surprisingly, timed oscillatory signals have even been observed at the very earliest stages of visual processing, including primary visual cortex. It remains unclear, however, whether this activity is behaviorally meaningful. We address this question in Chapter 3, Interval generation and oscillations in primary visual cortex.

1.2 Storing temporal intervals

The ability to generate intervals, which we discussed in the previous section, is not sufficient for a range of problems. Say, for instance, a subject was shown two successive visual stimuli (Cue A and B) that persisted for different durations and then was asked which was longer. While the subject may have generated an internal representation of the ongoing interval, it is not clear how it could be directly stored to make this comparison; theoretically, it might be possible to internally generate these intervals and then choose the cue associated with the interval that lasts longer. This seems, implausible, however, as the decision can be made near instantaneously. This suggests that, instead, the intervals associated with each cue are stored in some way. The mechanisms underlying that storage process are explored in this chapter.

In our discussion of interval generation in the preceding section, we described common temporal production tasks but glossed over the fact that in many of these tasks it is

necessary to have a representation of the target interval. In the peak-interval procedure, for instance, it is necessary to have a sense of when the probability of reward is highest (which corresponds to the peak rate of the reward-seeking action). Therefore, even in production tasks, there must be an element of interval storage. This is especially explicit in reproduction tasks, where a standard interval is shown and a subject is required to reproduce it.

But there are also a number of tasks for assessing interval storage which isolate its mechanism and do not have an explicit production component. Interval classification is a very common method for this (12). Though there are many variants, classification tasks essentially boil down to the task described above for deciding whether the interval associated with cue A or B is longer. In a typical set up, the subject is shown two reference intervals during training and told that one is short and one is long. During testing, the subject is shown a variety of intermediate intervals and must indicate (verbally or with a keypress) whether a given test interval is closer to the short or long reference interval. A psychometric curve for the probability of selecting “long” can then be created by averaging the decisions for each test interval. Usually, this results in a sigmoidal curve where test intervals at the extremes are easy to discriminate, but intervals near the middle of the two reference intervals are challenging. The bisection point is the temporal value at which the subject is equally likely to guess that the interval is short or long. Accurately determining the location of the bisection point is considered critical to understanding temporal storage and temporal perception, generally (50).

Before delving into the neural mechanisms underlying temporal storage and the location of the bisection point, it is important to describe several key insights from behavioral observations. One particularly influential finding in the field of psychology is that changes in quantities are perceived in proportion to the magnitude of those quantities. This is called Weber's law (51) and the intuition is as follows: if one were blindfolded and given a 5kg block in one hand, and another block in the other hand, how heavy would that block need to be so that it could be reliably distinguished as heavier or lighter? In other words, what is the just-noticeable difference (JND)? A reasonable guess in this case might be 1kg. But what if, instead, the subject was given a 50kg block; would it be possible to notice this 1kg difference? Probably not. In fact, Weber's law suggests that the JND is proportionate to the quantity being measured, and would therefore be 5kg in this case. Though perhaps overly simplistic (52), this law has been observed to hold in a variety of contexts (53–55), including time perception (56). (By the same intuition, it is easier to tell the difference between 5 and 6 seconds than 50 and 51 seconds.) Scalar Expectancy Theory (SET) (57), one of the most influential theoretical accounts of timing, relies heavily on this observation; in fact, the scalar in SET refers to the fact that accuracy in timing is a scalar multiple of the quantity being measured. SET provides a description for how comparisons of sample intervals in a classification task take place. According to SET, the ratio of the test interval to the short reference interval is compared to the ratio of the long reference interval to the test interval, and the reference interval associated with the smaller of these ratios is chosen. This comparison, while perhaps not initially as intuitive as a simple arithmetic comparison, is motivated by the fact that the reference intervals are different magnitudes and, thus, are associated with different JNDs. To illustrate this point, it is useful to think about where

the bisection point between two reference intervals would lie; if the reference intervals were 1 second and 5 seconds, respectively, then SET would predict that the bisection point (x) lies below the arithmetic mean of 3 seconds, at ~ 2.236 seconds, because the ratios of $1:x$ and $x:5$ are equivalent at that point.

Though SET makes precise predictions about the location of the bisection point, noise can arise from its underlying neural processes. SET proposes a pacemaker-accumulator (PA) model for interval storage (57, 58), in which a pacemaker emits discrete pulses which are counted by an accumulator, when a stimulus drives completion of a circuit between them. The pacemaker component has been suggested to be driven by a neural oscillator (59), as it provides a robust and rhythmic (clock-like) signal. In this way, production and storage mechanisms may be intertwined: a pulse-like oscillator could simultaneously generate an interval and send its information to an accumulator for temporary storage. Following reinforcement, the scalar value in the accumulator is written to long-term memory. Thus, the scalar value in memory serves as the representation for the duration of the interval. When comparing a test interval to a reference interval, therefore, comparison may occur between these scalar quantities.

Noise can enter this system at multiple levels. For one, the pacemaker itself may operate at different speeds. If it runs too fast, the interval will be perceived as longer than it is in reality but if it runs too slow, or its signal is not robust, the interval will be perceived as too short. Second, the gating mechanism could be faulty, being either too permissive or too restrictive. Third, the long-term memory store could be noisy, such that the scalar quantity changes over time. When doing a comparison, therefore, it would matter how far in the

past the scalar quantities were transferred to memory. Pharmacological studies have, indeed, dissociated these effects by showing selective adjustment of clock speed and memory processes (60).

As accurately measuring the bisection point is important for theories of timing (50), it is important to account for these sources of noise. Unfortunately, the bisection point is most commonly measured using only classification tasks. It is, therefore, difficult to control for these sources of noise. One straightforward approach to address this problem is to combine a standard classification task with a production task in which subjects must generate what they believe to be the standard reference intervals (1). Combining interval generation with the classification task in this way affords the opportunity to see how memory biases influence storage. Such a task, along with its results and implications, is described in Chapter 4.

It is important to note that the plausibility of the pacemaker-accumulator model has been challenged recently. Though there have been some demonstrations that implicate its conceptual components, such as the pharmacological studies described earlier (60), the central critique of the model is that it is not rooted in biological plausibility (61). Alternatives to SET have been suggested, such as Killeen's Behavioral Theory of Timing (62) and its derivative, the Learning-to-Time model (63), but, ultimately, they are more behaviorally than biologically motivated as well. Still other models eschew the notion of a clock entirely, favoring, instead, a memory-based representation for time-keeping (64); this, too, is criticized as biologically implausible (if not conceptually implausible owing to the need for an arbitrarily high number of integrators to represent various temporal

durations (65)). The research landscape is, therefore, open to alternative theories firmly rooted in biology.

Along this line, a current, popular alternative to the PA model is the Striatal Beat Frequency (SBF) model (66). In this model, various cortical oscillators are initiated by a start gun (proposed to be dopaminergic output from the VTA) and medium spiny neurons (MSNs) of the striatum decode their output. Since all of these oscillators operate at different frequencies, they are at different scalar values at the time of reinforcement; therefore, the vector of scalar quantities decoded by the striatum at the time of reinforcement serves as the memory for the interval. When trying to time an interval, therefore, the state of the ongoing oscillations is compared to this remembered vector and, when matched, the interval is terminated. The SBF is appealing because it has roots in biology and offers a mechanism by which intervals can be stored. It also contains some of the high level components that would be subject to noise (e.g. pulse-like oscillators running at various speeds and memory for the scalar vector). However, it is hard to imagine how such a storage mechanism could be used for the classic case of interval comparison. While it would be possible to determine whether a given interval were near identical to a prior interval, it is unclear how the code could be used to determine whether one interval were longer than another (and by how much). Moreover, at this point, more testing and experimental support for SBF is needed (61).

While it is unclear which timing model is most appropriate for explaining interval storage, memory is nevertheless a key component of them all. In Chapter 4, we will investigate

how biases in memory can affect time perception and, consequently, performance on a bisection task.

1.3 Evaluating temporal intervals

Interval generation and storage are fundamental to timing, but they also subserve decision-making when no explicit timing behavior is required. For instance, imagine a subject were presented with two cues, A and B, each associated with a different length interval, as before. Having learned those intervals, the subject is offered the option of choosing A or B, with the stipulation that reward will be received after waiting the duration of the interval associated with that stimulus. In this case, the subject will probably want to choose the stimulus associated with the shorter delay. Note, however, that this choice is not strictly timing based. Rather, the subject is incorporating temporal information into an ultimate decision. We define this process of making decisions that leverage temporal information as interval evaluation.

The example described above is a simple illustration of a powerful concept in interval evaluation: temporal discounting. Simply put, temporal discounting is the concept that a reward displaced farther in time is valued less than when it is imminent. This concept is tightly intertwined with the concept of subjective value, which is the perceived value of an outcome to an agent. Generally speaking, animals have a preference for imminent rewards, such that the subjective value of an option decreases as the time to reward increases. But this raises an interesting question: exactly how much does subjective value decrease with

time? That is, what is the shape of the temporal discounting function? And, further, what variables, if any, influence it?

Investigation into the exact form of the temporal discounting function has long been a topic of vigorous research. It is of broad relevance to economists, psychologists, and neuroscientists alike because it has deep implications for animal and human behavior. At a high-level, it is generally accepted that the temporal discounting function is monotonically decreasing. At a finer level, the discounting function has traditionally been modeled as a decreasing exponential in economics (67). This is appealing because it is simple and intuitive; subjective value declines at a rate proportional to its current value which implies that, in absolute terms, the subjective value declines much more rapidly for nearby than for distant time points. Intuitively, this makes sense: you probably care a lot more about getting a reward today versus tomorrow than about getting it in ten years versus ten years and a day.

Despite its simplicity and intuitive appeal, however, the exponential discounting model fails another test of intuition. If given the choice between \$10 today and \$15 in a month, it is likely that many people would choose the earlier, smaller option. (The exact numbers are not important; what is important is that there are some values for which there would be a preference for the earlier, smaller option.) Now imagine that these same people were given the choice between \$10 in a year and \$15 in a year and month. In this case, it would not be surprising for many of these same people to choose the \$15 in a year and month (larger, later option). Intuitively, the rationale for this is that by adding a year to both options, the month delay for the higher option all of a sudden does not seem matter as

much. This kind of behavior would not be predicted by an exponential discounting model, however, because in both cases the marginal gain of \$5/month is the same. Since the subjective discounting rate is constant in an exponential model, the choice of taking \$5/month should be the same regardless of context. We can even take this a step further. Instead of having two option sets (\$10 today vs \$15 in a month and \$10 in a year vs \$15 in a year and a month) imagine that we only had the second option: \$10 in a year vs \$15 in a year and a month. Imagine that subjects are allowed to choose which option they prefer today but also adjust their choice until they have received a reward. As before, an individual choosing today might choose \$15 in a year and a month (larger, later option). But what happens as the day approaches? In a year from now, the individual will be in the exact same situation as for the other option set: choosing between \$10 today and \$15 tomorrow. At that point, the subject may well prefer the \$10 option (smaller, earlier option). Therefore, as time elapses, the preferred option may change from the larger, later reward to the smaller, earlier reward. This phenomenon is known as a preference reversal, and it has been observed in animals and humans (68).

To explain these patterns of human and animal behavior, psychologists have developed hyperbolic temporal discounting models (67). Compared to an exponential model, a hyperbolic model discounts more steeply at early times but less steeply at late times. Therefore, in our example comparison between the two option sets, the additional \$5/month is more steeply discounted today than in a year and, thus, it makes sense to choose the smaller, earlier reward in one case (\$10 today vs \$15 in a month) and the larger, later reward in the other (\$10 in a year vs \$15 in a year and a month). Similar logic applies to the preference reversal: as time elapses, the steepness of discounting changes such that

the preference shifts from the larger, later reward (distant in time; gentle discounting) to the smaller, earlier reward (near in time; steep discounting). Generally speaking, hyperbolic or hyperbolic-like models have been found to be superior fits to behavioral data than exponential models (69, 70). Recent work has even demonstrated that a hyperbolic-like discounting function arises naturally from attempting to maximize reward rate, given some practical constraints (71).

Another related body of work deals with maximizing reward rates across space. For decades, ecologists believed that animals foraged according to Brownian motion—that is, random walks in their environment (72). Recent improvements in tracking devices and study methodologies led to the realization that, in fact, animals in the wild often do not search according to Brownian motion; in fact, their foraging behavior is characterized by a higher frequency of long excursions that is well-described by another process: the Lévy flight (73, 74). Essentially, the distribution that arises from this type of process is power-law distributed. This finding is of great interest, in part, because these types of superdiffusive movement patterns have been observed for a range of physical phenomena (75). Thus, it is surprising that animals seem to abide by these same movement dynamics.

This finding is of still greater interest as modeling efforts have shown that, in some cases, Lévy foraging patterns may be optimal (76). Recently, however, studies have pointed out that this model of optimality is rather brittle—that is, it holds for only very particular and unrealistic constraints and parameters (77). Aside from the fragility of the model itself, one of the implicit, unrealistic assumptions underlying this work is that foragers have no spatial memory and have no capacity to produce systematic, deterministic searches.

Why, then, do foragers seemingly exhibit these Lévy walks? Might there be a more biologically-plausible explanation for them? Since spatial search clearly involves considerable temporal investment, it is reasonable to assume that these temporal costs are accounted for in the search algorithm. Therefore, the insights related to temporal discounting can be brought to bear on this problem. We explore this connection in Chapter 4, and describe the results and implications for foraging theory. Thus, we describe a key way in which information about temporal intervals is incorporated into decision-making.

In the following chapters we will describe our insights into visually-guided interval generation (Chapter 2), storage (Chapter 3), and evaluation (Chapter 4) in cognitively-complex animals. In chapter 5, we will describe how these findings might be integrated into a unified view of timing.

Chapter 2. Interval generation and oscillations in primary visual cortex

Abstract

Several lines of recent work have challenged the long-standing belief that sensory cortex, and primary visual cortex (V1) in particular, faithfully represents the physical world. One such line of work has suggested that V1 can represent even the non-sensory outcomes that a stimulus portends. Indeed, it has been shown that theta oscillations in the local field potential (LFP) of V1 can generate the temporal delay between a visual stimulus and an expected reward, following conditioning. We extend this work by presenting evidence that these oscillations relate to a stimulus-driven, timing behavior. In particular, we show that with training, high precision and accuracy in timed behavior tracks theta oscillatory power in V1. In addition, we find that the duration of these theta oscillations covaries with the time of action execution. These LFP oscillations are intimately related to spiking responses at the single unit level, and, aggregating correlated input across ensembles of increasing size increases the predictive power of the timing signal. Together, these observations suggest that oscillatory activity in V1 carries behaviorally-relevant timing information and, thus, they extend our understanding of V1's role in stimulus-driven behaviors and the role of oscillations in interval generation.

2.1 Introduction

Generating timed responses to environmental stimuli is crucial for survival. Such stimulus-driven behaviors require knowledge of both what to expect and when, and many high-level brain areas have been shown to report this information. Neurons in the striatum (78–82), orbitofrontal cortex (83–86), and amygdala (85) have been found to express temporal predictions about outcomes, while dorsolateral premotor cortex (87–89), prefrontal cortex (90), and distinct regions of the striatum (91) have been implicated in translating this temporal information into action. Sensory regions like primary visual cortex (V1)—the earliest stage of cortical visual processing—are typically regarded as contributing only to the first phase of such behaviors: perception (92, 93). Recent work suggests, however, that experience-dependent plasticity in V1 can also give rise to information about when to expect an outcome (30, 33). It has even been shown that such sustained modulations in firing rate in V1 contribute to visually-timed behaviors (36).

A distinct signal in V1—oscillations in the local field potential (LFP)—has also generally been interpreted as relaying perceptual information. One of the key roles for oscillations, particularly in the gamma range, may be to enhance binding of visual features to create a complete visual percept (46, 47). Another crucial function of oscillations is to facilitate anticipation of upcoming stimuli, though this type of predictive information is often reported as lasting on the order of only tens or hundreds of milliseconds (44, 45, 94). But recent observations have also pointed to a role for oscillations in stimulus prediction on the order of seconds (30, 48)—the temporal range that is crucial in most cognitive tasks. Moreover, it has been found that theta oscillations in the LFP of well-trained rodents are

related to even non-sensory outcome predictions (49). Specifically, the duration of theta oscillations in V1 was found to correlate with the average temporal delay between a visual stimulus and an expected water reward. While it is interesting that this distinct signal carries temporal information, it is unclear whether it is behaviorally relevant.

To address this, we analyzed data from a task (36) in which rodents with chronic electrode implants in V1 must execute a visually-cued timed action in order to achieve reward. Surprisingly, we found that these visual cues evoked theta oscillations in V1 whose presence corresponds, on a per trial basis, to trials with improved performance on the timing task. Further, we find that the duration of these oscillations covaries with the time of an action, and that this relationship evolves with training. This theta oscillatory activity in the LFP is intimately related to the activity of single units, which can be observed to spike in phase with the LFP oscillation. Specifically, we find that synchronously firing neural ensembles carry predictive information about the timing of the action. Thus, these findings further our understanding of V1's role in stimulus-driven behaviors, provide evidence for theoretical accounts of timing which implicate neuronal oscillators (7, 95, 96), and extend our knowledge of the role for theta oscillations.

2.2 Results: Oscillatory states appear in V1 during a visually-cued timing task

Eight wildtype rats were trained on a timing task (36). In this task, the animal enters a nosepoke to initiate a trial, waited a random delay without licking, received a full-field, monocular visual stimulus (100ms, green LED, delivered through head-mounted goggles), and then licked at a chosen time. The time that the animal chooses to lick post-stimulus determines the amount of reward it obtains on a given trial. Specifically, the amount of water reward available rises linearly with time up until 1.5 seconds, at which point it drops to and remains at zero (Figure 1a). In this way, animals are encouraged to time their licks from the visual stimulus so that they fall near, but not past, the peak of the reward ramp.

Animals trained in this task exhibit cue-evoked theta oscillations in the local field potential recordings from the primary visual cortex. This theta oscillation can be seen in the average voltage trace across trials of a session when aligned to stimulus onset, as in Figure 1b. In this example, the average voltage trace exhibits appreciable oscillatory strength for about one second following visual stimulation. Separating the responses per trial (Figure 1c) reveals differences in the presence, amplitude, and duration, of theta oscillations across trials (Figure 1c, inset).

In order to quantify these across-trial differences in the presence, amplitude, and duration of oscillations, we transform this raw voltage signal into a metric of oscillation strength. We focus our analysis within a 4 to 9 Hz frequency range as the preponderance of the signal power falls within this range (Figure 1d). Using this range, we generate a “concentrated

energy” score—a measure of the power and purity of the oscillation (methods)—for every time point within each trial, as done previously (49) (Figure 1e). Qualitatively, trials with large oscillations in voltage (as in Figure 1c) have high concentrated energy scores (as in Figure 1e).

Using these concentrated energy scores, we can investigate how the oscillation strength—defined as the mean concentrated energy within a 200-700ms time window—varies across trials. By inspection, the probability density function (Figure 1f) of the oscillatory strength (Methods) is well described for this session by a bimodal fit (bottom), but not a unimodal fit (top), suggesting that there are distinct oscillatory states across trials. Therefore, we compared the quality of each fit by calculating the difference in the Akaike information criterion (AIC) scores (Methods). For this example, the ΔAIC is large and negative (~ -99.76) which indicates that the bimodal model is heavily favored over the unimodal model. Applying this process across all sessions, we found that the bimodal model is overwhelmingly preferred ($p=6.87e-66$, $W_{414}=1186$, $z=-17.14$; Figure 1g, histogram), for a variety of metrics (Figure 2a) and when compared to a number of alternative models (methods; Figure 2b,c). Given that trials appear to have either a high or low-power oscillation, a threshold (Figure 1h) for sorting trials into “oscillation” and “non-oscillation” trials was lawfully applied, as done previously (49). Ordering the trials from Figure 1c by the strength of their oscillation makes the difference in oscillatory power across trials visually apparent (Figure 1i). Finally, we define an oscillation’s duration as the interval between the first moment post-cue that the concentrated energy score surpasses this threshold for detection and the first moment it falls below it..

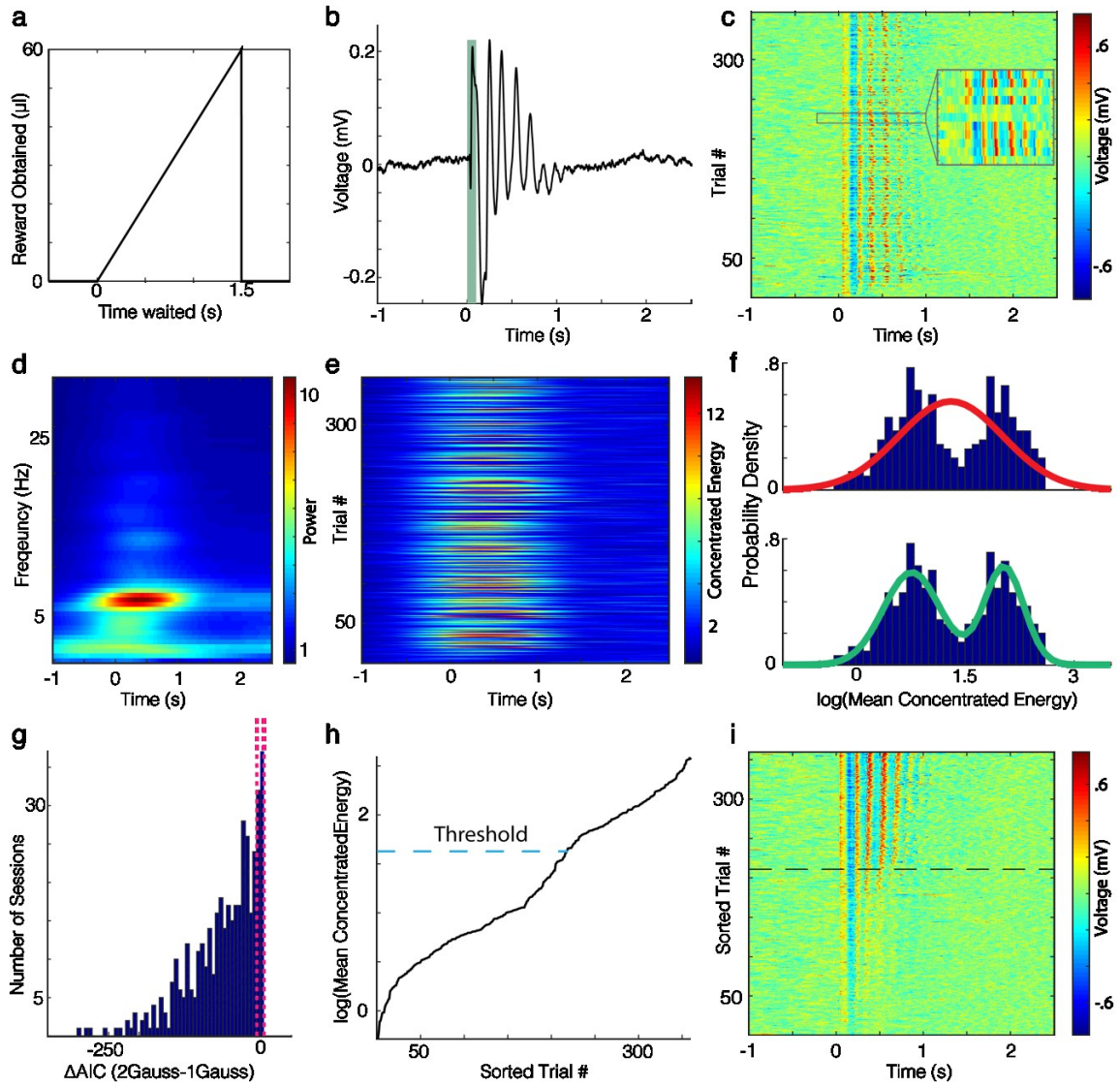


Figure 1 *Oscillatory states are present in V1 during a visually-guided timing task*

a) Schematic of the task reward structure, in which waiting longer to lick following a visual stimulus (time zero) results in a larger volume of water delivery at the lick tube. Maximum delivery occurs at 1.5 seconds, and drops to zero thereafter, so that animals must time their lick. **b)** The average voltage trace in the local field potential (LFP) taken from an electrode in an example session, with a green bar overlaid to indicate when the visual stimulus was on. Qualitatively, voltage values oscillate for ~ 1 second post-stimulus. **c)**

Voltage traces per trial for the example session. **d)** Average time-frequency representation of the trials in **c**. **e)** Concentrated energy through time of the trials in **c**. **f)** The empirical probability density function (PDF) for the $\log(\text{mean concentrated energy})$ scores on each trial shown in **e** are shown in blue. The mean concentrated energy is calculated in a 200-700ms window post-stimulus. A unimodal Gaussian fit is shown in red (top) and a bimodal Gaussian fit is shown in green (bottom). **g)** The distribution of the difference in Akaike Information Criterion (AIC) values for each model across all sessions is left-shifted, indicating an overall preference for the bimodal model. The dotted lines around zero are the bounds at which the relative likelihood of a model compared to another model is 5%. **h)** Sorted concentrated energy scores for the example session with a dotted line indicating the threshold used for determining whether a trial has an oscillation. If the concentrated energy score crosses this threshold during the 200-700ms window post-stimulus, it is considered to have an oscillation. **i)** The raw voltage trace in **c** sorted by the mean concentrated energy in the analysis window on a given trial. Oscillations were detected for trials above the dotted line.

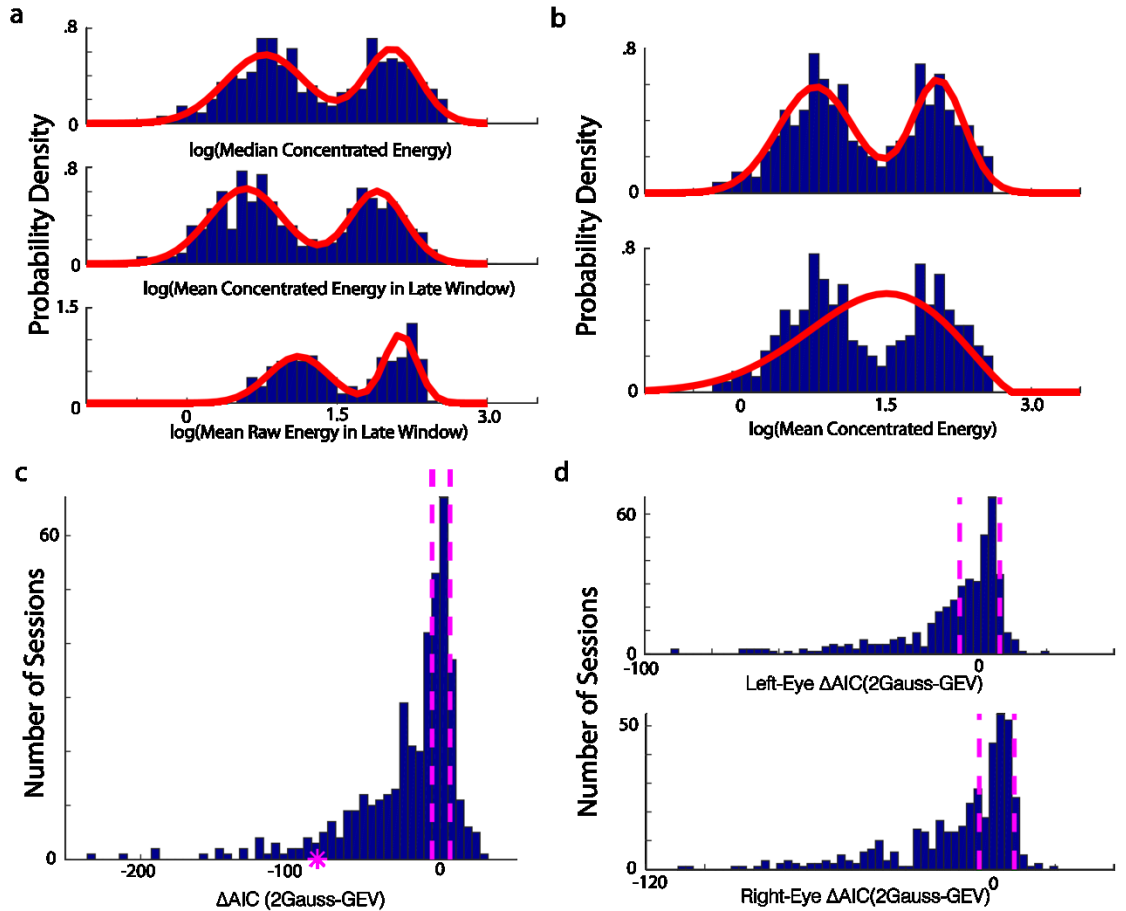


Figure 2 *Trial-by-trial local field potential signals appear bimodal*

a) Empirical probability density function (PDF) for the example in Figure 1 using several metrics, including median concentrated energy (top), mean concentrated energy in a late analysis window [500-1000ms post-stimulus] (middle), and mean raw energy in a late analysis window (bottom). Bimodal Gaussian fits are shown in red. **b)** The PDF for the log(mean concentrated energy) scores in a 200-700ms window post-stimulus with a bimodal Gaussian fit (red line, top) and generalized extreme value distribution fit [GEV] (red line, bottom). **c)** The distribution of the difference in Akaike Information Criterion

(AIC) values for each model across all sessions is left-shifted, indicating an overall preference for the bimodal Gaussian model compared to the GEV model. The dotted lines around zero are the bounds at which the relative likelihood of a model compared to another model is 5%. **d)** Same as in **c** except that trials are broken down by whether the left eye (top) or right eye (bottom) was visually stimulated.

2.3 Results: Lick timing precision and accuracy improve during theta oscillation states

Having defined cue-evoked oscillations and their duration, we next addressed whether across-trial differences in the performance of the visually-cued timing behavior tracks with changes in the oscillatory state. To visualize whether performance is related to the presence/absence of cue-evoked theta oscillations, we plot, per trial, the time of the first lick post-stimulus (the behavioral variable relevant for reward acquisition) atop the concentrated energy values (see Figure 3a, top for an example session). Viewed in this way, it is apparent that there is considerable variability in the time of the first lick (white squares), but challenging to see what, if any, relationship there is between concentrated energy and first lick time. However, sorting trials by the strength of the oscillation (Figure 3a, bottom) reveals that there is considerably greater precision in time to initiate licking on trials with higher oscillatory power. To quantify this difference, we compared the temporal distribution of first lick times (under five seconds post-stimulus (>95% to avoid outliers) on oscillation and non-oscillation trials (Figure 3b; threshold shown by black dotted line). First lick times on oscillation trials tend to be more tightly packed (purple line) than on non-oscillation trials (green line). Indeed, this tends to be the case across all sessions recorded on this channel (Figure 3c; $p=4.05e-11$, $W_{66}=2139$, $z=6.60$, two-tailed Wilcoxon signed rank test against median=0) and all channels ($p=4.8e-54$, $W_{408}=78618$, $z=15.48$). Moreover, the difference in variability across sessions from this channel tends to be more pronounced in well-trained animals (i.e. rats performing at least three consecutive sessions with a median wait time of one second or greater), compared to naïve, on this channel

(methods; $p=0.01$, $U=5274$, $z=2.43$, $n_1=66$, $n_2=75$, two-sided Mann-Whitney U-test) and across all channels (Figure 3d; $p=1.4062e-15$, $U=205955$, $z=7.98$, $n_1=408$, $n_2=457$). Since this increased variability on non-oscillation trials predominantly comes from a higher fraction of early licks, the central tendency of the lick times across sessions is significantly lower on non-oscillation trials (median of ~ 1006 ms) than oscillation trials (median of ~ 1103 ms) ($p=1.51e-14$, $U=193710$, $z=7.69$, $n_1=409$, $n_2=410$, two-sided Mann-Whitney U-test). This means that, on average, licks on oscillation trials occur farther along the ramp, where more water is available and, thus, are more accurate. Therefore, the precision and accuracy of timed licks are considerably higher on trials with strong oscillations.

Since the presence of an oscillation detected at a given electrode covaries with behavioral improvements, we hypothesized that there would be larger behavioral improvements during trials with more spatially widespread oscillations in V1. Because we analyzed LFP recordings from six channels (3 per hemisphere) per session, we can assess how the timed lick behavior varies with the number of electrodes reporting an oscillation on a given trial. Variability systematically decreases (Figure 3e, top; $p=8.27e-05$, slope= $-1.91e+04$, $r=.98$) and the central tendency systematically increases ($p=0.020$, slope= 23.78 ms, $r=0.83$) as the number of electrodes reporting oscillations grows. These effects translate into a systematic increase in the amount of water obtained per trial (Figure 3e, bottom; $p=4.9e-04$, slope= 3.43 , $r=0.96$). Thus, the greater the spatial extent of cue-evoked oscillations within V1, the greater the precision and accuracy of timed reward-seeking actions, and the greater the obtained reward.

These observations suggest that cue-evoked theta oscillatory states observed in V1 may be effectors of timed behavior, but this relationship might arise from other sources. Because there is a random delay period between nosepoke entry and visual stimulus onset, this higher variability in lick precision on non-oscillation trials might arise from higher variability in time waited prior to the stimulus. Countering this hypothesis, we find that the difference in lick variability between oscillation and non-oscillation trials is considerably higher than the difference in wait-time variability (Figure 4b; $p=3.94e-30$, $z=11.4$, $U=201251$, $n_1=414$, $n_2=414$, two-sided Mann-Whitney U-test). Furthermore, the lick variability is consistently higher on non-oscillation trials, holding the time waited since nosepoke entry constant (Figure 4d). The same is true when controlling for inter-trial interval duration and trial number within session (Figures 4e and f, respectively), suggesting that these variables do not account for differences in timed licking.

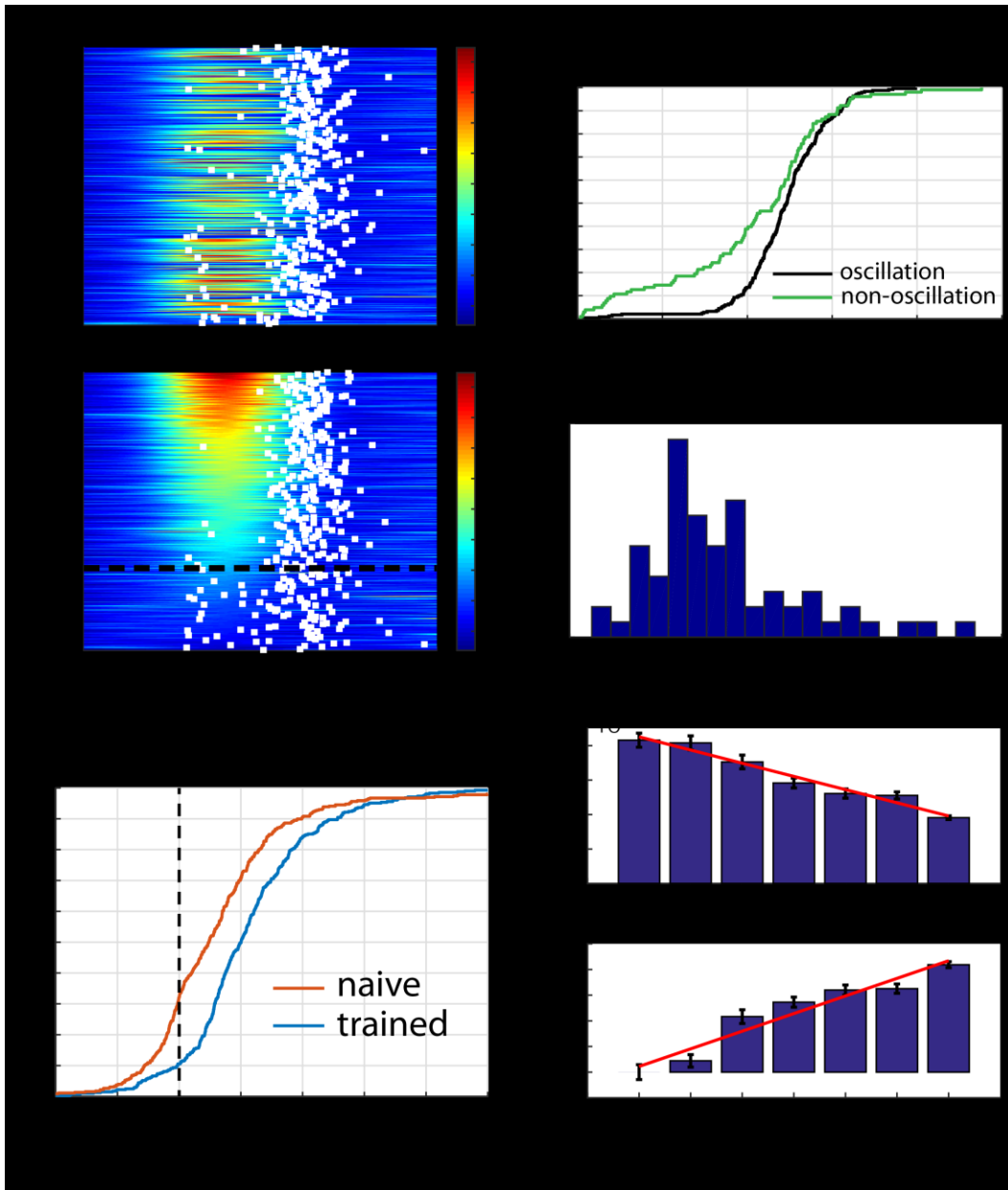


Figure 3 *Lick time precision is higher during oscillatory states.*

a) Concentrated energy values with first lick times (white squares) post-stimulus overlaid for each trial of an example session in chronological order (top) and sorted by oscillation duration (bottom). The dashed black line is the threshold for being categorized as oscillatory. **b)** Empirical cumulative density functions for the first lick times post-stimulus

on oscillation (black) and non-oscillation (green) trials in **a**. **c**) Histogram of the difference in lick variability on oscillation and non-oscillation trials for each session recorded on a given electrode. **d**) Differences in lick time variability on oscillatory and non-oscillatory trials for all sessions and channels of trained (blue) and naïve (red) animals. **e**) (top) Lick time variability decreases as the number of electrodes on which an oscillation was detected increases for a given trial. Standard error bars shown in black, with regression line in red. (bottom) The percent of water obtained over baseline (defined as trials in which no oscillations were detected on any electrodes) increases as the number of electrodes showing an oscillation increases. Standard error bars shown in black, with regression line in red.

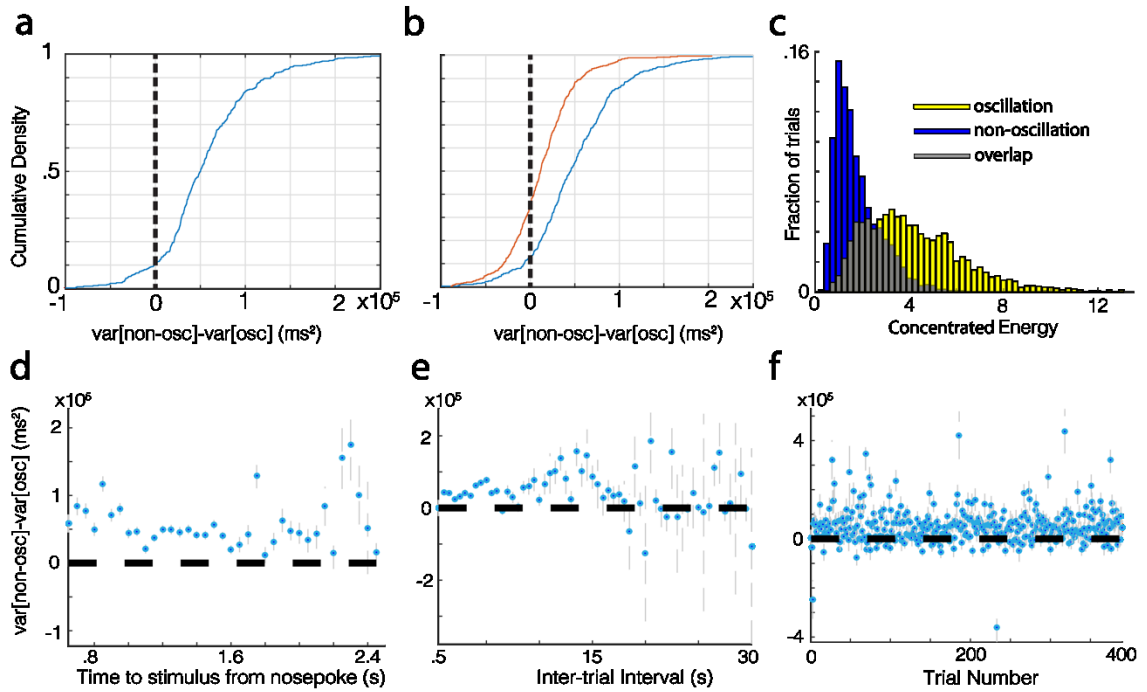


Figure 4 *Trial and session statistics do not account for differences in lick precision between oscillatory and non-oscillatory trials*

a) Differences between lick time variability on oscillatory and non-oscillatory trials across all sessions and channels. **b)** Differences in lick time variability (blue) are considerably larger than differences in stimulus onset time (from nose-poke entry) variability (red) on trials in which there was no licking pre-stimulus. **c)** The concentrated energy scores taken from a 50ms window prior to the first lick on oscillation (blue) and non-oscillation (yellow) trials from all sessions and channels. **d)** Differences in lick variability between oscillatory and non-oscillatory trials for trials within a given range of times to stimulus onset (from nose-poke entry) from 0 to 2.5s in 100ms steps, collapsed across all sessions and channels. **e)** Differences in lick variability between oscillatory and non-oscillatory trials for trials

within a given range of inter-trial intervals from 0 to 10s in 100ms steps, collapsed across all sessions and channels. **f)** Differences in lick variability between oscillatory and non-oscillatory trials for a given trial number in a session, collapsed across all sessions and channels.

2.4 Results: Timed reward-seeking action tracks oscillation duration on a per-trial basis

Given these differences in behavior with respect to the presence and spatial extent of cue-evoked theta oscillations within V1, we next assessed whether the duration of these oscillations is directly related to the timing of the reward-seeking action (lick initiation). Figure 5a shows the first lick time per trial (pink squares) plotted over the concentrated energy values for an example session, sorted by oscillation duration. Indeed, lick initiation tends to follow the edge of the oscillations' termination (black circles). By transforming this data into a scatter plot (Figure 5b), it appears that there is a positive relationship between first lick time and oscillation duration. Indeed, across all sessions from this electrode, the distribution of regression slopes is significantly right-shifted (Figure 5c, histogram; $p=3.29e-05$, $W_{69}=1902$, $z=4.15$, two-tailed Wilcoxon signed rank test against median=0), meaning that there tends to be a positive linear relationship between first lick time and oscillation duration. This relationship holds across all sessions and channels (Figure 5d, blue line; $p=3.43e-25$, $W_{414}=65641$, $z=10.28$), and is more pronounced in well-trained compared to naïve animals (Figure 5d, blue vs red line; $p=3.72e-10$, $U=196120$, $z=6.27$, $n_1=414$, $n_2=486$; , two-sided Mann-Whitney U-test). The same is also true when collapsing across channels per session (Figure 6a, top), and using a variety of other metrics and filters (Figure 6a, middle and bottom; Figure 6b). Moreover, the mean slope across sessions is significantly higher ($p<<.05$) than the distribution of mean slopes for shuffled lick time data (Figure 5e; black dotted line is actual mean slope). Finally, as described previously (49), the amplitude of the visually evoked potential (VEP)—the acute response

to the visual stimulus—is also related to the duration of the oscillation, but it is a considerably worse predictor of lick time than oscillation duration (Figure 6c, bottom).

Given these observations, we investigated whether the strength of the oscillation influences the relationship between first lick time and oscillation duration. Since the oscillation would likely exert less influence over behavior the weaker it is, we hypothesize that the relationship between first lick time and oscillation duration would degrade with oscillation strength (as appears to be the case in Figure 5a). Indeed, filtering by trials with the strongest oscillations (that is, taking the x percent strongest oscillations, as defined by the mean concentrated energy in a 200-700ms window post-stimulus, in a given session) yields the strongest correlations (Figure 5f). Coupled with the observations above, this indicates that the duration of cue-evoked oscillations relates to the timing of reward-seeking actions.

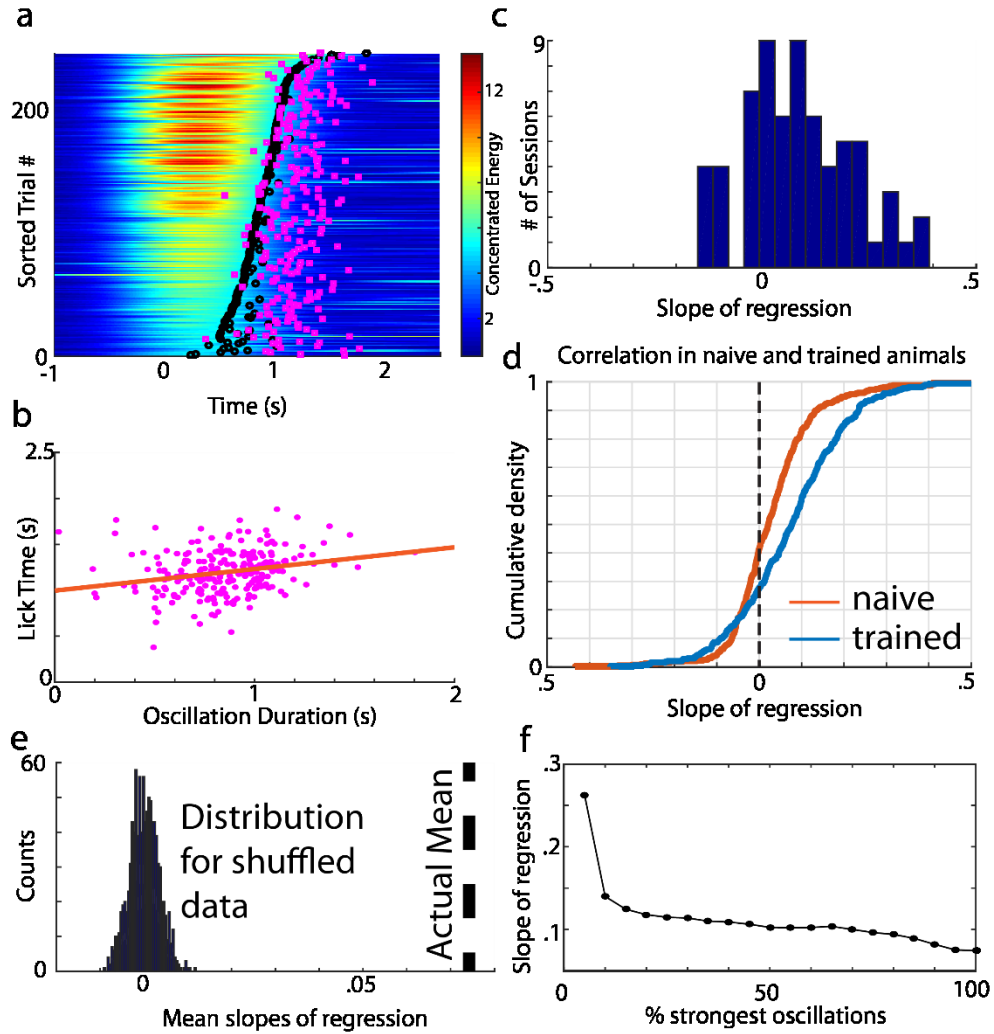


Figure 5 *Lick time correlates with oscillation duration in trained animals*

a) Concentrated energy values with first lick times overlaid (pink squares) on trials sorted by oscillation duration. **b)** Scatter plot showing the relationship between oscillation duration and first lick time for the trials in **a** with a regression line shown in orange. **c)** The distribution of the slopes of regression for each session recorded on a given channel. **d)** The empirical cumulative distribution of the slopes of regression for all sessions and channels from naïve (red) and trained (blue) animals. **e)** The null distribution of slopes for the sessions taken from the trained cohort, calculated by randomly shuffling the

relationship between the lick time and oscillation duration 1000 times. The actual mean slope across session is shown by the black dotted line. **f)** The slope of regression decreases as the percentage of trials with the strongest oscillations is systematically increased. To do this systematic sweep, we sorted trials recorded on a given session/electrode by their mean concentrated energy and took the top x percent of trials. Therefore, the x-axis ranges from 5% (in which only the trials in the top 5% of oscillation strength are included) to 100% (in which all trials are included).

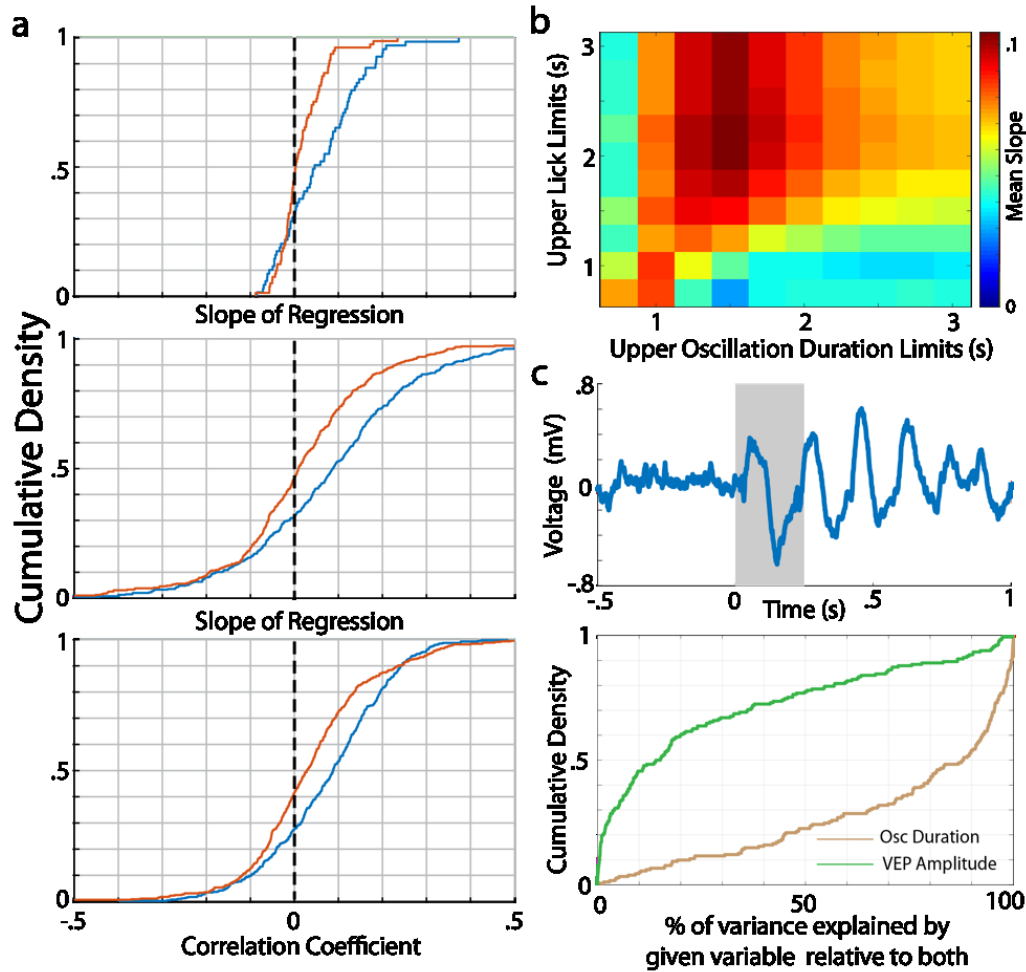


Figure 6 *Lick time correlates with oscillation duration across a wide range of metrics and parameters*

a) Slopes of regression for trained animals (blue) are right-shifted compared to naïve animals (red) when combining across channels per session (top) and using unrewarded trials only (middle). This trend can also be observed for the correlation coefficient (bottom) across all sessions and channels. b) Mean slope of regression across all sessions and channels for a variety of upper lick time and oscillation duration limits. c) (top) Local field potential trace from a single trial with a 250ms gray bar overlaid to highlight the visually evoked potential [VEP]. (bottom) The percent of variance explained by a regression of lick

time against oscillation duration (brown) or VEP amplitude (green) relative to a model containing both variables.

2.5 Results: Cue-evoked single unit oscillations are predictive of timing performance

Having observed this timing-related activity at the level of the local field potential, we sought to investigate the response patterns of single neurons recorded during this task. An example response is shown in Figure 7a. The spike raster (top) and peristimulus time histogram (bottom) across the whole session (i.e. all trials with a stimulus) suggest that this neuron primarily responds acutely to the visual stimulus (presented at time zero). However, separating each trial by whether an oscillation was detected in the local field potential (for a given electrode within the same hemisphere) reveals that there are, in fact, quite different response patterns during oscillation and non-oscillation trials (Figure 7b and c). In particular, there is a long-duration oscillatory firing pattern on the oscillation trials, whereas there is predominantly an acute stimulus response on non-oscillation trials. Indeed, many neurons (~66%) show a significant difference in their responses on oscillation and non-oscillation trials (Figure 8a; methods). This difference is quantified as the Autocorrelation Difference Index (ADI; methods), for which positive scores indicate more oscillatory spiking activity on LFP-identified oscillation trials. The ADI for this example neuron is ~ 1.46 , and the distribution of ADI's across all neurons is positively-shifted (Figure 9b, histogram; $p = 5.27e-34$, $W_{263} = 32152$, $z = 12.16$, two-tailed Wilcoxon signed rank test against median=0).

Given this rhythmic discharge pattern, we characterized how oscillatory single unit activity was synchronized with the local field potential signal. To assess this, we converted the local field potential voltage into a phase angle at every point in time and asked how well

the spikes aligned to a particular phase of the signal (methods). For this example, the spikes (white squares) appear to be concentrated before the peak of the oscillatory envelope (Figure 9b, left; Figure 8c; $p=1.50e-88$, $z=182.33$, Rayleigh's test for non-uniformity). Indeed, the spikes from most neurons across the population cluster around this phase (Figure 9b, right), indicating that these single units tend to be part of ensembles of neurons which are locked with one another.

Given that the LFP oscillations are related to timing behavior and single unit activity is related to the LFP signal, we next assessed whether, and in what way, single unit oscillatory activity could be related to timing behavior. We addressed this issue by restricting our analysis to the spiking activity for each recorded neuron, setting the LFP data aside. For each neuron, we categorized each trial from its recorded session as oscillatory or non-oscillatory on the basis of its spike train (Methods), and then quantified the difference in first lick variance between these categories. As with categorizing trials on the basis of oscillations detected in the LFP, we found that sessions tended to have higher lick variance on non-oscillatory trials, which in this case corresponds to leftward-shifted scores (Figure 9d, blue line; $p=6.49e-05$, $W_{257}=11812$, $z=-3.99$). Further, given that neurons tended to be phase-locked to a particular phase of the LFP theta oscillation, we assessed whether aggregating evidence from multiple spike trains recorded simultaneously might boost the signal, improve classification, and consequently accentuate these behavioral differences. Indeed, by categorizing a trial based on the activity of multiple units, we found an even greater average difference in lick variance on oscillation and non-oscillation trials (Figure 9c, red line; $p=4.06e-05$, $W_{63}=416$, $z=-4.05$). In addition, the performance of timed reward-seeking behavior on oscillating trials improves with the size of the ensemble, as indexed

by an increase in the difference of lick variance between oscillation and non-oscillation trials (Figure 9d, sessions in gray, session averages in pink; $p=.03$, slope=-2.76, $r=.28$).

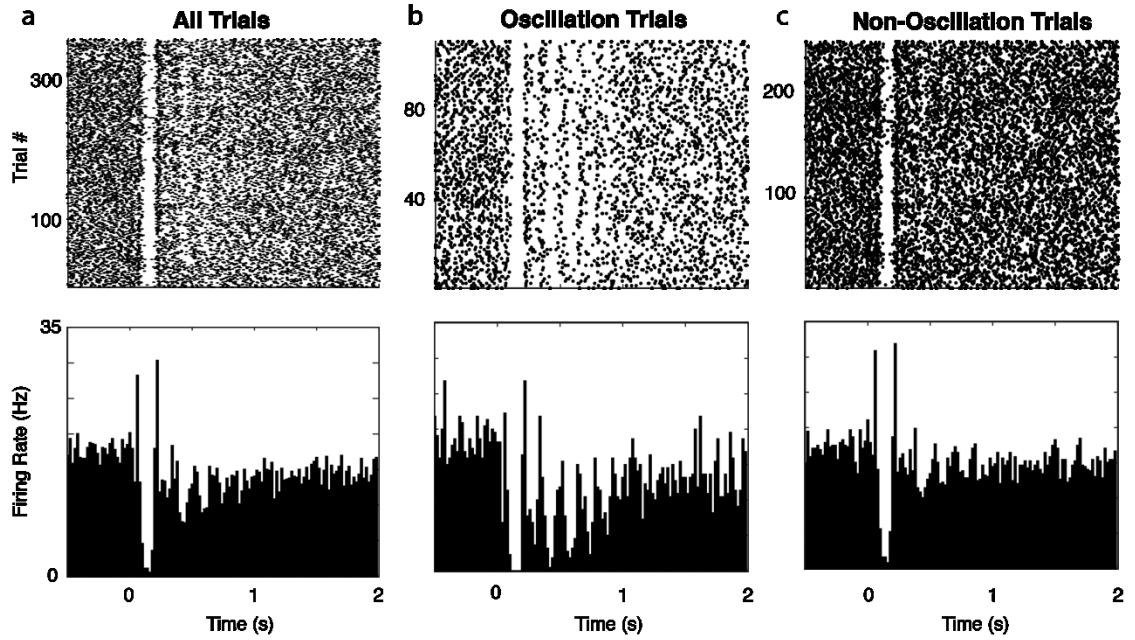


Figure 7 *Neural oscillations occur during LFP oscillations*

a) Spike rasters (top) for an example neuron on all trials, **b)** oscillation trials, and **c)** non-oscillation trials of a session. The peristimulus time histogram for each group is shown below.

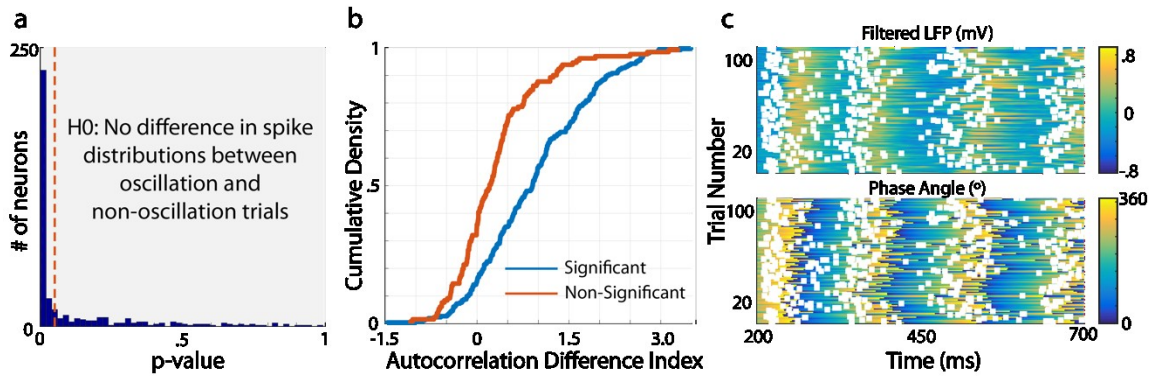


Figure 8 *Neurons spike at a consistent phase of the oscillations in the local field potential.*

a) P-values for the null hypothesis that there is no difference in spike distributions between trials with and without an oscillation in the local field potential for each neuron. The dotted red line indicates where $p=0.05$. b) The Autocorrelation Difference Index (which is a measure of the difference in the level of autocorrelation between spike-separated oscillation and non-oscillation trials) is considerably higher in neurons for which the null hypothesis stated in a is rejected (blue) than in those for which it is not (red). c) Heat maps showing the filtered local field potential (top) and phase angle (bottom) on LFP oscillation trials, with spikes from the example neuron in Figure 7 overlaid (white squares).

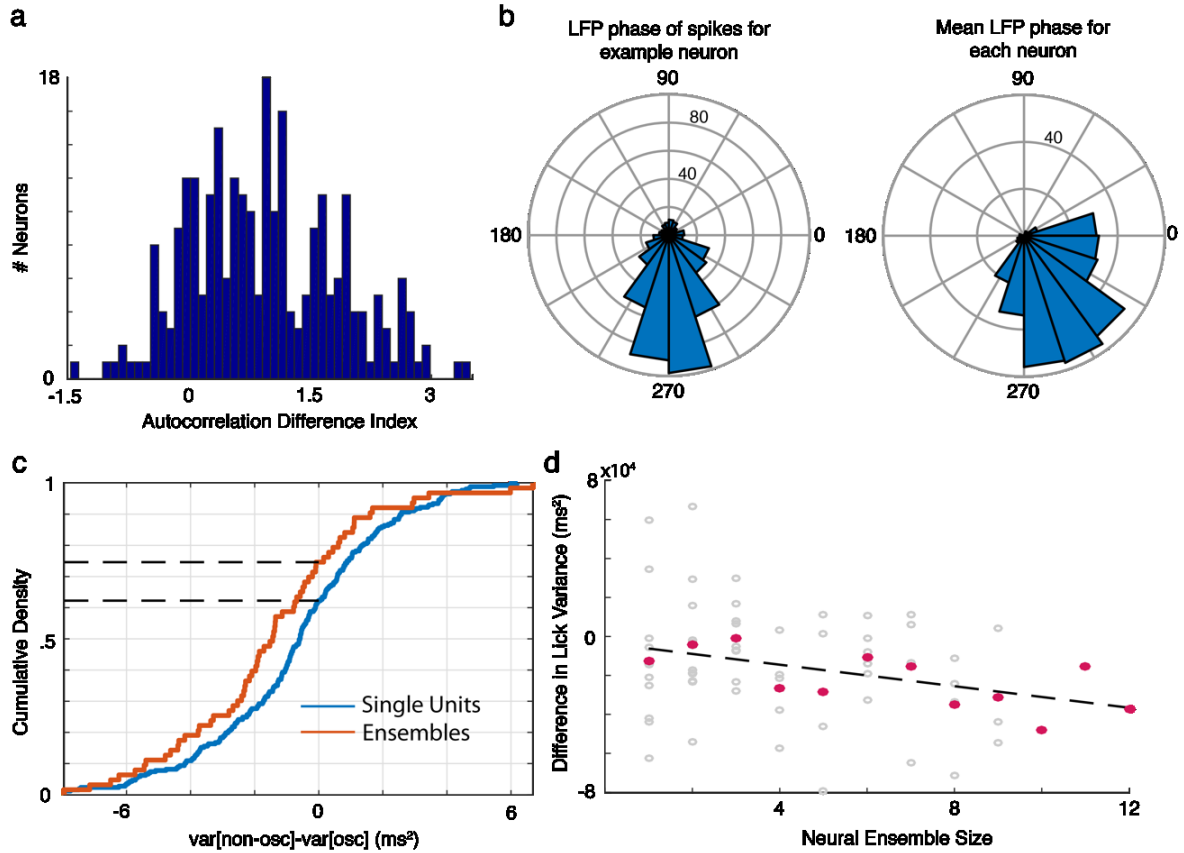


Figure 9 Timed lick behavior tracks single unit spike coherence

a) The distribution of the Autocorrelation Difference Index across all neurons is right-shifted, indicating that the spike train autocorrelation is higher on LFP oscillation trials. **b)** Polar plots indicating the distribution of LFP oscillation phase angles at which spikes occur for the example neuron (left) and the mean phase angle for each neuron in the population (right). **c)** Empirical cumulative distribution functions for the difference in lick variance on spike-separated oscillation and non-oscillation trials ($\text{var}[\text{osc}] - \text{var}[\text{non-osc}]$) for individual neurons (blue) and neural ensembles (red). **d)** Relationship between neural ensemble size and difference in lick variance on each session (gray dots), with a regression line (dotted black line), and session means per ensemble size (pink dots).

2.6 Results: The likelihood of evoking an oscillation covaries with the recently experienced reward rate

Since timing is more precise and accurate during oscillatory states in V1, we wondered what behavioral variable(s) might influence the likelihood of observing an oscillation on a given trial. To assess this, we created a logistic regression model with several candidate explanatory variables, in which the dependent variable was the fraction of channels detecting an oscillation (out of six). Of the variables tested, the inter-trial interval (that is, the time from nosepoke exit to subsequent trial initiation) was consistently the most informative (i.e. the distribution of its t-statistic across sessions was shifted farthest from zero) (Figure 10a). Because the regression statistics can be influenced by extreme values, we probed this relationship further by plotting the likelihood of oscillation with respect to inter-trial interval alone (Figure 10b). It can be seen from this plot that longer inter-trial intervals decrease the probability of evoking an oscillation. Such a relationship may arise if the cortical state was tracking some behavioral rate, such as the trial rate, photic rate (i.e. the rate of visual stimulation), or reward rate recently experienced until that moment by the animal. Therefore, we sought to dissociate these possibilities. Specifically, we compared the receiver operating characteristic (ROC) values—a measure of the discriminability between two distributions, in this case the rates on oscillation vs non-oscillation trials—across all sessions. For the filter parameter (which sets the integration dynamics for calculating the behavioral rates) associated with the maximal mean ROC (methods), all three variables are good predictors of oscillation likelihood, but the reward rate is the best predictor of the three (Figure 10c). In fact, the reward rate was consistently the best

predictor over the full range of time windows analyzed (that is, the windows over the rates were calculated) (Figure 10d). This suggests that oscillations are most prevalent during periods of high experienced reward rate in this behavioral timing task.

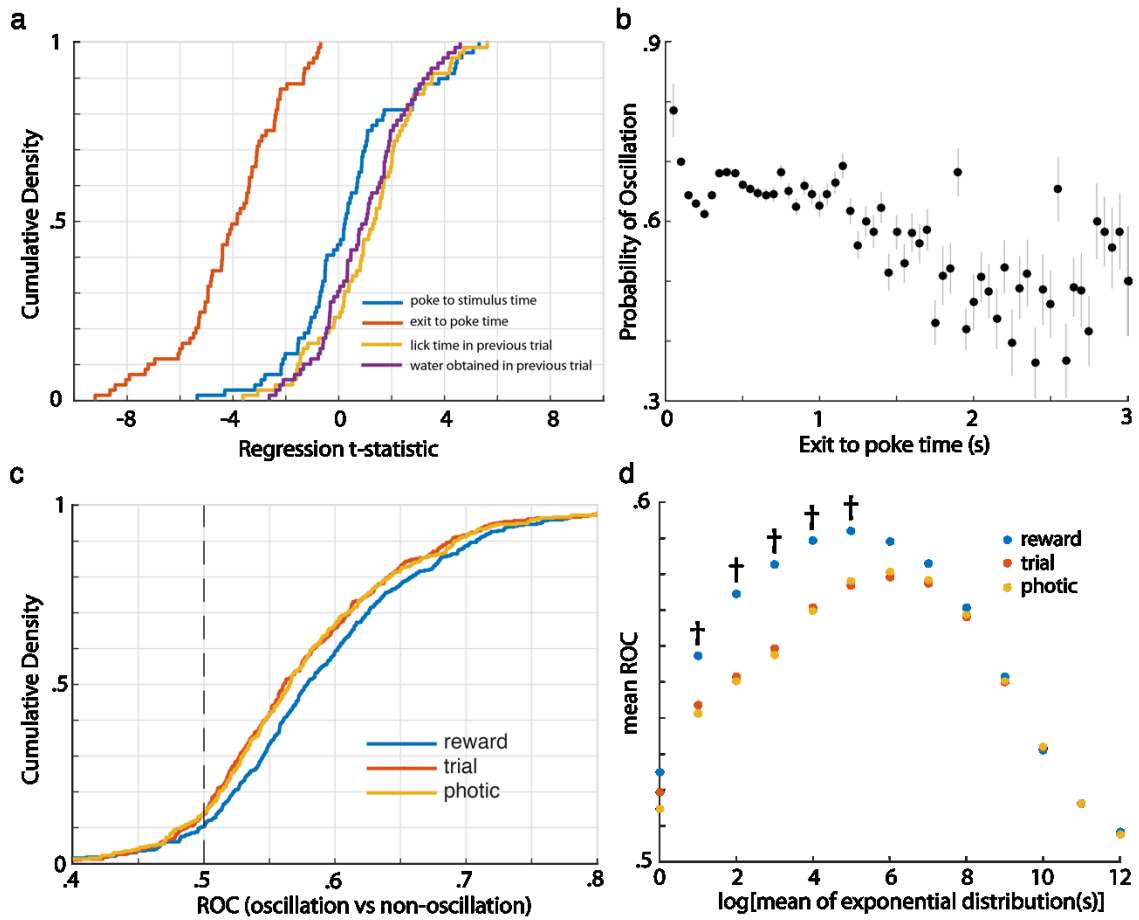


Figure 10 *Reward rate is related to oscillation likelihood*

a) Distributions of t-statistics across sessions for several variables in a logistic regression model in which the dependent variable is the fraction of electrodes displaying an oscillation on a given trial (out of six). Of the variables considered here, the distribution of t-statistics for the inter-trial interval (red line)—the time between exit on the previous trial to subsequent trial initiation—is the farthest shifted from zero. **b)** Relationship between the probability of oscillation and the inter-trial interval (exit to poke time). Probabilities are calculated by taking the number of oscillations divided by the total number of observations (i.e. all analyzed channels and trials) falling within a range of inter-trial intervals 500ms

wide, sweeping from .5s to 30s. **c)** Empirical cumulative distribution functions (CDFs) for the receiver operating characteristic (ROC) values, across sessions, associated with the difference in various behavioral rates (reward, trial, and photic) between oscillation and non-oscillation trials. These CDFs correspond to the exponential filter (used to calculate the rates) yielding the maximal mean ROC (methods). **d)** The mean ROC values for each rate variable across sessions, for each exponential filter size tested. Daggers denote where the mean ROC value associated with reward rate is significantly different from that associated with trial rate.

2.7 Materials and Methods

2.7.1 Behavioral task and neural recordings

Experimental procedures were as previously described (36). Briefly, water-deprived, adult, male, wild-type, Long-Evans rats were trained to perform a visually-cued timing task, in which they entered a nosepoke, waited a random delay without licking, received a 100 ms full-field, monocular visual stimulus, executed a lick, and obtained a water reward (on 5/6 visually-cued trials). The amount of reward available upon licking post-stimulus increased linearly up to 1.5 seconds, after which no reward was available (Figure 1a). After animals were sufficiently trained (average wait times exceeded one second for three consecutive days), they were stereotaxically implanted bilaterally with 2x8 electrode arrays targeted toward layer IV of the binocular zone of primary visual cortex (V1). Following recovery and water deprivation, animals performed the task while neural recordings were collected, amplified, and filtered by Neurlanx (Bozeman, MT) hardware. For a different cohort of animals, referred to here as naïve, implantation occurred prior to training (and the ramp of available reward extended only to 1, instead of 1.5, seconds). All procedures were conducted in accordance with the NIH Guide for the Care and Use of Laboratory Animals and were approved by The Johns Hopkins University Institutional Animal Care and Use Committee. Six spatially-distant electrodes (3 per hemisphere) were selected for local field potential analysis, to reduce redundancy in the signals.

2.7.2 Local field potential processing

Neural signals were continuously sampled at 32kHz, downsampled to 2.2kHz, and bandpass filtered (1-400Hz). This filtered LFP signal was then converted to concentrated energy scores by applying the methodology in (49). Here, concentrated energy is defined as the mean energy divided by the purity. To calculate the mean energy, we first generate a time-frequency representation from the filtered LFP by applying Gabor filters with frequencies from 4 to 9 Hz in .5 Hz steps (standard deviation of Gaussian kernel=.5). The mean of this time-frequency representation across all frequency values for each point in time is defined as the mean energy. Purity, a measure of how concentrated the energy was across the range of frequencies assessed, was calculated as:

$$purity = \frac{\sum f^2 * e_{norm}}{(\sum f * e_{norm})^2}$$

where f is the frequency values and e_{norm} is the energy at each frequency at every point in time normalized to the total energy at that time.

2.7.3 Oscillation detection and duration

The concentrated energy scores during a session were used to detect the presence of an oscillation and duration, as described previously (49). To categorize trials into oscillatory and non-oscillatory groups, we first created a threshold according to the formula:

$$threshold = (CE_{max} - CE_{min})/c$$

where CE_{max} and CE_{min} are the maximum and minimum mean concentrated energy scores (taken from a 200-700ms window following a visual stimulus) for any visually-cued trial

across the session, respectively, and c is a constant equal to 2.5. An oscillation trial is then defined as any trial where the concentrated energy value crosses this threshold at any point in the 200-700ms post-stimulus window. For trials with an oscillation, the duration of the oscillation was the amount of time between when the concentrated energy exceeded this threshold to when it subsequently fell below the threshold.

2.7.4 Oscillation states

In order to establish whether it is appropriate to treat trials as belonging to one of two classes (oscillatory or non-oscillatory), we modeled the post-stimulus responses across trials. To do this, we took the mean concentrated energy from a 200-700ms window post-stimulus on each trial and attempted to find a good fit to this distribution. We started with the most straightforward hypothesis that the concentrated energy values across trials arose from a Gaussian process, $\mathcal{N}(\mu, \sigma)$, which would result in a unimodal distribution. This was tested against a mixed model in which two Gaussian processes are linearly combined, $p * \mathcal{N}(\mu_1, \sigma_1) + (1 - p) * \mathcal{N}(\mu_2, \sigma_2)$, which would result in a bimodal distribution. To compare these “1-gaussian” and “2-gaussian” models, we calculated the Akaike information criterion (AICc) values for each. The AIC takes into account the likelihood (derived from maximum likelihood estimation) and also the model complexity, such that models with more parameters are penalized. In this case, the 2-gaussian model has 5 parameters whereas the 1-gaussian model has only 2 parameters. AICc is a correction for small samples and is calculated as $AICc = AIC + 2k(k + 1)/(n - k - 1)$. The difference in AICc values (or, more specifically, $\exp((AICc_1 - AICc_2)/2)$) provides a measure, then, of the relative likelihoods of the models.

Because a unimodal Gaussian model is a simplistic alternative, we also tested against a variety of more plausible models. Specifically, we tried to find the best alternative to the 2-gaussian model among 17 continuous distributions implemented in a custom MATLAB script by Mike Sheppard (2012) [Fit all valid parametric probability distributions to data, MATLAB Central File Exchange, Retrieved November 17, 2015] which includes, among others, the following distributions: Beta, Exponential, Gamma, Generalized extreme value, Inverse Gaussian, Logistic, Log-logistic, Lognormal, Normal, Rayleigh, and Weibull. Of these, ten provided reasonable fits to the data in less than 30% of cases and, thus, were excluded from the data. Of the remaining seven candidates (which provided reasonable fits in 100% of cases), the Generalized extreme value distribution had the lowest overall AICc value across sessions and, therefore, was chosen as the best alternative to the 2-gaussian model. Unlike the unimodal Gaussian model, this model has skew and, thus, can fit the distribution of concentrated energies across trials better.

2.7.5 Visually-evoked potential correlation

The acute response to the visual stimulus, termed the visually-evoked potential (VEP), is defined here as the voltage modulation in the local field potential during the first 200ms post-stimulus. To assess whether the correlation between the timed lick and oscillation can be explained by an earlier physiological event, we assessed whether the magnitude of the visually evoked potential (that is, the absolute difference between the peak and the trough in the voltage trace during this 200ms period) might be predictive of lick time. Specifically, we calculated the percent of variance explained by a single variable (either oscillation duration or VEP amplitude) compared to a linear regression with both variables, across all sessions and channels.

2.7.6 Spike-LFP phase locking

Spiking data was manually sorted using Offline Sorter software from Plexon (Dallas, TX). Finding the phase of the oscillation at which these spikes occurred required converting the filtered LFP signal into a phase position at each time point. This was achieved, as previously described (49, 97, 98), by decomposing the signal with a discrete, Meyer-type wavelet transform into its 3.9 to 7.9Hz components, applying a Hilbert transform on the reconstituted signal, and computing the angle of this result, z , with the following equation: $angle(z) = imag(\log(z))$. Rayleigh's test for circular uniform distributions was then used to determine whether the phase angles at which the spikes occurred was isotropic.

2.7.7 Spike train analysis

In order to compare the degree of rhythmic activity on oscillatory and non-oscillatory trials, we created the Autocorrelation Difference Index (ADI). The ADI is the difference in the autocorrelation scores on oscillation and non-oscillation trials, which are defined as the sum of the sample autocorrelation function from 100 to 300ms (which encompasses the range of the oscillatory periods) derived from the peristimulus time histogram (PSTH).

To separate trials based on their spike trains alone, we assessed whether the autocorrelation score defined above increased or decreased as each trial was removed from a session's overall PSTH. If removing a trial decreased the overall autocorrelation, it was considered an oscillatory trial and vice versa. For the ensemble analysis, each neuron in the ensemble (that is, the group of neurons recorded simultaneously during a session) was given a vote

based on the aforementioned criterion, and the majority vote determined whether a particular trial was labeled as oscillatory.

2.7.8 Oscillation prevalence modeling

To dissociate the contributions

of various behavioral rates (reward, trial, and photic) to the likelihood of evoking an oscillation, we systematically swept through a parameter space of integration filters that incorporated past behavioral statistics. For completeness, we used both a uniform and exponential distribution as filters. The distribution of means tested for each filter type were identical, and were 2^x seconds, where x took on all integer values from 0 to 11, inclusive. The differentiability between the rates computed for all these parameters on oscillation and non-oscillation trials was measured on each session using the receiver operating characteristic (ROC). The mean ROC for a particular filter, mean parameter, and rate type was the average ROC value computed in this way across sessions and channels. We define the maximal mean ROC as the highest mean ROC for a given filter type (across all mean parameters and rate types).

2.7.9 Assessing the acute effect of licking

We examined the possibility that the lick itself could affect an ongoing oscillation, thereby artificially creating a distinction between oscillatory and non-oscillatory states. Three analysis were brought to bear on this question. First, we asked whether licking acutely suppresses an oscillation. To address this, we calculated the average difference in concentrated energy between a 50ms window before and after a lick and compared it to the

null distribution of concentrated energy differences obtained by repeatedly ($n = 1000$) shuffling the relationship between the lick times and trial number. Second, we investigated whether there was a phase relationship between licking and oscillations, in a manner similar to that described above in **Spike-LFP Phase Locking**, but for licks. Third, we asked whether there was a discernable difference in oscillatory power even prior to licking. To address this, we calculated the distribution of concentrated energy scores in 50ms windows prior to the first lick on a given trial for oscillation and non-oscillation trials separately.

2.8 Discussion

Appropriately timing actions in response to sensory stimuli is a necessary ability for survival. Here, we show that oscillatory states in primary visual cortex may contribute to this ability. Specifically, we show that there is an enhancement of precision and accuracy of timed reward-seeking responses following a visual cue, when that cue evokes theta oscillations in V1. The more widespread across V1 this theta oscillation is, the greater the improvement in timing performance. An appealing hypothesis to explain the difference in timed lick behavior between oscillatory and non-oscillatory states is that an ongoing oscillation in V1 exerts an influence on the animal's decision to lick (perhaps via a downstream motor region) by suppressing licking throughout its duration. Under this hypothesis, we would expect the time of the first lick to covary with the duration of the oscillation. Indeed, this relationship was stronger for well-trained compared to naïve animals, suggesting that the association between the oscillatory state and the timed behavior is learned. Furthermore, we found strong evidence for this oscillatory state in the spiking data of simultaneously recorded neurons. These oscillatory firing signals are related to enhanced timing precision and, in addition, act in concert as ensembles to boost the predictive signal. Together, these data suggest that there is a distinct oscillatory state in primary visual cortex that is related to the performance of visually-timed actions.

An alternative to this interpretation is that lick initiation itself shuts down ongoing oscillations. If this were the case, non-oscillation trials would appear to have earlier (and perhaps more variable) lick times, as a lick during the scoring window would increase the likelihood of being categorized as a non-oscillation trial. This explanation is not

satisfactory for a number of reasons, however. First, a prior study (49) in which animals could and did lick freely post-stimulus (and before the typical delay to reward) did not detect a suppression in ongoing oscillatory power. In line with this observation, we find that the first lick following a visual stimulus does not acutely suppress an ongoing oscillation ($p=.90$, by random shuffling; methods). Second, as shown previously (49), we did not find any phase relationship between licking and oscillations, suggesting that the oscillation was not being driven by motor output ($p>.05$, Rayleigh's test for non-uniformity; methods). Third, we found that the distribution of oscillation strengths is already much lower for non-oscillation than oscillation trials prior to a lick (Figure 4c; $p<.001$, $U=2.89e09$, $z=-261.86$, $n_1=59466$, $n_2=143514$, two-sided Mann-Whitney U-test; methods) which suggests that these differences exist before the action. In sum, these observations suggest that the timing activity in V1 is not merely a consequence of the behavioral action itself.

Our findings thus further our understanding of V1's role in stimulus-driven behaviors. Traditionally, V1 was thought to contribute only to the first stage of such behaviors: sensation. Along these lines, primary visual cortex has been regarded as a feature detector which relays faithful representations of the visual world to downstream regions. This view has been challenged by recent work suggesting that V1 can actively generate predictions about visual input (99–103) and can be influenced by behavioral variables such as attentional states (104–108) and reinforcement (109–111) (e.g. water reward). Whereas these findings pertain to influences on perception, our findings provide evidence that V1 makes predictions about non-visual outcomes. Specifically, we find that following the acute visual response, V1 exhibits long-lasting theta oscillations that subtend the interval between stimulus and action during a timing task. Thus, these oscillations in primary visual

cortex are a signature of V1's involvement beyond perception and into the decision-making phase of a timed, stimulus-driven behavior.

These observations also extend our knowledge about the role and behavioral significance of theta oscillations. In the hippocampus, theta oscillations have been implicated in several cognitive functions, including voluntary movement, learning, and memory processes (112). This rhythm is believed to contribute to these processes partly through facilitation of information transfer with prefrontal cortex (113, 114). Indeed, oscillatory synchrony is a common mechanism for inter-regional communication which has been shown in a number of circuits (115), including those involving visual cortex (116–119). In our visuomotor task, this mechanism may allow the output from primary visual cortex to be effectively read out by a motor region that ultimately initiates the action. Within visual cortex itself, oscillations are often studied from a perceptual perspective and have been found to enhance responding to particular stimuli (120–122) and enable feature binding (46, 47). Recent work has found, however, that oscillatory states in primary visual cortex may also be related to expectancy of future outcomes (48, 49). We extend these findings by showing that theta oscillations in V1 are related to the precision and accuracy of visually-timed actions. Though theoretical accounts of timing often implicate oscillatory processes in such timed behaviors (7), evidence supporting these theories has been lacking (61). Finding this kind of signal as the earliest stage of cortical visual processing is particularly surprising and may suggest that such a mechanism is a common feature of local circuits.

These findings also raise the question of why there are multiple (i.e. oscillatory and non-oscillatory) states in V1. One straightforward possibility is that maintenance of an oscillatory response pattern is energetically taxing and, therefore, must be limited. Another, compatible possibility—given the relationship between reward rate and oscillation prevalence (Figure 10)—is that animals performing the timing task are seeking to balance knowledge accumulation with reward accumulation (i.e. the exploration vs exploitation trade-off) (123). Under this construction, it may be advantageous for an agent to exploit its knowledge of the environment by tracking a theta oscillation and waiting a precise amount of time when the reward rate is high, but explore the environment otherwise. In support of this hypothesis, a prior study found that experimentally increasing the reward rate increased the likelihood of evoking an oscillation (49). Future studies that precisely manipulate reward rate during a behavioral timing task will help elucidate the role this factor plays in governing cortical state and temporal decision-making.

A potentially rich avenue of future exploration would be to investigate what downstream regions are receiving and processing this information from V1. One plausible candidate is motor cortex, which might directly use the signals emanating from V1 to exert control over the action (in this case, licking or suppression of licking). In this simple circuit, the oscillatory signal might facilitate information transfer between these regions, as has been shown for similar circuits (115, 118, 124), even those involving primary visual cortex (116, 117), or might simply provide a much clearer and robust signal for motor cortex to interpret. In a similar vein, this oscillatory signal might be processed in the basal ganglia, a subcortical region crucial for voluntary movement, which is active even prior to self-initiated actions (91). A popular theoretical model for this type of interaction is the striatal

beat-frequency model, in which medium spiny neurons of the striatum detect an activity pattern across cortical oscillators in order to demarcate a temporal interval. It is also possible that areas comprising the reward system receive this output from V1. An appealing candidate in this regard is the ventral tegmental area (VTA) in the midbrain, which must receive reward-expectancy information in order to generate the prediction errors that are crucial for reinforcement learning. Given these possibilities, it would be informative to simultaneously record from these brain areas and V1 as animals perform this visually-cued timing task.

Another central question is how this oscillatory expectation signal in V1 arises. Along these lines, modelling work has suggested that reinforcement signals induce the synaptic changes underlying cortical reward timing (125) and experimental work has demonstrated that cholinergic innervation from the basal forebrain is both necessary (34) and sufficient (35) for generating such signals in V1. Other neuromodulator systems, like the dopaminergic and serotonergic systems, may also play a role. As the dopaminergic system has been implicated in tracking vigor and reward rate (126), it might also contribute to the association between oscillation prevalence and reward rate described here (Figure 10). It might be interesting, therefore, to study how disrupting or inducing these systems impacts the oscillatory signals and the behavior on this visually-cued timing task. It is also likely that inhibitory interneurons—which are often implicated as key players in generating cortical oscillatory rhythms (127)—contribute to the oscillatory expectation signal in V1. In this regard, selective manipulation of Parvalbumin, Somatostatin, and Vasoactive Intestinal Polypeptide-expressing inhibitory interneurons, which are abundant in cortex,

may provide further insight into the origins and functions of oscillatory states in primary visual cortex.

Author Contributions

The study was conceived by Joshua M. Levy and Marshall G. Hussain Shuler. Joshua M. Levy performed all analyses, with help from Camila L. Zold, on data collected by Vijay M.K. Namboodiri. Joshua M. Levy and Marshall G. Hussain Shuler wrote the manuscript.

Chapter 3. Interval storage and memory bias effects

Abstract

A common method for studying interval storage is classification, in which a subject must indicate whether a given probe duration is nearer a previously learned short or long reference interval. This task is designed to reveal the probe duration that is equally likely to be labeled as short or long, known as the temporal bisection point. Studies have found that this bisection point is influenced by a variety of factors including the ratio of the target intervals, the spacing of the probe durations, the modalities of the stimuli, the attentional load, and the inter-trial duration. While several of these factors are thought to be mediated by memory effects, the prototypical classification task affords no opportunity to measure these memory effects directly. Here, we present a novel bisection task, termed the “Bisection by Classification and Production” (BiCaP) task, in which classification trials are interleaved with trials in which subjects must produce either the short or long referents or their midpoint. Using this method, we found a significant correlation between the means of the remembered referents and the bisection points for both classification and production trials. We then cross-validated the bisection points for production and classification trials by showing that they were not statistically differentiable. In addition to these population-level effects, we found within subjects evidence for co-variation across a session between the production bisection points and the means of the remembered referents. Finally, by using two sets of referent durations, we showed that only memory bias-corrected measures

were consistent with a previously reported effect in which the ratio of the referents affects the location of the bisection point. These results argue that memory effects should be considered in temporal tasks.

3.1 Introduction

Organisms rely on a wide range of temporal information to guide their behavior (7). At one end of the spectrum, organisms require sub-second information to guide movement (128, 129). At the other end, their circadian rhythms are entrained by temporal cycles that span days (130). In between these extremes, organisms must be able to evaluate the length of temporal intervals on the order of seconds to hours to guide their decision-making (4, 5, 131, 132). Because of the importance of this type of temporal information, interval timing has been studied extensively in laboratory settings.

A common method for studying interval timing in humans is a classification task (133, 134). While the precise form of this task has been modified frequently, its essential component is that subjects are required to classify sample temporal intervals as short or long. Typically, this classification relies on the subject remembering previously learned short and long reference intervals (i.e. similarity method). The obtained data is the percentage that the subject chooses to label an interval “long” as a function of probe duration length. From this data, the bisection point, or probe duration at which a subject is equally likely to choose “short” or “long”, can be calculated.

Several theories of timing and time perception make predictions about the location of the bisection point. One of the most influential theories of timing, scalar expectancy theory (57), posits that the bisection point lies at the geometric mean of the short and long reference intervals (134). Another timing theory, which assumes a difference rule for comparing a probe duration to the short and long referents, predicts that the bisection point

lies at the arithmetic mean of the referents (133). More contemporary theories have been brought to bear in an attempt to systematically explain the observed variations in the bisection point location from the harmonic mean to the arithmetic mean (Killeen et al., 1997; Kopec and Brody, 2010) and rationalize such variations in terms of reward-rate maximization (71) and optimal temporal risk assessment (137, 138). Given that these many theoretical accounts of timing make specific predictions about the location of the bisection point, obtaining accurate and meaningful measurements of the bisection point is crucial.

Indeed, many factors have been shown to affect the location of the bisection point. These factors include the ratio of the target intervals (50, 139), the spacing of the probe durations (140, 141), the modalities of the stimuli (142–146), the attentional load (147–150), and the inter-trial duration (151, 152). Several of these factors are thought to affect memory and, thereby, the subjective representation of time. Increasing the cognitive load, for example, by requiring subjects to observe emotionally-charged faces can cause either an overestimation or underestimation of time on a temporal bisection task, depending on whether the stimulus is arousing (e.g. angry face) or attention-demanding (e.g. shameful face), respectively (149). Analogously, requiring subjects to engage in tasks which demand working memory, like remembering a series of digits, will cause distortions in temporal production (147, 148). Similarly, varying inter-trial duration is believed to affect the degree of memory trace degradation and, thereby, whether a subject is more likely to label an interval “short” (choose-short effect) or “long” (choose-long effect) (151, 152).

It is not surprising that these factors affect time perception given that memory is a key component of several interval timing models. In pacemaker accumulator models, the

number of pulses generated by a pacemaker during the reference interval is stored in memory and compared against the number of pulses generated by a probe duration (58). This comparison serves as a proxy for comparing the length of a probe duration to the referent. Thus, affecting the rate of the pacemaker during the referent/probe duration, or altering values stored in memory, can affect the subjective representation of time. Pharmacological manipulations showing a dissociation of the effects on memory from effects on perception have bolstered this view (60, 153). Another model of interval timing, the striatal beat-frequency model, also reserves a key role for memory (66, 154). In this model, striatal neurons compare ongoing cortical oscillatory patterns to prior patterns of activation that co-occurred with the expiration of an interval. Still other models have posited that the strength of a memory trace is itself an internal clock (64, 155) which naturally meshes with the notion that alterations in memory affect time perception.

Given the importance of memory in temporal perception, several variants of the prototypical bisection task have been developed to study its role. One variant of the similarity method, in which subjects are explicitly taught to recognize the short and long reference intervals, is the partition method, in which subjects must infer the range of intervals and, concomitantly, what constitutes a short and long interval (139, 141, 156). Interestingly, the results from these experiments indicate that both methods yield similar outcomes, suggesting that subjects do not compare probe durations directly to referents. Instead, it is believed that subjects translate these referent durations into a mental representation threshold above which a probe duration is classified as long and below which a probe duration is classified as short, a process which may be integral in cross-domain comparisons of quantities (157). Another variant of the prototypical task in which

referents are provided at the beginning of the session only (i.e. “no-referents” method), is the “fixed-referents” task, in which the same referents are displayed before each trial (158). By replaying the reference intervals before each trial, the contribution of memory to the decision process should be reduced. Yet another variant, the “roving-referents” task (159, 160) changes the referent intervals on a trial-by-trial basis, thereby reducing or eliminating the effect of memory.

Entirely different methods have also been employed to study temporal perception. One of the most prevalently used methods is a reproduction task in which subjects observe a temporal interval on each trial and must reproduce it as accurately as possible (161, 162). In this way, the translation of real time into subjective time can be observed across a wide range of time points while minimizing the role of memory. Another method requires subjects to periodically produce taps at a frequency set by a guiding stimulus (163). In this method, the readout is the temporal error in tapping after the guide stimulus has been removed. Yet another production method asks subjects to wait for a time specified by a verbal cue (e.g. 4 seconds). While relevant to some applications, this method does not fully control for subjects’ prior experience and also may be confounded by the interaction between magnitude (e.g. numerosity) and temporal perception (164–166). Though informative, these experimental methods do not, by construction, reserve a large role for memory and are, therefore, not ideal for studying its effects.

Our goal was to develop a method for directly assessing how memory affects the bisection point location in prototypical bisection tasks. To do this, we developed the “Bisection by Classification and Production” (BiCaP) task which interleaves trials in which subjects must

use their memory to produce the short or long reference intervals or their midpoint with trials in which they must classify probe durations as short or long. Both classification and production trials yield an estimate of the bisection point (the point at which the subject classifies the interval “long” 50% of the time and the produced midpoint interval, respectively). We anticipated that the bisection point generated from each method would not be differentiable. Further, we hypothesized that the biases in the memory of the referents, as measured on a fraction of production trials, would co-vary with the location of the bisection point for both classification and production trials. This is indeed what we found. Additionally, the BiCaP task is a novel and powerful method for studying temporal perception generally.

3.2 Results: Performance on the BiCaP Task

To assess the effects of memory on the bisection point, we developed the “Bisection by Classification and Production” (BiCaP) task (Figure 11a), which consists of classification (top) and production (bottom) trials. Using this design, we were able to compare the bisection point produced from classification trials with the midpoint from production trials and, simultaneously, assess what the subjects believe the reference intervals to be. We used two sets of reference intervals, 1/5 seconds and 2/4 seconds, for different cohorts.

We analyzed data from subjects in the 1/5s group to generate descriptive statistics for classification and production trials. As expected, data on classification trials in this group showed a monotonically increasing relationship between the length of the probe duration and the proportion that the interval was classified “long” (Figure 11b, black dots with SEMs across subjects). After fitting a sigmoid function to the data ($R^2=0.99$), we found that the interpolated point at which the subject was equally likely to classify a probe duration as short or long (i.e. the bisection point) was 2.859s. This point has an associated Weber ratio, which is a measure of the standard deviation around a point divided by its mean. For classification, the Weber ratio is the difference limen, defined as half the difference in interval lengths at the points where the subject responded long 75% and 25% of the time, divided by the bisection point. The Weber ratio of the classification bisection point for the 1/5 group was 0.212.

Mean responses on production trials are shown in the same panel (Figure 11b, lines). The mean produced bisection point, shown in red, is 3.269s \pm 0.066s (SEM). The mean

produced short and long interval, shown in black, is $0.948s \pm 0.032$ and $5.844s \pm 0.128s$, respectively. Whereas the mean produced short interval was only slightly shorter than 1 second, the mean produced long interval was nearly a whole second above its true value of 5 seconds. Therefore, while the arithmetic mean of the referent intervals is 3 seconds, the bias-corrected arithmetic mean (i.e. the AM of the produced short and long reference intervals), shown by a solid green line, was $3.396s \pm 0.066s$.

Next, we assessed whether the scalar property (57), which states that the standard deviation in time estimation grows linearly with temporal magnitude, holds for

individual subjects in the 1/5 group. To do this, we calculated the Weber-like fraction (167), or coefficient of variation (i.e. standard deviation/mean), for production across the range of times tested (i.e. short reference, midpoint, and long reference). The median values for the population of subjects are plotted with the error bars indicating the interquartile range (Figure 11b, middle). To test whether Weber's law holds across the pool of subjects, we compared the coefficient of variation (CV) for the population across the three intervals (short reference, production bisection point and long reference). We found a significant difference in median ($p = 0.012$, $\chi^2(29)=8.83$, Kruskal Wallis test) for produced intervals with the 1s and 5s references. Thus, our data does not support Weber's law in the production of these intervals. Such a decreasing trend for the CV has also been observed in humans previously, wherein shorter intervals have larger CVs than longer ones (168).

These analyses were repeated for the data from the 2/4 group. As was the case for the 1/5 group, the proportion of probe durations classified "long" monotonically increased with the length of the probe duration (Figure 11c, black dots). The classification bisection point

was 3.180s and the Weber fraction was 0.155. As before, averaged responses on production trials are shown in the same panel (Figure 11c, lines). The mean production bisection point was $3.347s \pm 0.061s$. The mean production time for the short and long interval was $2.347s \pm 0.054s$ and $4.767s \pm 0.101s$, respectively. Consequently, the bias-corrected arithmetic mean of the two referents is larger than 3 ($3.557s \pm 0.057s$). Repeating the same analysis with the Weber fractions for produced intervals in the 2/4 group, we found no difference in median across the range of intervals ($p=0.24$, $\chi^2(29)=2.82$, Kruskal Wallis test), which is consistent with Weber's law.

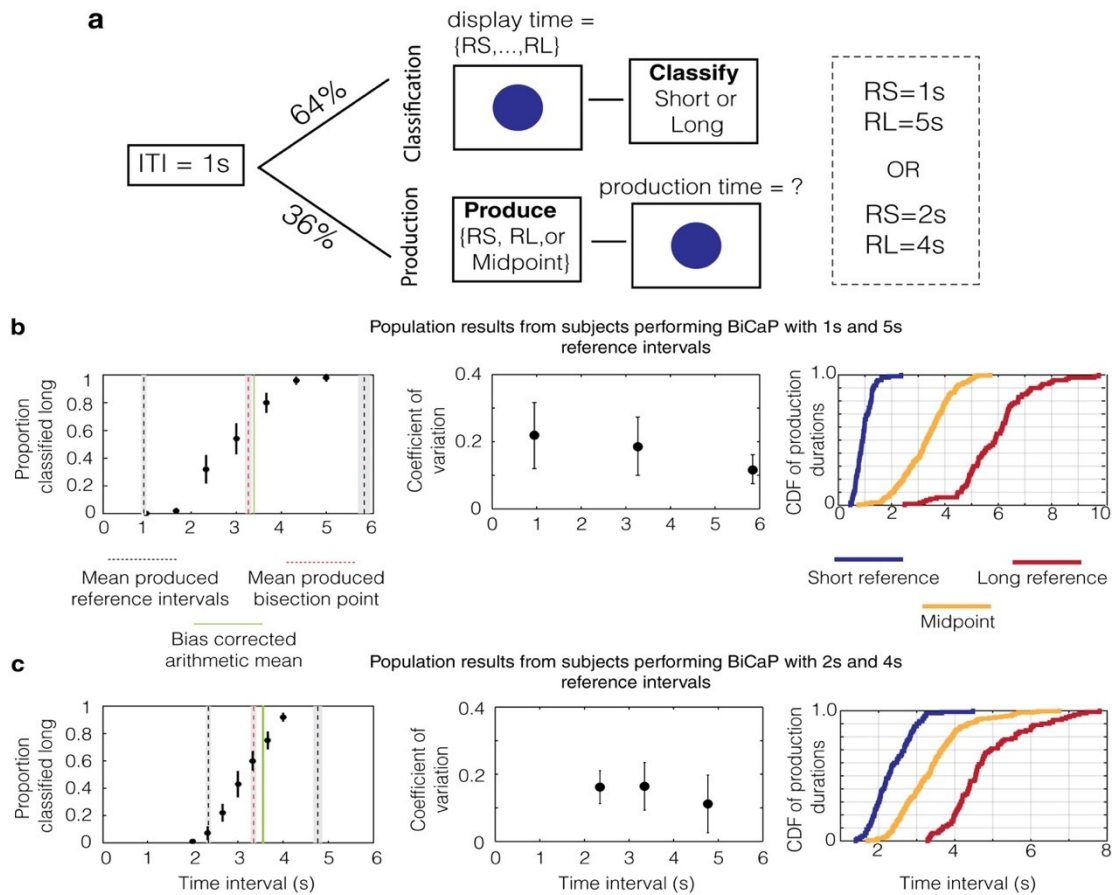


Figure 11 *Performance on the BiCaP Task*

a. Design of the BiCaP task which consists of two trial types—classification and production—pseudo-randomly interleaved. **b.** The proportion that a given probe duration is classified long (left panel, black dots with SEMs across subjects) for the population in the 1/5s referent group. Mean produced intervals for the short reference (black dotted line), long reference (black dotted line), and midpoint (red dotted line) are shown along with the SEM (gray bars). The bias-corrected arithmetic mean (AM) (i.e. the AM of the produced short and long referent intervals) is shown in green. Note that both the produced midpoint and the bias-corrected AM lie above the true AM of the 1/5s reference intervals (i.e. 3 seconds). The mean coefficient of variation (CV) across subjects for each production

interval is shown with SEMs on the middle panel. The empirical cumulative distribution function (CDF) of production times for the short reference (blue), long reference (red), and midpoint (yellow) is shown on the right panel. **c.** The population data for the 2/4s group.

3.3 Results: The location of the bisection point covaries with memory biases

Next, we sought to assess the degree to which memory biases may have affected the location of the bisection point on both classification and production trials. To this end, we examined the correlation between the bias-corrected mean and the bisection points across subjects for classification trials ($p=0.022$, $R^2=0.26$) and production trials ($p=1.9 \times 10^{-7}$, $R^2=0.79$) and found both to be significant (Figure 12a, top). (Separating by groups, we found: classification 1/5s: $p=0.175$, $R^2=0.22$; production 1/5s: $p=0.002$, $R^2=0.70$; classification 2/4s: $p=0.098$, $R^2=0.30$, production 2/4s: $p=3.14 \times 10^{-5}$, $R^2=0.90$). We examined the co-variation between classification and production bisection points (Figure 12c) and also found no significant difference between these groups ($p = 0.15$, two-tailed Mann-Whitney U test, $U_{18} = 356$, $z = -1.45$).

Whereas classification is a purely perceptual measure of the subjective estimate of time, production includes both a perceptual component and a motor component. If the movement time associated with the motor component is automatically compensated for by the brain, we could treat the movement time to be zero (as we have done above). If it is not, however, the movement time would be likely added to the end of the interval. Using a prior study in which the mean movement time of clicking a computer mouse was estimated to be approximately 175 ms (using EEG to detect the moment of movement initiation) (Houlihan et al., 1998) as a guide, we subtracted this number from the subjects' responses on production times. As expected, this manipulation did not affect the degree of correlation between the bias-corrected mean and the bisection points (Figure 12b). It did, however,

make the difference between production and classification bisection points even weaker ($p = 0.64$, $U_{18} = 392$, $z = -0.47$) (Figure 12d).

We next sought to determine whether there was evidence for memory bias within data from individual subjects. To do this, we divided each subject's session into ten equal blocks and asked whether the average midpoint production in a given block correlated with the mean of the produced short and long referent in that block. We found that for the 1s/5s group, data from eight out of ten subjects showed positive slopes of regression (Figure 13a, left). We compared the average slope across subjects (Figure 13a, red star) to that of the null distribution of slopes calculated by bootstrapping (Methods) and found that it was significantly different ($p < .001$). We repeated this analysis for the 2s/4s group. We found that data from nine out of ten subjects in this group showed positive slopes (Figure 13b, left) and the average slope across subjects was, again, significantly higher than that expected by chance (Figure 13b, red star; $p = .007$). Therefore, we found evidence from individual subjects that memory bias across the session in the production of the referents correlated with the produced bisection point.

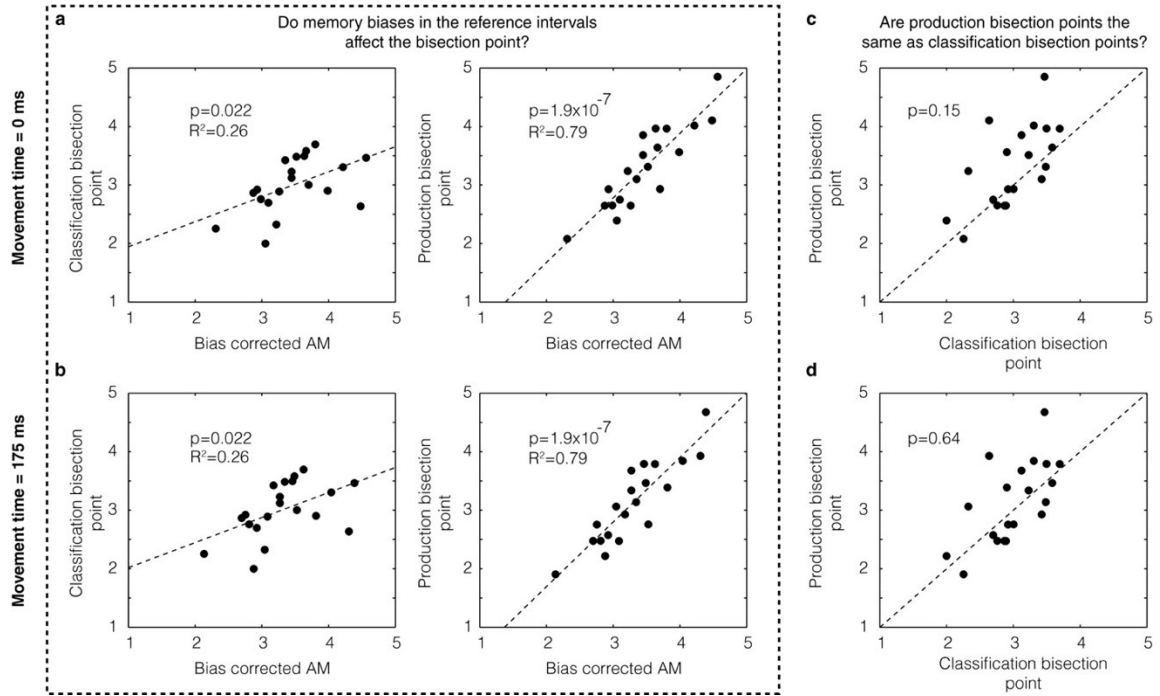


Figure 12 *Memory bias in production and classification*

a. We found a statistically significant correlation between the bias-corrected AM and the classification bisection point ($p=0.022$) assuming a movement time 0 ms (left panel). We also found a highly significant correlation ($p=1.9 \times 10^{-7}$) with the bias-corrected AM for the production bisection point (right panel). **b.** These results do not change assuming a different movement time (i.e. 175 ms). Production bisection points were not statistically distinguishable from classification bisection points **c.** if movement time was assumed to be zero ($p = 0.15$, two-tailed Mann-Whitney U test, $U_{18} = 356$, $z = -1.45$) or **d.** if movement time was assumed to be 175ms ($p = 0.64$, $U_{18} = 392$, $z = -0.47$).

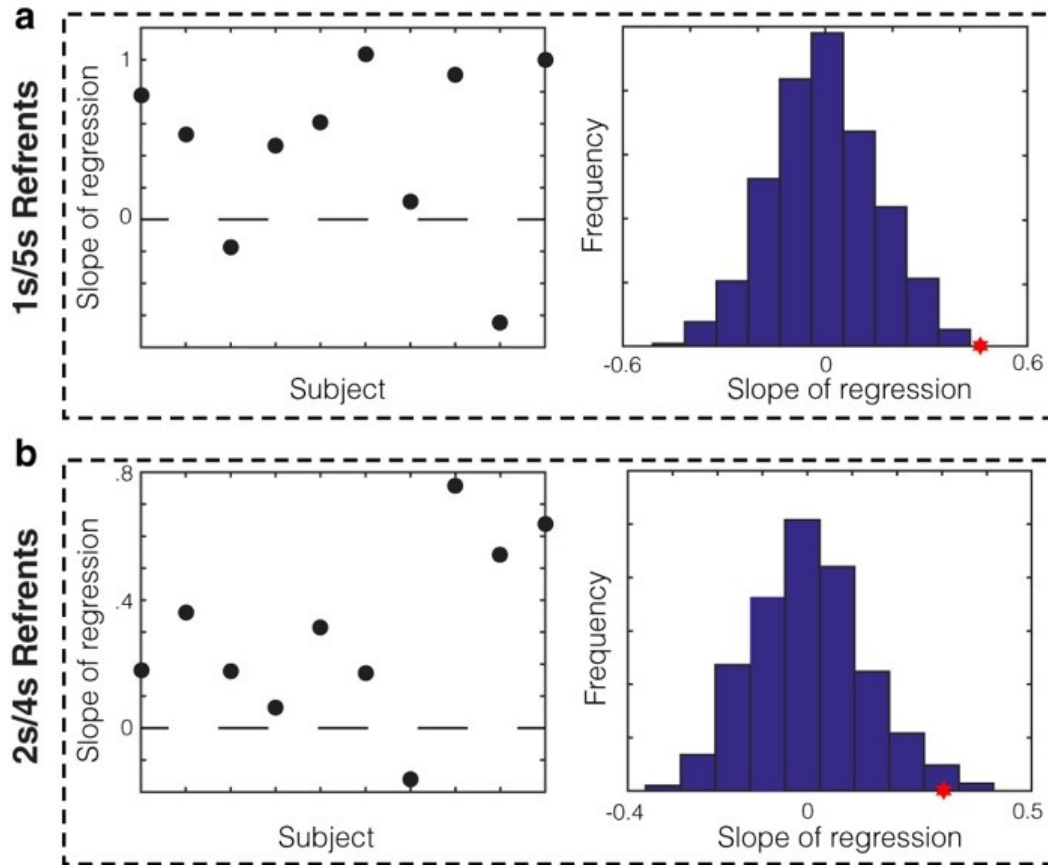


Figure 13 *Within-subject analysis of memory bias in production*

a. Slope of regression in the 1/5s referent group between the mean of the produced referents and the averaged midpoint production per block for each subject. Data from 8/10 subjects show positive slopes. The sampling distribution of slopes was calculated by bootstrapping (right). The average slope for the 1/5s groups (red star) was significantly higher than the null distribution ($p < .001$). **b.** This analysis was repeated for the 2/4s referent group. Data from 9/10 subjects showed positive slopes and the average slope was significantly higher than that of the null distribution ($p = .007$).

3.4 Results: The bias-corrected bisection point exhibits the referent ratio effect

Prior work has shown that the ratio of referent intervals can affect the location of the bisection point (50, 139). A meta-analysis of classification data (136) reported that the bisection point lies near the geometric mean (GM) for ratios of 2 or less and lies near the arithmetic mean (AM) for ratios of 4 or greater. Since our referent interval sets spanned this range, we are able to assess whether our data follows this trend. We first performed these calculations for the population without taking into account memory bias. Neither the production nor the classification bisection points exhibited the referent ratio effect: the production bisection points for both groups were significantly greater than the arithmetic mean (1/5s: $p = 9.2 \times 10^{-5}$, $W_{199}=6845$, $z=-3.91$; 2/4s: $p = 1.16 \times 10^{-6}$, $W_{199}=5995$, $z=-4.86$, two-tailed Wilcoxon signed rank test against median=3) and the classification bisection points were higher for the 2/4 group (3.180s) than the 1/5 group (2.859s) and were found to be significantly different by bootstrapping ($p < 0.001$).

Given that the bisection points correlate with a bias-corrected measure, we sought to determine whether the referent ratio effect could be observed for the remembered referents instead. To this end, we created a distance index defined as:

$$\text{Distance index} = \frac{\text{bisection point} - \text{bias corrected GM}}{\text{bias corrected AM} - \text{bias corrected GM}}$$

Thus, when $D.I = 0$, the bisection point equals the bias-corrected GM and when $D.I=1$, the bisection point equals the bias-corrected AM. Analyzing the data this way, we found evidence for the referent ratio effect in production trials (but not classification trials for

which the power was likely too low). Qualitatively, the mean of the distance index for the 1/5s group was higher than that of the 2/4s group for both classification and production trials (Figure 14a), even when assuming a non-zero movement time (Figure 14b). Quantitatively, the production bisection point for the 1/5s group was significantly different from the GM (Two-tailed Mann-Whitney U test with $n = 10$, $p = 0.0091$, $U = 140$, $z = 2.608$; $n = 10$, $p = 0.0046$, $U = 143$, $z = 2.8347$, for 0ms and 175ms movement times, respectively) but not the AM ($p = 1$, $U = 105$, $z = 0$, for both movement times). While these comparisons were not significant for the 2/4s group, the production bisection points for the 1/5s and 2/4s groups were significantly different in closeness to the GM and AM (0.0376, $U = 77$, $z = -2.0788$ for both movement times), as expected by the referent ratio effect.

Are bisection points closer to GM or AM?

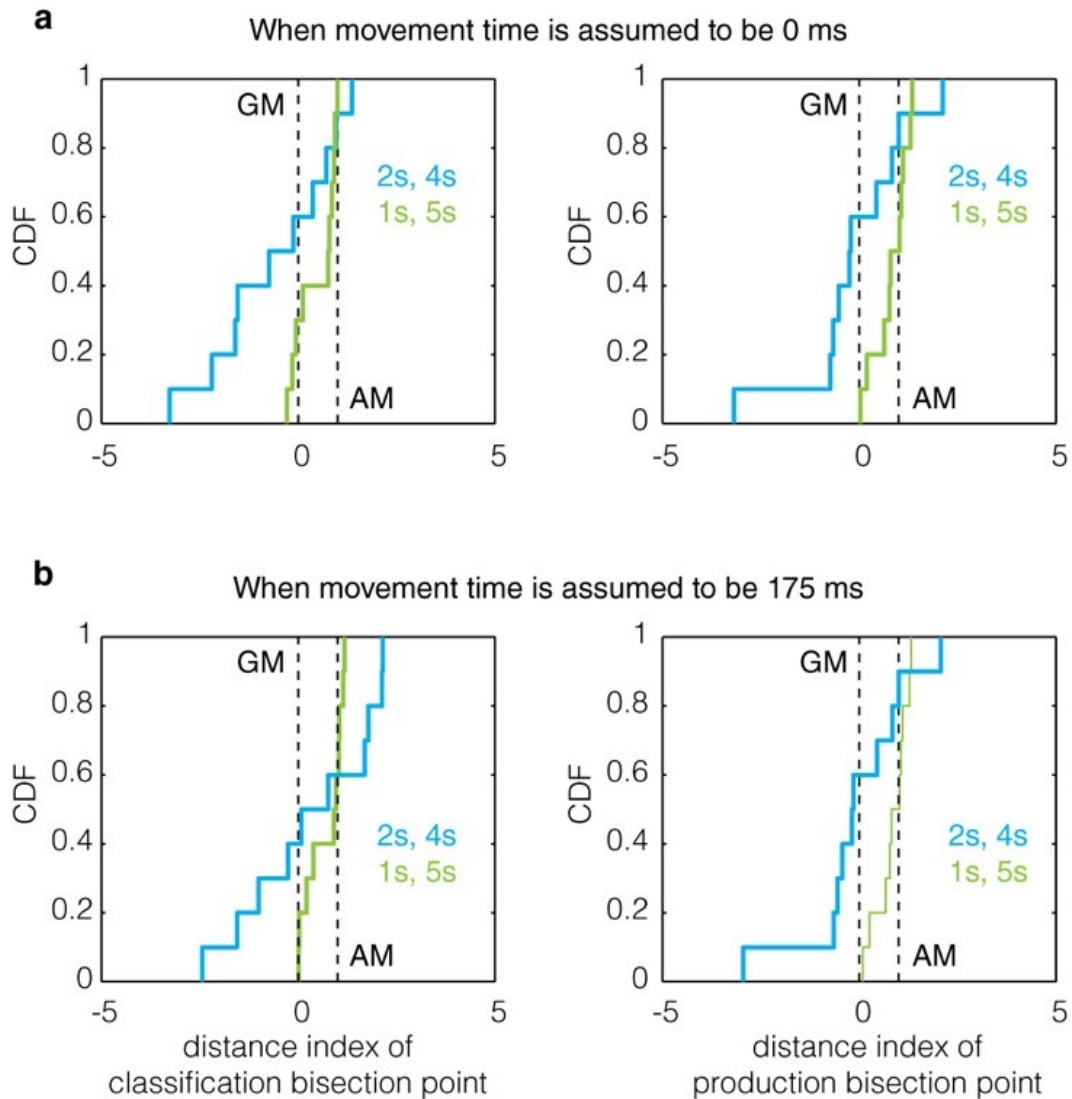


Figure 14 *The effect of referent ratio on the bisection point location*

Previous work has demonstrated that the bisection point transitions toward the arithmetic mean (AM) from the geometric mean (GM) as the ratio of the referents increases (50, 136, 139). Here, we show the cumulative distribution function (CDF) of the distance indexes (defined in Results) for classification and production bisection points. Qualitatively, the data obeys this trend as the median bisection point across all subjects is closer to the AM

for the 1/5s group (referent ratio of 5) than the 2/4s group (referent ratio of 2) for both classification (left) and production (right) trials assuming **a.** a movement time of 0 ms and **b.** a movement time of 175 ms. A quantitative treatment of this data can be found in Results.

3.5 Material and Methods

3.5.1 Subjects

20 healthy, human subjects aged 22-38 participated in this study. All subjects were recruited from The Johns Hopkins University were naïve about the purpose of the study and gave consent to participate. All procedures were approved by the Institutional Review Board (IRB).

3.5.2 Apparatus

Subjects were placed in a quiet room in front of a MacBook Pro. Instructions were displayed on the screen and simultaneously read aloud by the experimenter. All responses were registered by clicks on a wireless mouse. For production trials, the subjects had to left-click to start and stop the interval. For classification trials, the subjects had to left- or right-click to classify the interval as short or long, respectively. Clicks prior to the end of the interval were not registered. To proceed to a subsequent trial, the subject was required to tap the space bar once. The trial type was indicated at the top of the screen. Stimuli were presented and responses were collected by custom-made code written in Java (JDK 6.0_65).

3.5.3 Task

Training

Prior to testing, subjects experienced a training phase that consisted of three parts. In the first part, *observation*, subjects were instructed to observe short and long intervals. Each

interval was labeled as either “SHORT” or “LONG” at the top of the screen. 12 observation trials were given. In the second part, *classification training*, subjects were shown an unlabeled short or long reference interval and instructed to classify. Depending on whether they classified it correctly or incorrectly, they were shown a smiley or frowny face for 1 second. In order to pass classification training, the subject had to correctly classify 3 short and 3 long intervals consecutively by type (with the trial types interleaved with one another). In the third part, *production training*, subjects were instructed to produce the short or long reference interval by instructions at the top of the screen. Depending on whether the response was close enough (i.e. within a window centered on the appropriate interval whose half-width was a Weber fraction of 0.2), they were shown a smiley or frowny face for 1 second. The value of the Weber fraction was chosen to be close to the fraction observed for well-trained subjects on classification and production tasks; a meta-analysis of classification data shows that the Weber fraction is around .2 for human subjects (136) and a similar production procedure to the one used here found a Weber fraction around .15 in well-trained humans who receive do not receive feedback and do not chronometrically count (169).

Additionally, subjects received feedback about how far from the appropriate interval they were off (in milliseconds, rounded to the nearest integer). This feedback would appear on the left or right side of the screen depending on whether the response was short or long, respectively. The text was in green font for correct responses and red for incorrect responses.

Production training itself was divided into three stages, in which the subject produced short referents only, long referents only, and then short and long referents inter-mixed. For training on the short trials only, the mean \pm the standard deviation of the subject's last 8 responses needed to be between the lower (LB_{short}) and upper (UB_{short}) bound (in seconds). The same calculation was performed for the long trials except the range was LB_{long} and UB_{long} . During the final part, in which trials were inter-mixed, these criteria were applied to short and long trials separately.

Subjects were placed into one of two groups. In one group, the 1v5 group, the subjects (10) were trained with a short referent that was 1 second in length and a long referent that was 5 seconds in length. For production training in this group, $LB_{short} = .6s$, $UB_{short} = 1.4s$, $LB_{long} = 3.75s$, and $UB_{long} = 6.25s$. In other words, the mean \pm the standard deviation on short production trials had to be between .6s and 1.4s over the last 8 responses, whereas the mean \pm the standard deviation on long production trials had to be between 3.75s and 6.25s. In the other group, the 2v4 group, subjects (10) were trained with a short referent that was 2 seconds and the long referent that was 4 seconds. For production training in this group, $LB_{short} = 1.5s$, $UB_{short} = 2.5s$, $LB_{long} = 3s$, and $UB_{long} = 5s$. The subjects were never explicitly told which group they were in nor what the length of the referent stimuli were.

Experimental Testing

After passing training, subjects were told they would be asked to "1. CLASSIFY the sample interval (based on whether it's closer to the short or long target interval) or 2. PRODUCE the short interval, long interval or MIDPOINT between them" during testing. All subjects performed a novel task called the "Bisection by Classification and Production" (BiCaP).

This task combines a prototypical classification task (133, 134) with novel aspects. For the classification component, subjects were required to classify a probe duration as either short or long (by left- or right-clicking, respectively). The novel aspect of the task, the production component, required subjects to produce the short referent, the long referent, or the midpoint between them (by left-clicking to start and stop the interval). Note that while subjects produced the long and short referents during training, they were required to produce a third interval, the midpoint, during testing. Trial types were indicated at the top of the screen. For classification trials, the instruction was “CLASSIFY” whereas for the production trials the instruction was “PRODUCE SHORT”, “PRODUCE LONG”, or “PRODUCE MIDPOINT”. No feedback was provided during testing.

Stimuli

The stimuli were blue ovals (122 x 73 pixels) that appeared at the center of a white background (1220 x 730 pixels). The duration that the blue interval appeared on the screen constituted the length of the interval. On classification trials, the subject could left or right-click after the stimulus had ended. On production trials, a blue oval would appear upon clicking to start the interval and would disappear upon clicking to end the interval.

During training, only short and long referents were displayed. On each trial, the probability of receiving a short or long referent (or being asked to produce the short or long referent in the third stage of production training) was equal. During testing, many probe durations were displayed. For the 2v4 group, the probe durations used were {2.0, 2.33, 2.66, 3.0, 3.33, 3.66, 4.0} and for the 1v5 group, the probe durations were {1.00, 1.67, 2.33, 3.00, 3.67, 4.33, 5.00} (i.e. 7 linearly spaced intervals between the short and long referent,

inclusive). In all, 110 trials were performed by each subject during testing. A block structure was used in which each block consisted of 11 trials and there were ten blocks per session. A block consisted of 7 classification trials (one of each probe duration), 2 midpoint production trials, and 2 referent production trials (1 short and 1 long). Within a block, the presentation order was random.

3.5.4 Analysis of classification

To analyze classification data, we numerically fit a psychometric function for the probability that an interval t is labeled as closer to “long” by the generalized logistic function shown below

$$p(\text{"long"}) = \frac{p_3 - p_4}{1 + e^{-\frac{(t-p_2)}{p_1}}} + p_4$$

where p_1 , p_2 , p_3 and p_4 represent free-fit parameters. Once the best fit parameters were obtained using non-linear regression, the bisection point (the duration for which $p(\text{"long"})=0.5$) was calculated as

$$Bis = p_2 - p_1 \log\left(\frac{p_3 - 0.5}{0.5 - p_4}\right)$$

The Weber fraction was measured the difference limen, which is defined as half the difference in the durations corresponding to $p(\text{"long"})=0.75$ and $p(\text{"long"})=0.25$, divided by the bisection point. This is shown below

$$Error = \frac{p_1}{2} \left(\log\left(\frac{p_3 - 0.25}{0.25 - p_4} \cdot \frac{0.75 - p_4}{p_3 - 0.75}\right) \right)$$

The sensory Weber fraction was calculated as the ratio between the error and bisection point.

In order to calculate the 95% confidence intervals, we used bootstrapping. This was performed for 1000 runs by randomly drawing different trials with replacement and calculating the resultant Weber fraction for each run. The 95% confidence intervals were measured from this sampling distribution.

To test whether the slopes of covariation between the bias-corrected arithmetic mean (i.e. the mean of the produced short and long referent intervals) with respect to production bisection point and classification bisection point were significantly different, we used bootstrapping. For each bootstrap, we randomly selected subjects with replacement and calculated the difference in these slopes. This procedure was repeated 2,000 times to obtain a two-tailed p value for whether the sampling distribution of the difference in slopes was significant. To look for within-subject evidence of memory bias in the production bisection point, we divided the data from each subject's session into 10 equal blocks of 11 trials each (which was the experimentally imposed block length). For each block we averaged the two midpoint productions and computed the mean of the short and long referent productions. We then regressed the averaged midpoint against the mean of the referent productions per block and obtained the slope of regression for each subject. The mean of the slopes across subjects within the 1s/5s or 2s/4s cohort was compared to a null distribution of slopes from each cohort. The null distribution was created by randomly shuffling the data within a subject's session, computing the slope of regression for each subject, and taking the average of the slopes from each subject. This procedure

was repeated 1,000 times to obtain a two-tailed p value for whether the average of the slopes across subjects within each cohort was significantly different from the mean of the null distribution.

3.6 Discussion

Considering the effect of memory bias on the bisection point location is critical as different theoretical accounts of timing make different predictions about where it lies (50). Theories that hypothesize a linear mapping between real time and subjectively represented time, and assume a difference rule in comparing a probe duration to each of the referents, predict that the bisection point lies at the arithmetic mean (133). Scalar timing theory, which favors a ratio rule for comparing a probe duration to each referent, predicts that the bisection point lies instead at the geometric mean (134). Still other theories, which perhaps best accord with the preponderance of the behavioral data, predict that the bisection point location will vary, based on task parameters and subjective statistics, all the way from the arithmetic mean down to the harmonic mean (71, 135, 136). Given the importance of the bisection point location to these theories, it is critical to account for the sources of bias in measuring the bisection point.

We sought to measure the memory bias in bisection point location by employing both temporal classification and production methods. While several studies have examined the similarities and differences between temporal classification and production (163, 170), the “Bisection by Classification and Production” (BiCaP) task we used is unique in that these methods are employed simultaneously (by interleaving different trial types within a single session). Using this method, we were able to directly address whether memory biases can affect the location of the bisection point. Indeed, we found that the bias-corrected arithmetic mean, calculated from the mean produced time of the short and long referents, co-varied with the classification bisection point (Figure 12, column 1). We also found co-

variation with the production bisection point (Figure 12, column 2). While we found significant co-variation between the bias-corrected arithmetic mean and the production bisection point within the 1/5s and 2/4s groups separately, we did not observe the same within each group for the classification bisection point. Perhaps the bias-corrected arithmetic mean is not as predictive of the classification bisection point location as it is derived from production trials, and, consequently, higher power would be needed to reveal significance within these groups. We also found evidence for within-subject co-variation between the production bisection point and the mean of the remembered referents across the session (Figure 13). Taken together, we show that considering memory bias of the referents helps account for the variability in the bisection point observed on both classification and production trials. Such bias is difficult to directly measure in prototypical classification tasks in which only data about the bisection point (both its location and associated CV) is obtained.

An alternative explanation of our findings is that the observed biases are attributable to clock speed changes. This interpretation is challenged by the fact that we do not observe biases in production of the one second reference duration whereas we do observe a large bias for production of the five second duration. It is possible, however, that this differential observation is due to the fact that different mechanisms may underlie sub- and supra-second timing (171). To further address this question, we looked at whether a clock speed interpretation could apply to the 2/4s group. If clock speed is accounting for the observed effects, then we might expect to find a change in produced times of the reference durations from training to testing. Assuming the clock speed changes were linear, we should expect to see a proportional change for the short reference duration as the long reference duration

(which in this case, are 2 and 4 seconds, respectively). To test this, we performed a two-sided Wilcoxon signed rank test and found that the medians of the ratios for the 2s duration (that is, the ratio of the production duration during testing to the duration during training) were significantly different from those of the 4s duration ($p = .0039$). We repeated this for the 1/5s group and, not surprisingly, found that the medians were again significantly different ($p = .0059$). This suggests that our effects are not attributable to linear variations in clock speed. It is difficult, of course, to rule out the possibility that some arbitrary non-linear clock speed variation may account for our effects, but a linear relationship in commonly assumed is pacemaker-accumulator models (60).

Importantly, prior work has studied the effects of reference memory and found no effect on time perception (158, 172, 173). Allan and Gerhardt directly addressed this issue by comparing the prototypical bisection task to a “roving-referents” task (159, 160), in which new referents are shown prior to every trial and the subjects must determine whether a probe interval is more similar to the first or second referent. In this study, no difference was observed between the prototypical task and the roving referents version of the task. One explanation for this conflicting result is that this study was performed in the sub-second range with intervals that spanned 400 to 750ms. As mentioned above, many empirical findings suggest that there is a perceptual dichotomy between sub- and supra-second timing (171) and it has been shown that different brain regions are engaged in sub and supra-second timing tasks (174). Consequently, it is possible that memory biases are much smaller in the sub-second range where the interval storage may be more accurate. In addition, the ratios of the reference durations used in that study were all less than the ratios used here (five for the 1/5s group and two for the 2/4s group). Since errors in time

perception are known to grow with the duration of the intervals to be timed (Gibbon, 1977), we reason that errors in temporal memory may grow with the length of the intervals to be remembered and, consequently, memory biases in the bisection point may be larger for higher reference durations. Given our finding, it would be interesting in the future to administer the BiCaP task using reference durations in the sub-second range.

In addition to directly addressing the contribution of memory bias to the measurement of the bisection point, the results from the BiCaP task also afforded the opportunity to look at whether production and classification rely on common timing mechanisms, a question which has been elegantly addressed in prior work (163, 170, 175–177). We were able to build on this body of work in several ways. First, whereas most previous studies have relied on comparisons across different experimental blocks, the BiCaP task involves comparisons among trial types within a single session. This approach may, therefore, better control for state effects, thereby decreasing the likelihood that subjects rely on short-term muscle memory to guide performance in production trials. It should be noted, however, that inter-mixing these trial types may affect the performance on each type. As it is known, for instance, that the order of reference duration presentation can affect the bisection location (158), it is possible that the presence of a classification trial or a short reference production could affect, say, a midpoint production. It would be informative, therefore, to see how these results vary when trial-type blocks are used. Second, several of these studies have used rhythmic tapping tasks, in which the subject must produce periodic and repetitive movements, as a basis for comparison to classification. We chose a different approach as the motor movements themselves in tapping tasks contribute a large source of variability in the responses (176, 178). Third, while most previous human studies have focused on the

sub-second range, we were interested in the seconds range of temporal perception. Using this method, we found that the bisection point derived from production and classification trials could not be distinguished (Figure 12, column 3). This lends support to the hypothesis that these distinct methods share at least partially overlapping timing mechanisms (163, 170, 175).

We sought to address not only whether production and perception relied on similar timing mechanisms, but also what the nature of these mechanisms might be. By using two sets of referent probes (1/5s and 2/4s) we were better able to address this question as the location of the bisection point derived from classification has been shown to vary with the ratio of the referents used (50, 139). A meta-analysis showed that the bisection point will tend to be nearer the arithmetic mean for referent ratios exceeding 4 and be nearer the geometric mean for ratios lower than 2 (136). Our reference sets spanned this range (ratio of 5 for the 1/5s and ratio of 2 for 2/4s group) so we were able to investigate this question. Interestingly, the raw bisection points for classification and production clearly did not accord with this trend and, in fact, were not consistent with any known model (50). The fact that our raw bisection points do not accord with that of Wearden and Ferrara (1996) and others may be due to the fact that they use interval durations that are approximately an order of magnitude smaller; as it is known that different timing mechanisms are engaged for sub- and supra-second timing, (7) the memory bias may not be as large a factor in this temporal regime. However, when we looked at the location of the bisection points with respect to bias-corrected measures of the arithmetic (Figure 14, green lines) and geometric (Figure 14, blue lines) means, we found significant evidence that the production bisection point followed this trend (though the classification data was likely underpowered to address this

question). It is important to note, however, that the presence of the one second reference duration, which may engage multiple timing mechanisms as mentioned above, may affect the comparison between the 1/5s and 2/4s groups. It is also important to note that, in addition to the reference duration ratio, the bisection point location can also be affected by the probe spacing and the presence of feedback. Here, we chose a linear probe spacing which, compared to logarithmic spacing, has been shown to push the bisection point closer to the arithmetic mean in human subjects (136, 141). Therefore, it is possible that the bisection points in this study, which tended to be higher than the arithmetic mean, would have been pushed lower by a non-linear probe spacing. In addition, it is likely that the presence of feedback (similar to that used in training) on some fraction of trials would have yielded more veridical timing.

One aspect of our data violates a long-held tenet of time perception—scalar timing. Specifically, scalar expectancy theory predicts that as the standard deviation in temporal estimation grows with the temporal magnitude to be estimated (57). Although scalar timing is commonly cited as a fundamental feature of time perception, there are many examples in which it is violated (168, 179). Our data adds to these examples, as Weber’s law was violated for production trials in that the CVs of the production for the short, long, and midpoint intervals were significantly different in the 1/5s group. A potentially trivial explanation for this result is that the subjects were trained much more extensively on the referent intervals than on the midpoint intervals (which they were required to produce *de novo*, without any feedback, during testing). This does not explain why our results were consistent with Weber’s law in the 2/4s group, however. Another explanation, alluded to above, is that the one second reference duration engages another timing mechanism from

that engaged by the reference durations in the supra-second range. Interestingly, we did find evidence that the CV is inversely related to the bisection point on production trials in the 1/5s group (slope = -8.53, $p = .0042$, $R^2 = .6627$), as predicted by some theoretical accounts of timing (71, 137). This relationship was not significant for classification trials or for the 2/4s group.

In sum, we have shown evidence that memory bias can account for variation in the location of the bisection point for both classification and production. In addition, by interleaving these trial types, we were able to simultaneously measure the classification and production bisection points and found that they were not significantly different, suggesting that these tasks rely on at least partially overlapping timing mechanisms. Using bias-corrected measures we were able to recapitulate some previously reported effects of the referent ratio on the bisection point, which non-corrected measures could not explain. These results suggest that it is important to consider memory bias in timing and design future experiments to measure its effects.

Author Contributions

Joshua M. Levy, Vijay M.K. Namboodiri, and Marshall G. Hussain Shuler conceived of the study. Joshua M. Levy designed the code for the data collection. Vijay M.K. Namboodiri and Joshua M. Levy performed the analyses. Joshua M. Levy wrote the manuscript with help from Vijay M.K. Namboodiri and Marshall G. Hussain Shuler. Joshua M. Levy and Vijay M.K. Namboodiri contributed equally to this work. The listing of first author was determined by a coin flip.

Chapter 4. Interval evaluation and spatial foraging patterns

Abstract

Understanding the exploration patterns of foragers in the wild provides fundamental insight into animal behavior. Recent experimental evidence has demonstrated that path lengths (distances between consecutive turns) taken by foragers are well fit by a power-law distribution. Numerous theoretical contributions have posited that “Lévy random walks”—which can produce power-law path length distributions—are optimal for memoryless agents searching a sparse reward landscape. It is unclear, however, whether such a strategy is efficient for cognitively complex agents, from wild animals to humans. Here, we developed a model to explain the emergence of apparent power-law path length distributions in animals that can learn about their environments. In our model, the agent’s goal during search is to build an internal model of the distribution of rewards in space that takes into account the cost of time to reach distant locations (i.e. temporally discounting rewards). For an agent with such a goal, we find that an optimal model of exploration in fact produces hyperbolic path lengths, which are well-approximated by power laws. We then provide support for our model by showing that humans in a laboratory spatial exploration task search space systematically and modify their search patterns under a cost of time. In addition, we find that path length distributions in a large dataset obtained from free-ranging marine vertebrates are well described by our hyperbolic model. Thus, we provide a general theoretical framework for understanding spatial exploration patterns of

cognitively complex foragers through the lens of temporal discounting and interval evaluation.

4.1 Introduction

Understanding the movement patterns of wild animals is a fundamental question in ecology with implications for wildlife conservation. It has recently been hypothesized that random search patterns known as Lévy walks are optimal and underlie the observed power-law movement patterns of wild foragers. However, as Lévy walk models assume that foragers do not learn from experience, they may not apply generally to cognitive animals. Here, we present a novel decision-theoretic framework wherein animals attempting to optimally learn from their environments will show near-power law distributed path lengths due to temporal discounting (where the value of a reward diminishes with the delay in its receipt). We then provide experimental support for this framework in human exploration in a controlled laboratory setting and in animal foraging in the wild.

Lévy walks are a special kind of random walk whose path lengths form a power law distribution at their asymptotic limit (x): $p(x) \propto x^{-\mu}$; $1 < \mu < 3$; $x > x_{\min}$ (180–183). Numerous recent papers have demonstrated that foraging animals in the wild or under controlled conditions show path lengths consistent with power laws (74, 184–189), which are proposed to arise from an underlying Lévy walk process. Theoretical models have demonstrated that such a process can be optimal for memoryless agents searching for randomly distributed rewards across space under certain conditions (76, 180, 181). Together, these findings have led to the Lévy flight foraging hypothesis which states that such search patterns have arisen due to their evolutionary advantage (181, 182) However, since many animals, including humans, are cognitively complex and can learn from their environments, it is important to address whether such heavy-tailed path lengths are optimal

even for cognitively complex agents (05). The question of how memory influences foraging patterns has been approached in some contexts (190–193) but has not yet been sufficiently addressed (77, 194–196).

Because power-law path lengths have been observed in sparse and dynamic environments (e.g. open ocean), in which foragers rarely revisited previously rewarded locations (187, 188, 197, 198), it is reasonable to assume, as foundational models have, that there is little advantage to learning about the reward distributions at any given spatial location. Hence, under this assumption, prior studies constrained the class of models studied to random searches in the absence of learning. However, despite the fact that remembering spatial locations in environments such as open oceans may not be advantageous, it is widely believed that many ecological parameters, including prey distributions, show high degrees of spatial autocorrelation (199, 200). Moreover, it has been found that these distributions can exist as hierarchies, wherein large, global spatial structures comprise smaller, more local structures, and, that predators potentially learn these mean scales in the spatial distribution of prey (199, 200). Therefore, given the existence of patterns in the distribution of prey in relative space, it may be advantageous for predators to build representations, or models, of these patterns as opposed to performing purely random searches (05a,b). In this paper, we show that in order to optimally learn the reward distribution across relative spatial scales in the service of future reward rate maximization, foragers would produce approximate power-law path lengths, resembling Lévy walks.

Aim: optimally search for randomly distributed rewards in space

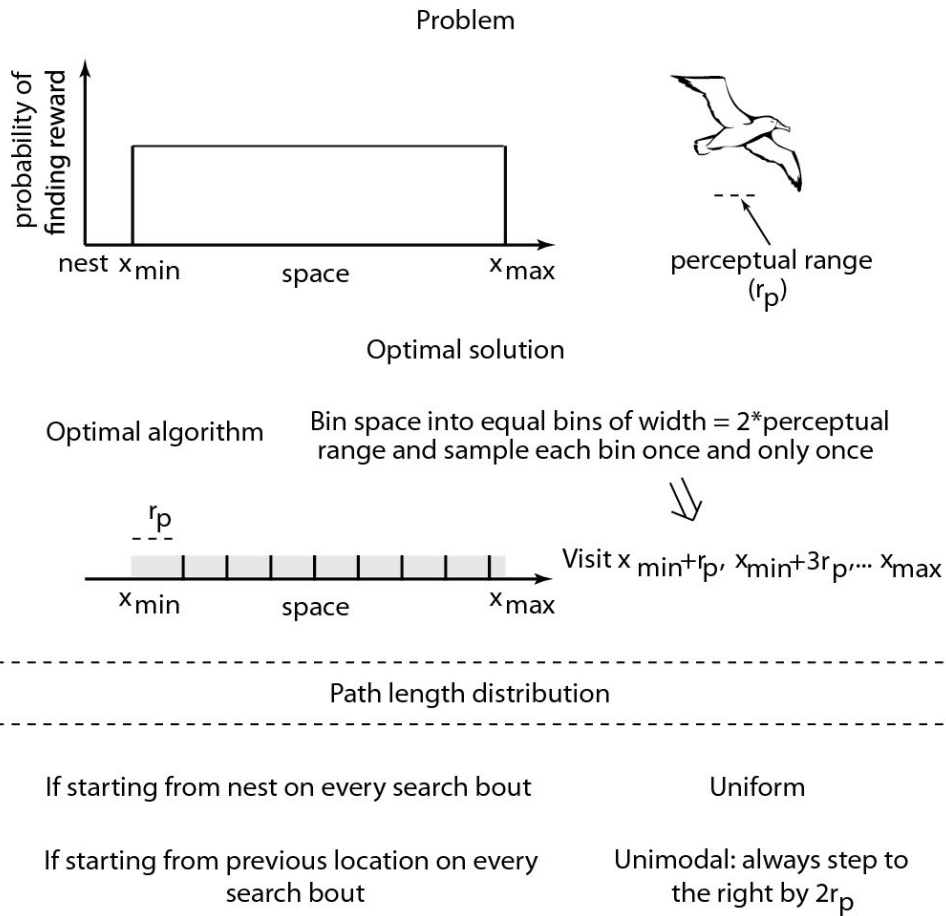


Figure 15 *Optimal search of a bounded area containing reward by a forager with spatial memory*

A forager with spatial memory searches a bounded area containing uniformly distributed rewards. The optimal solution, assuming that the forager has a limited perceptual range, is to tessellate the search region into bins defined by the perceptual range so that every location in the search space can be sensed by single visits to the locations $x_{\min} + r_p$, $x_{\min} + 3r_p$, $x_{\min} + 5r_p$, ... x_{\max} . If the forager has no spatial memory and hence cannot remember which location it visited on the previous search bout, it will be suboptimal.

4.2 Results: Optimal foraging under temporal constraints

How might foragers build a model of the relative spacing between food items? Consider the foraging behavior of albatrosses, for instance. A straightforward solution is to build a model of rewards obtained as a function of distance flown on each step (16c). Since the speed of movement during searching is often nearly constant for many foragers (e.g. 8, 16), this model can also be built with respect to the time flown on each step. The question faced by the forager then becomes how to sample different step lengths so as to maximize the ability to detect differences in reward distributions associated with each step length. However, foragers do not treat the same reward available at different delays equally: the later the receipt of a reward, the less its subjective value (202, 203). In other words, the subjective value of a reward expected after a long flight is smaller than that of the same reward obtained immediately. Many behavioral experiments have shown that the cost of time associated with a delayed reward takes a specific functional form: that of a hyperbolic (for $\mu=1$) or hyperbolic-like (for $\mu\neq 1$) function (202–209), shown below,

$$SV(r,t) = rD(r,t) = \frac{r}{(1 + \frac{t}{c})^\mu} \quad (1)$$

where $SV(r,t)$ and $D(r,t)$ represent the subjective value and discounting function, respectively, of a reward of magnitude r delayed by a time t . c and μ represent parameters that measure the rate at which the value of a delayed reward is discounted. In light of such a cost of time, exploration of a given flight time ought to be done under consideration of its utility for future exploitation. Thus, the foragers must explore so as to maximize their

ability to discriminate *subjective value* (not reward) distributions associated with different step lengths.

Here, we show that in order to maximize the ability to discriminate the subjective value distributions associated with different step lengths, the forager has to sample each step length in proportion to the uncertainty in subjective value associated with that step length. This strategy makes intuitive sense since the higher the uncertainty associated with an option, the more it must be sampled to learn its properties. Such a strategy of exploring in proportion to uncertainty has previously been assumed to be an exploration heuristic (210). However, we show that it is in fact optimal for maximizing discriminability (Figure 16). For a forager that initiates exploration under a uniform prior (i.e. no *a-priori* assumption regarding the distribution of rewards), sampling in proportion to uncertainty in subjective value equates to sampling in proportion to the discounting function associated with a flight time. As previously mentioned, the discounting function over flight time is hyperbolic. Therefore, for constant speed, the discounting function for a path length is also hyperbolic. Thus, we predict that the path length distribution of a forager attempting to explore the reward distribution across relative space will be

$$p(x) \propto \frac{1}{\left(1 + \frac{x}{c}\right)^\mu}; \text{ or rearranging by a constant, } p(x) \propto \frac{1}{(c+x)^\mu} \quad (2)$$

This is similar in appearance to a power law, but differs due to the presence of an additive constant c . Consequently, while it decays asymptotically as a power law, it predicts a constant probability at low values. Further, note that any distribution that is consistent with a strict power law (e.g. prior observations of foraging patterns (74, 187, 188)) will

necessarily be consistent with the above distribution since the power law distribution is a special case of Equation 2 in which $c=0$. Since foragers might limit the range of their exploration to a bounded interval of step lengths (e.g. due to behavioral/environmental constraints), the above probability distribution would only be expected to hold in a truncated domain (between x_{min} and x_{max}) under exploration. Further, in reward dense environments, we propose that observed path lengths would reflect not just the intended path lengths shown in Equation 2, but also the truncation due to prey encounter, thus resulting in exponential path lengths (as has previously been shown (186); Figure 17).

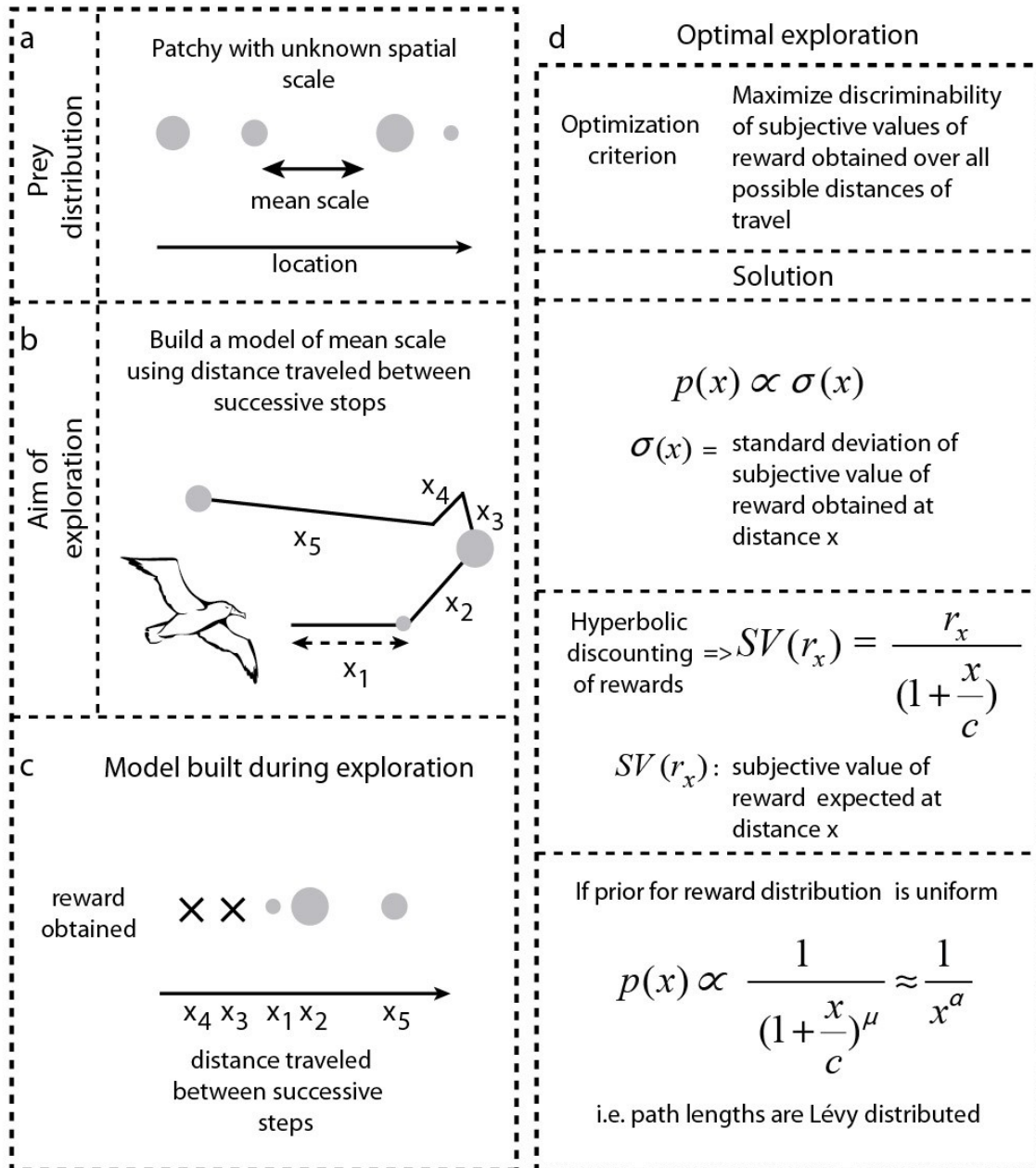
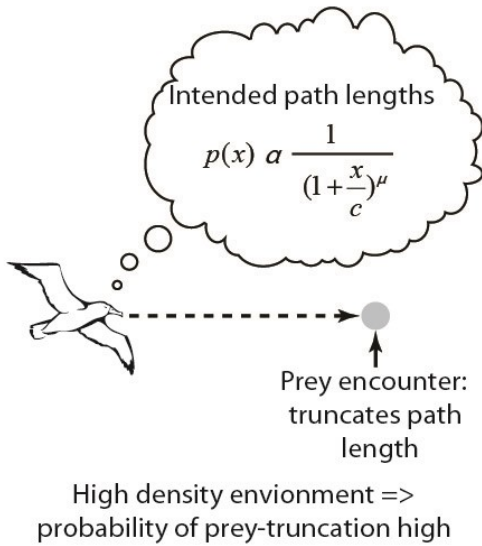


Figure 16 Model for adaptive benefits of apparent Lévy walks

a. The environments of foragers often show spatial autocorrelation with a mean spatial scale. Thus, it is likely that foragers attempt to build a model of the mean spatial scale by building a model of rewards obtained for different flight distances (**b & c**) (see text). **d.** An optimal model of exploration that maximizes discriminability requires foragers to sample

different flight distances (or durations) in proportion to the uncertainty in subjective value of rewards predicted at those distances. If the prior expectation of rewards is uniform, the sampling of different flight distances will produce a hyperbolic-like distribution—due to hyperbolic discounting—that can appear to be power law distributed.

a Environmental dependence of path lengths: truncation due to prey encounters



b Prey-truncated path lengths are exponential if prey is distributed uniformly

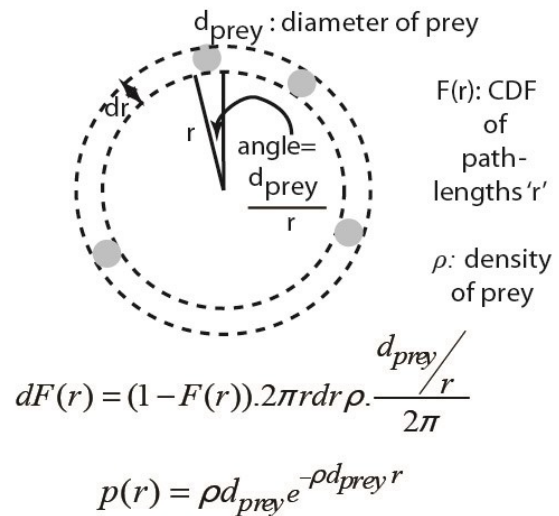


Figure 17 *Prey truncation leads to exponential path lengths when the density of food is high:*

Observed path lengths of foragers no longer reflect the intended path lengths when the distribution of prey is high due to prey-encounter truncation. The resultant path lengths can be shown to be exponential for a 2-D environment with randomly distributed prey.

4.3 Results: Human exploratory task

The model described above makes several predictions about search behavior of a cognitively-complex agent that we could test with humans in a controlled laboratory setting. Specifically, we sought to determine 1) whether humans search space in a random search pattern as expected from the Lévy walk model, or, in a systematic and deterministic way, and, 2) whether spatial search patterns are sensitive to the cost of time incurred in traversing the space. To test this, we designed a spatial exploration task for humans with and without the cost of time (Methods). In phase 1 (with a time cost) of this task, subjects could stop an image of a flying albatross in order to reveal a fish at a given spatial location. The goal of the subjects was to build a model of the distribution of fish as the knowledge acquired during this exploration phase could then be used on one exploitation trial to collect the largest fish possible. Crucially, flying longer distances across the screen took proportionally more time (the longest distance corresponded to waiting 10 seconds). Unknown to the subjects was that the distribution of fish sizes at any given location was uniform between fixed bounds. To test path lengths in the absence of a time-cost, we removed the distance-time relationship in phase 2 and allowed the subjects to explore by merely clicking a given location with a computer mouse. In other words, they no longer had to wait for the albatross to fly to that location.

We found that in both phases, the pattern of search was non-random. Subjects systematically explored the space by, for instance, undertaking longer and longer path lengths or undertaking shorter and shorter path lengths from the end of the screen (Figure 18b). Statistically, the probability of finding bouts of positive path length differences or

negative path length differences between consecutive paths was higher than chance in every subject for phase 2 ($p < 0.05$, runs test with Benjamini-Hochberg correction for multiple comparisons, $n=12$). For phase 1, the non-randomness in the search was statistically significant in 10 out of 12 subjects ($p < 0.05$, runs test with Benjamini-Hochberg correction for multiple comparisons). Thus, human spatial search in this random environment is not random. This conclusion is also bolstered by prior studies demonstrating that numerous animals remember spatial locations to produce non-random spatial search patterns in the wild (196, 211–217). We also found that the distribution of path lengths in phase 1 was significantly different from that in phase 2 (Figure 18c; $p < 0.001$, two-tailed two sample Kolmogorov Smirnov test) due to the cost of time, as predicted by our temporal discounting model. Thus, human data supports two key predictions of our model, viz. that spatial search by cognitively complex agents is systematic and non-random and that temporal discounting plays a fundamental role in the shaping of such search. These datasets are relatively small, however—as it is difficult to encourage human subjects to explore for long periods in a laboratory setting—and, therefore, are insufficient for model comparisons (though our model is consistent with the data). Therefore, to perform model comparisons, where a considerable amount of data is required, we turned to foraging data in the wild where, in some instances, thousands of path lengths have been recorded from individual animals.

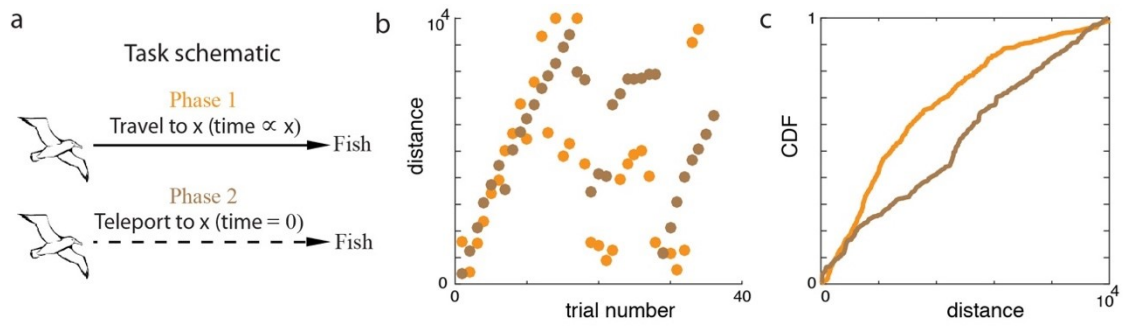


Figure 18 *Human spatial exploration task with and without temporal costs*

a. Schematic of the computer task (Methods): In phase 1, an albatross flies across the screen from a “nest” at a constant speed. Thus, the flight time is proportional to the distance flown. The farthest end of the ocean corresponds to ten seconds of flight time. In phase 2, subjects can make the albatross jump to a spot (i.e. teleport). Thus, flight time is independent of distance and is zero. **b.** Data from example subjects showing systematic search behavior across space. **c.** Raw CDF of the population data across subjects for phase 1 and phase 2 showing sensitivity of exploration to the cost of time.

4.4 Results: Path length distributions of wild animals are well-fit by a hyperbolic model

Given the preponderance of evidence that foraging path lengths are well-fit by the power law distribution (74, 184–187), the immediate question to be addressed is whether the hyperbolic distribution of path lengths expected from Equation **Error! Reference source not found.** can be well-described by a power law. Since the above distribution (and a power law) is defined in a bounded domain, we tested against a truncated power law (see Methods for details). We found that for random numbers generated using Equation **Error! Reference source not found.**, Akaike Information Criterion weights (w_{AIC}) overwhelmingly supports a truncated power law compared to a truncated exponential ($w_{AIC_{tp}}=1.000$ and $w_{AIC_{exp}}=0.000$) for all parameters tested (Figure 19a).

At this point, we wondered whether previously analyzed foraging data (187) may be well-explained by our model. For this analysis, we compared a hyperbolic model to a power law model, as the power law distribution was found to provide a good fit to the data (187) and is generally compared against the exponential distribution to assert the presence of Lévy walks (74, 76, 184–186, 188, 189). To be clear, we compared against the power law distribution, not the family of distributions which have power-law distributions at their asymptotic limits—to which a hyperbolic and power law model both belong. One important point to note here is that while a strict power-law distribution is a special case of the hyperbolic distribution, it is not trivially true that in a direct comparison between the two models, the data will be better fit by a hyperbolic distribution. Specifically, a

hyperbolic distribution will have a faster decay at large values and slower decay at small values when compared to the closest power law. Thus, for real data that are approximated by a power law (better than an exponential distribution), it may well be that the data is inconsistent with this specific prediction for a hyperbolic model. In such a case, the best fit hyperbolic model will reduce to the best fit power law and hence, model selection (by $wAIC$) would favor the pure power-law model over the hyperbolic model owing to fewer parameters.

Since differentiating between two highly similar distributions requires considerable statistical power, we limited our test to eight individual marine animals, comprising four blue sharks *Prionace glauca* (PG) and four basking sharks *Cetorhinus maximus* (CM), for which a substantial number of path lengths ($>10,000$) were recorded. The results for two individuals, blue sharks PG2 and PG4, are shown in Figure 19b and c, respectively. In both cases, the hyperbolic fit (cyan) provides an excellent fit to the data. Notably, the truncated power law fit is visually compelling for PG2 (Figure 19b) but not PG4 (Figure 19c). Indeed, individual PG2 represents a typical case where the fits are not easily distinguishable visually (as in the simulation in Figure 19a), but where the $wAIC$ overwhelmingly favors a hyperbolic model. Examining all individuals, we found that the hyperbolic model provided a superior explanation of the data when compared to power law and exponential models in all but one individual (Table 1). In this individual (CM3), the exponential model provided the best fit, potentially due to prey encounter-related truncation (186). In all other cases, the hyperbolic model was overwhelmingly favored ($wAIC=1.000$), except in PG3 where support was not as clear-cut ($wAIC=.708$). Hence, our theoretical model provides a superior fit to previously collected foraging data.

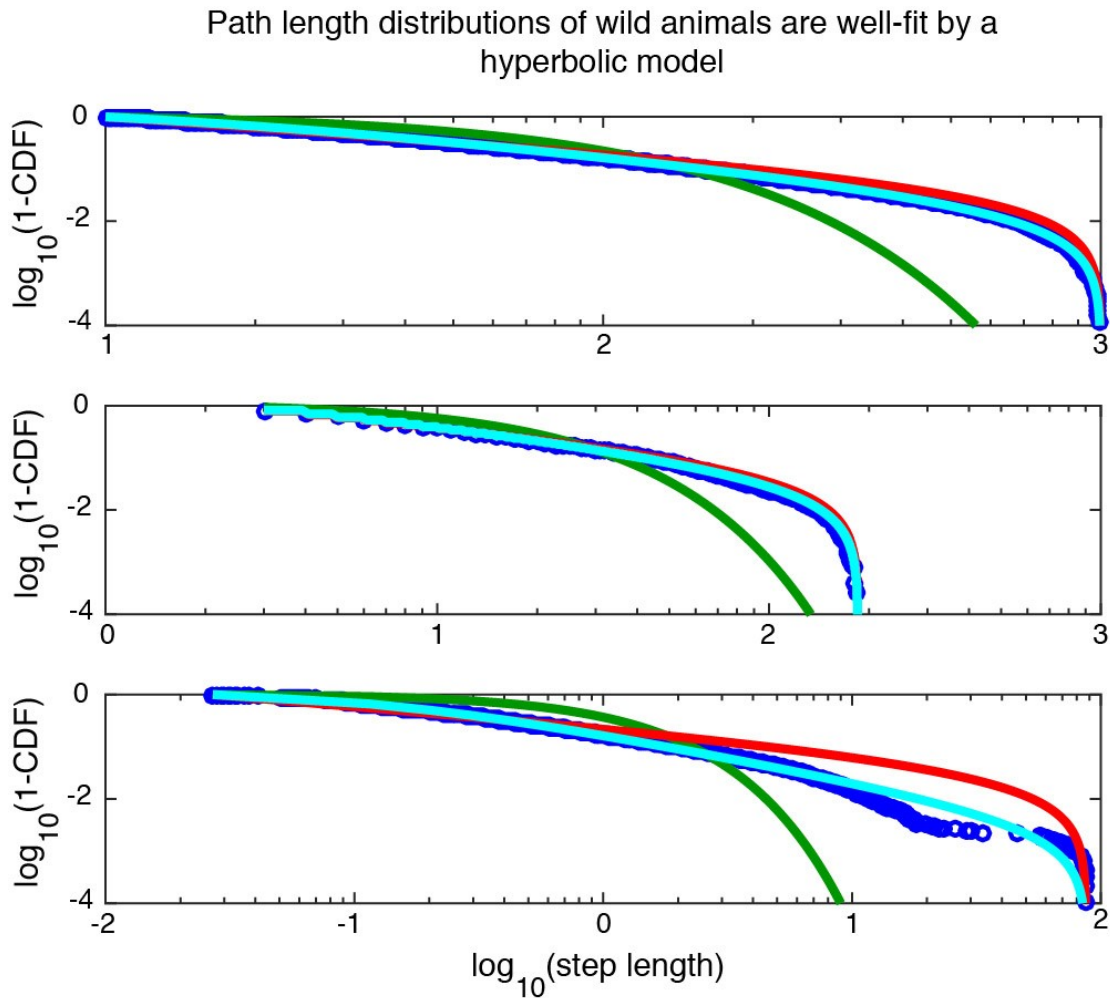


Figure 19 *Previously collected data from wild animals is well-fit by a hyperbolic model than a power law model*

a. Random data generated from a hyperbolic distribution (blue dots) can be well-approximated by a power law distribution (red), but not by an exponential distribution (green): 25000 random numbers were generated from a hyperbolic distribution (Equation 2; Methods) with truncation set to be between 10 and 1000. The best fit truncated power law describes the data significantly better than the best fit exponential ($wAIC_{tp}=1.000$ and $wAIC_{exp}=0.000$). **b.** Previously collected data (blue dots) that is well fit by a hyperbolic

model (cyan) and power law model (red), but not an exponential model (green). c. Data from a subject in which the hyperbolic model is considerably preferred to any alternative model.

	Type	x _{min}	x _{max}	μ _{pl}	μ _{hyp}	c _{hyp}	KS D statistic			wAIC		
							pl	hyp	exp	pl	hyp	exp
CM1	Disc	1	322	-1.19	-1.41	1.19	0.061	0.026	0.356	<10 ⁻⁶	1.000	<10 ⁻⁶
CM2	Disc	6	91	-2.07	-3.03	7.20	0.056	0.083	0.127	<10 ⁻⁶	1.000	<10 ⁻⁶
CM3	Disc	7	68	-1.49	-8	88.64	0.077	0.051	0.059	1×10 ⁻⁹¹	1×10 ⁻¹¹	1.000
CM4	Disc	7	63	-1.44	-1.79	4.25	0.015	0.007	0.061	2×10 ⁻⁴	1.000	<10 ⁻⁶
PG1	Disc	2	185	-2.10	-2.24	0.36	0.013	0.003	0.248	<10 ⁻⁶	1.000	<10 ⁻⁶
PG2	Disc	3	185	-1.63	-1.82	1.23	0.022	0.007	0.219	<10 ⁻⁶	1.000	<10 ⁻⁶
PG3	Disc	4	218	-1.70	-1.77	0.57	0.025	0.018	0.222	0.292	0.708	<10 ⁻⁶
PG4	Cont	0.027	87.3	-1.38	-1.90	0.13	0.150	0.031	0.376	<10 ⁻⁶	1.000	<10 ⁻⁶

Table 1 Results of fitting truncated power law (pl), truncated hyperbolic (hyp) and truncated exponential models to data previously collected from individual marine animals.

CM, basking shark; PG, blue shark. The first seven animals had quantized data (Type=Disc) that could be considered as resulting from a discrete probability distribution. For these animals, we divided the data by their common factor to get the discrete data (e.g. the first animal had unique observations 1,2,3,...,322). x_{min} and x_{max} represents the best fit truncation across all three distributions (Methods). The best fit parameters, goodness of fit (Kolmogorov-Smirnov D statistic), and relative quality of fit (wAIC) are shown.

4.5 Results: Optimal exploration with noisy temporal representations

In our model for foraging animals in the wild, we previously assumed perfect ability to estimate the time flown on a given step. Since we know that the error in estimating longer intervals is larger than that of smaller ones (218), we derived the optimal exploration model for the biologically realistic case in which time perception is subjective and noisy (Appendix). In this model, the sampling per bin of path length (or equivalently, real time) for maximizing discriminability of rewards associated with that path length will be determined by the degree of nonlinearity in time perception as different bins in subjective time are scaled differently depending on the non-linearity (Figure 20c). Theoretically, it has been proposed previously that the degree of non-linearity in time perception is directly related to the discounting function in subjective time (71) (Figure 20d, left). Consequently, we show—based on our prior theory of temporal perception and decision-making (71, 219–221)—that the optimal path length distribution would be

$$p(x) \propto \frac{1}{(vT_{ime} + x)^3} \quad (3)$$

Here, v is the speed of the animal. The term T_{ime} is the interval over which the past reward rate experienced by an animal is estimated so as to make appropriate intertemporal decisions that maximize reward rates (71, 219, 220). Importantly, this term governs the non-linearity of time perception and the steepness of temporal discounting (71, 219–221). Thus, the power-law that best approximates the above distribution would have an exponent determined by the non-linearity of time perception (20d).

It is important to note that the derivations mentioned above necessarily simplify the foraging problem faced by animals in the wild. For instance, one factor that we did not yet take into account is that animals might account for other sources of risk such as that resulting from competition in their exploratory model. In such a case, we show in the Appendix that the probability distribution of path length durations can be calculated as

$$p(t) \propto \frac{1}{(T_{ime} + t)^3 (1 + k\alpha r^\alpha t)^\alpha} \quad (2)$$

where k and α represent the magnitude of competition such that an increase in their values represent more competition and hence, shorter path lengths. r in Equation (2) can be thought of as the mean reward expected in an environment; the higher the mean reward expected, the larger the competition and shorter the path lengths. The asymptotic limit of Equation (2), for positive α , will have a power law exponent greater than 3 and hence, will be outside the Lévy range of exponents. However, in cases where the asymptotic limit cannot be reached, as is often the case in biology where path lengths are often truncated either by the physical world or potentially by some internal limit set by the forager, a best fit truncated power law will *appear* to have a lower exponent than the real generative process, with the apparent exponent lying between 0 and $3+1/\alpha$.

An even more complete model of animal movements would involve additional factors. Nevertheless, the simplified model presented here demonstrates that path lengths of foragers with spatial memory that build a map of their environment for future exploitation can be heavy-tailed and nearly power-law distributed.

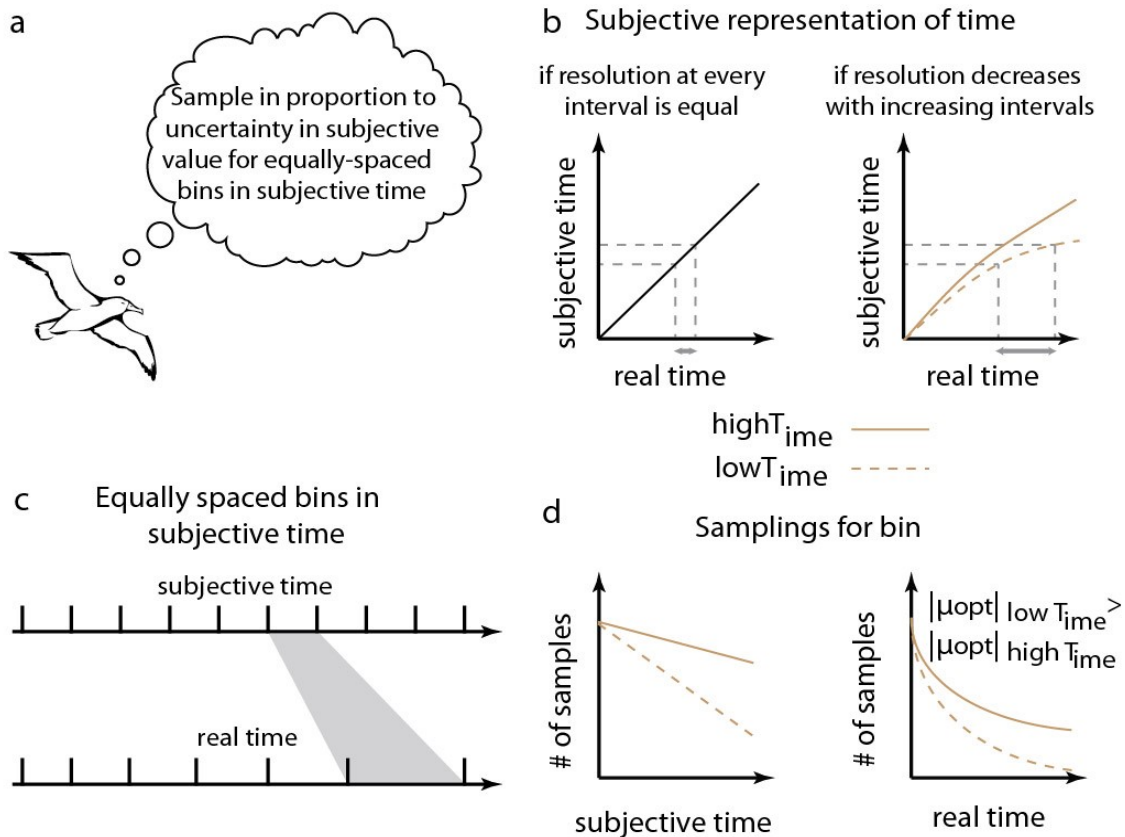


Figure 20 *Optimal exploration when temporal representations are noisy.*

a. Optimal algorithm for exploration. b. If temporal resolution is constant at every interval, subjective representation of time can be represented as a linear function of real time, with constant noise. However, it is known that errors in timing increase with the interval being timed (Buhusi and Meck, 2005b). In this case, subjective representation of time can be represented as a non-linear function with the non-linearity controlled by the parameter Time (Namboodiri et al., 2014a, 2014b, 2014c). c. When subjective representation of time is non-linear (concave), equal bins in subjective time correspond to bins of increasing width in real time. d. A theory of reward-rate maximization (Namboodiri et al., 2014a, 2014b, 2014c) predicts linear sampling for optimal exploration in subjective time, with the slope

determined by Time. In real time, this sampling becomes hyperbolic with its decay controlled by Time.

4.6 Materials and Methods

4.6.1 Experimental Design

Subjects

The 12 subjects that participated in this experiment were healthy individuals aged 22-35 recruited from Johns Hopkins University. All procedures were approved by the Institutional Review Board (IRB) and all subjects gave oral consent prior to the start of the experiment, as required by the IRB.

Exploration Task

We developed an exploration task for human subjects. Our task was divided into two phases. At the start of each trial in phase 1, an image of an albatross would begin flying (i.e. moving) from its “nest” left to right across the “sky” (i.e. light blue patch of screen). Subjects were instructed to stop the albatross at any point by clicking a mouse. When the albatross was stopped, it would instantaneously dive into the “water” (i.e. dark blue patch of screen) and an image of a fish would be revealed. Unknown to the subject, the size of the fish was drawn from a uniform distribution with five discrete outcomes. After the fish was displayed for 1 second, the albatross returned to its nest and immediately began to fly in the next trial.

In phase 1, it would take the albatross 10 seconds to fly the entire length of the screen. The speed of the albatross was constant and was 109 pixels per second. If the subject waited for the albatross to traverse the entire screen (i.e. waited 10 seconds), the albatross

automatically dove into the water and a fish was revealed. This only happened on rare occasions, however, as the subjects usually stopped the albatross well short of 10 seconds.

Prior to the start of phase 1, subjects were informed that they would have exactly 3 minutes to explore the region and “discover where the biggest fish swim.” They were also informed that at the end of the phase, they would be given just one chance to catch the largest fish they could and that their payout would be “determined exclusively by the size of the fish on this one trial” and not by the fish caught during exploration. In this way, the subjects were incentivized to explore the region.

Following phase 1, phase 2 began. In phase 2, the subjects were instructed that the albatross was flying over a different region of the ocean and, thus, they had to explore again to know where the biggest fish swim. The albatross remained in its nest until the subject clicked on a region of space (as indicated by a gray region that ran the length of the screen) to which it instantaneously teleported. Therefore, there was no time cost in exploring farther regions of space, as there was in phase 1. The instructions for phase 2 were similar to those for phase 1 except that subjects were informed that they had 1 minute to explore the region. This limit was imposed so that subjects would complete a similar number of trials in phase 1 and phase 2 (since trials in phase 2 are shorter as the albatross teleports rather than flies). Aesthetic changes (background color, fish image, and fish size) were made between phases to encourage exploration by underscoring the instruction that the environments in phase 1 and 2 were distinct.

Procedure

Subjects were placed in a quiet room in front of a 13-inch MacBook Pro. On-screen instructions were read aloud by the experimenter to ensure that the subject understood them. At the end of the experiment, subjects answered a questionnaire administered by the experimenter and were monetarily compensated for their participation.

Display

The experiment was controlled by custom-made code written in Java (JDK 6.0_65). The display was 1220 pixels wide and 730 pixels high. The area of the fish image (i.e. the size of the fish) was a random integer value between 1 and 5 scaled by a constant factor.

4.6.2 Animal foraging data

Blue ($n = 4$) and basking sharks ($n = 4$) were each fitted with a pressure-sensitive data logger that recorded an individual time series of depth measurements as the fish swam through the water column, as described previously (187). Raw depth measurements from loggers were converted into move step-lengths (the distance between consecutive turns) by calculating the vertical movement step (in m) between successive vertical changes in direction (from down to up and vice versa), as described previously (187).

4.6.3 Procedure to fit data

The general approach used here to test the appropriateness of different models is to 1) estimate the respective parameters using maximum likelihood estimation (MLE) for the *same* set of possible truncations across all models, 2) set the best truncation to that resulting in the lowest Kolmogorov-Smirnov (KS) D statistic across all models and all truncations, and 3) quantify relative likelihoods of models using Akaike Information Criterion (AIC).

The truncated hyperbolic-like distribution, shown in Equation (2), needed to be statistically characterized (Appendix). The truncated power law distribution is a particular example of a truncated hyperbolic distribution for $c=0$. To test whether data generated from this distribution can be mistaken for a power law distribution, we generated data using the following random number generator

$$t = \left[(t_{\min} + c)^{1-\mu} + \left\{ (t_{\max} + c)^{1-\mu} - (t_{\min} + c)^{1-\mu} \right\} u \right]^{\frac{1}{1-\mu}} - c$$

where t is the random variate following the truncated hyperbolic-like distribution, t_{\min} and t_{\max} are the minimum and maximum truncation limits, c and μ are the parameters of the distribution, and u is a uniform random variate. For the purpose of 0, t_{\min} was set at 10 and t_{\max} at 1000. The procedure for fitting and testing of power law, hyperbolic and exponential models is explained below.

We fit the data using three models: exponential, truncated power law, and truncated hyperbolic. As discussed in prior work^{1,2}, upper truncation is important for power law and hyperbolic models, but not exponential models, as such heavy-tailed models cannot last for an infinite domain in the real world. Additionally, a lower truncation is necessary for the power law model as it is not defined for a flight time of zero. Consequently, as done previously^{1,2}, we used a truncation for all the models tested. Unlike before, however, we did not tune the truncation parameters to each model. Rather, we tuned them across all models by picking the truncation that resulted in the lowest Kolmogorov Smirnov D-statistic across all models and all truncations. The different values of the truncation tested were as follows: for discrete data, the low truncation possibilities were set to 1, 2, ..., 7 and

the upper truncation to 80th , 84th,..., 100th percentiles of the unique observations in the data, whereas for continuous data, the possible options for the minimum truncation were set to 0th, 4th,..., 20th percentiles and the upper truncation was chosen from 80, 84, ...100 (percentile) for which at least 80% of the data was retained. Thus, if the lower truncation was set to 20th percentile, the upper truncation had to be the 100th percentile, whereas the possible upper truncations with a lower truncation of 16th percentile were 96th and 100th percentiles. Thus, truncation limits are not free-fitting parameters for each distribution that add cost to the AIC. The benefit of using this approach is that the exact same data is used for comparison across all the models, thus avoiding different domains of the probability distribution functions for the different distributions tested.

The ML estimate for the exponent in the truncated power law model was numerically calculated by solving Equation (16). Similarly, the ML estimate for c and μ for the truncated hyperbolic model was numerically calculated by solving equations (14) and (15) . Lastly, the ML estimate for the truncated exponential model was calculated by solving Equations (23) or (25).

We used AIC to compare the three models. Since the truncation parameters were set to be the same for all models, these were not counted as free-fit parameters in the calculation of AIC. Thus, the AIC for the different models were calculated as shown below (each AIC was calculated using the correction for small sample sizes, i.e. they were AICc). The numbers of free-fit parameters for the different models were: one for “tp”, one for “exp”, and, two for “hyp”.

$$AIC_p = 2 - 2\log(L_p) + \frac{4}{n-2} \quad (3)$$

$$AIC_{hyp} = 4 - 2\log(L_{hyp}) + \frac{12}{n-3} \quad (4)$$

$$AIC_{exp} = 2 - 2\log(L_{exp}) + \frac{4}{n-2} \quad (5)$$

4.7 Discussion

In this work, we first argued that even though natural environments of foragers are often highly stochastic such that remembering reward distributions associated with a specific location might not be useful, there still might be additional statistical regularities that cognitively complex foragers may exploit. Specifically, if foragers aim to build models of reward distribution across relative space, we showed that an optimal model of exploration would require sampling in proportion to the uncertainty of subjective value associated with a reward obtained after a given path length. Since it is often observed that the subjective value of rewards obtained after a delay is discounted hyperbolically with respect to the delay, we showed that the resultant path lengths would be hyperbolically distributed. In support of our model, we found that humans engaged in a laboratory exploration task searched space systematically and account for the cost of time in traversing space. Next, we showed that data generated from a hyperbolic distribution is better fit by a power law distribution than an exponential distribution and that previously collected data from foraging animals in the wild can be better explained by a hyperbolic model than a power law model. Additionally, we extended our model to show that for foragers in the wild with noisy temporal perception, the exponent of the best fit power law is governed by the non-linearity of time perception and the amount of competition faced from other foragers. Thus, we argue that search patterns in complex agents are unlikely to be purely random in situations where cognitive modeling is advantageous, and that approximate power-law path lengths emerge due to the temporal discounting of farther rewards. Hence, our model provides a novel and principled way of understanding search patterns and, thus, contributes to the ongoing discussion regarding the mechanistic origins of power-law path lengths in

foragers (222–233).

It is important to note that the human exploratory task presented here has superficial differences from the general model of exploration of relative space that was proposed earlier for foragers in the wild. The main difference is that while foragers in the wild were predicted to explore relative locations in space (i.e. locations relative to their current position), humans in this task are exploring absolute locations in space (i.e. locations relative to a fixed location). However, there is a fundamental equivalence between both cases in that exploration is performed with respect to the distance traveled on each search bout. In this sense, exploration of absolute space in one dimension is just a special case of exploration in relative space. Consequently, the discounting of rewards for future exploitation is defined with respect to the distance traveled during exploratory bouts in both cases. Thus, our laboratory task provides a test for the conceptual framework we developed here.

In the following section, we consider potential predicted deviations from the simplified model presented here. We presented a model for animal movements in the wild by assuming that animals are building a model of the subjective value of reward distributions across relative space. Our calculations would thus be expected to be true only when animals are in fact building such a model. Since animals would likely not spend their entire foraging time building such a model, in these cases, one must expect deviations from the hyperbolic distribution of path lengths predicted here. One such instance would be when animals are exploiting knowledge gained from the aforementioned exploration. If foragers realized that there is indeed a scale over which prey are distributed across space, they would fly these

distances under exploitation. Thus, for exploitation, one would predict unimodal distributions of path lengths if the foragers are flying an optimal distance. Another prediction of our framework would be that paths of foragers might show directional preferences. If there is anisotropic autocorrelation in the spatial distribution of prey, the foragers would likely also learn the optimal angle to travel. Thus, one would predict non-uniform spread of directions of travel.

Further, even when foragers are building a model of subjective value of reward distributions across relative space, our calculations have ignored complications such as models of risk associated, for instance, with competition from other foragers. These complications would introduce quantitative deviations from the simplified framework presented here (see Section 0). On a related note, it must also be pointed out that optimizing discriminability between all choices is not required to optimize the ability to pick the maximum reward in a static environment. However, since reward environments are rarely static, it is likely that animals evolved a mechanism to build models of the world appropriate for mapping the entire distribution of subjective values. Another caveat is in relation to the dimensionality of the environment to explore. Here, the assumption was that the dependence of interest to the animal is on the distance from the previous reward (i.e. autocorrelation). This results in a 1-D exploration problem irrespective of the dimensionality of the environment. Further, we have assumed radial symmetry in autocorrelation. Despite these caveats, our calculations illustrate how path lengths of foragers in the wild can be heavy-tailed, as experimentally observed.

Author contributions

V.M.K.N., J.M.L., S.M. and M.G.H.S were involved in the conceptualization of the theoretical contributions. V.M.K.N., J.M.L. and M.G.H.S. designed the experimental contribution. J.M.L. wrote the program for the experimental paradigm. D.W.S. provided previously collected foraging data in the wild. V.M.K.N. performed the analyses with help from J.M.L. and wrote the manuscript with help from J.M.L., S.M., D.W.S. and M.G.H.S. V.M.K.N. and J.M.L. contributed equally to this work.

Chapter 5. General discussion

In the previous chapters, we described elements of three key aspects of visually-guided timing: interval generation, storage and evaluation. In this chapter, we briefly summarize our findings, discuss their relationship to one another, and describe their implications for models of timing.

In Chapter 2, we found evidence for behaviorally-relevant interval generation at the earliest stage of cortical visual processing, the primary visual cortex (V1). Specifically, we found that reward-seeking timed behavior tracks distinct theta oscillation states in V1. During these states, both the behavioral precision and accuracy on the timing task was much improved, and the degree of improvement was largest when the oscillatory signal was spatially widespread. Importantly, the duration of these oscillations covaries with the timing of the reward-seeking action on a per trial basis. Surprisingly, using these LFP-defined states to separate single unit activity revealed otherwise unappreciated patterns of activity. We devised a strategy to capture these activity patterns using spikes trains alone and found that behavioral performance on the timing task improved during periods of high coherence. Finally, we found that the prevalence of these states covaried with the rate of experienced reward, thus linking them to motivation and the balance between exploration and exploitation. Together, these findings point to a behavioral role for theta oscillations in V1, and for interval generation even at the earliest level of sensory cortex.

In Chapter 3, we described drawbacks with current methods of measuring temporal storage, highlighting classification, in which subjects must assess whether a given interval is more

similar to a short or long reference interval. Specifically, we described the possible sources of noise in measuring the temporal bisection point, the sample interval at which subjects are equally likely to label an interval as “short” or “long”, and the implications its measurement has for theories of timing. One prominent source of bias in the bisection point may arise from noisy memory processes, as memory is a fundamental component of mechanistic models of time perception, and we therefore sought to directly measure memory biases by creating a novel task, “Bisection by Classification and Production” (BiCaP). Using this task, we found that the classification bisection point varied with the bias-corrected arithmetic mean (calculated from the mean produced time of the short and long reference intervals) and covaried with the production bisection point. In addition, we found evidence for within-subject covariation between the production bisection point and the mean of the remembered reference intervals across the session. Together, these findings suggest that memory bias can contribute to the variability in interval storage, thus highlighting the need to account for it in experimental measurements and theoretical models.

In Chapter 4, we discussed interval evaluation through the lens of studying how cognitively-complex foragers use temporal information to efficiently forage. We found that an agent who maximizes information about temporally-discounted outcomes will exhibit search patterns which are well-approximated by power-law path lengths (which have been extensively observed in nature (180–186), but are, in fact, hyperbolic. We test our model with data collected from humans engaged in a laboratory exploration task and animals foraging in the wild and find that key predictions of our model are supported, including that our hyperbolic model outperforms extant models in describing the data. We

also extend our model to the realistic case in which temporal estimates are subjective and noisy. Together, our results provide a compelling demonstration of how interval evaluation may impact complex decisions.

Though investigated independently, the aspects of timing investigated in each of these chapters are intimately related. In fact, in each chapter there are implicit references to the other aspects of timing. Though we focused on interval generation in Chapter 2, successfully accomplishing the task requires that the rodents store information about the interval (storage) and attach behavioral significance to it (evaluation). Though we focused on interval storage in Chapter 3, subjects also needed to generate intervals in order to produce them. Finally, though we focused on interval evaluation in Chapter 4, making optimal foraging decision requires that animals had experience with (generation) and stored prior intervals. This is not a coincidence: most real-world timing behaviors require these multiple aspects of timing.

This gives us hope that we can understand the multiple axes of interval timing, and rationalize our findings, within a unified framework. At a high level, our results support a view in which a behavioral arc proceeds sequentially from interval generation to storage to evaluation. First, given that timing-related theta oscillations are observed at even the earliest level of cortical processing, primary visual cortex (Chapter 2), they may be a common mechanism of interval generation. Second, since memory biases in interval production correlate with movements in classification measurements (Chapter 3), interval storage and generation are likely to rely on at least partially overlapping mechanisms. Lastly, complex evaluations take place on these stored intervals, as demonstrated by spatial

exploration patterns in foraging (Chapter 4). Thus, interval generation, storage, and evaluation may be explicitly connected.

At a finer resolution, we can assess whether our results are consistent with extant timing models, such as the influential Pacemaker-Accumulator model (58). In this model, a pacemaker outputs discrete ticks which are counted by an accumulator and, subsequently, sent to working and long-term memory. Temporal classification decisions are then made by comparing the interval in working memory with the reference interval stored in long-term-memory. Scalar Expectancy Theory (SET) (57) is the most commonly cited implementation of a PA model. Traditionally, the pacemaker in SET has been conceptualized as a centralized apparatus emitting Poisson-distributed pulses. Yet, this idea has fallen out of favor as evidence for such a pacemaker is lacking (234). On the other hand, many examples of emergent oscillatory activity have been found. Along this line, the type of oscillatory activity we observed in primary visual cortex (Chapter 2) would serve as an excellent pacemaker: its output is highly structured and consistent and offers a high signal-to-noise ratio. In fact, such oscillatory activity has been proposed as a pacemaker before (59). Our data also supports the notion of a distinct memory store for intervals; we found that biases in memory for specific durations could account for shifts in the temporal bisection point better than generalized shifts in clock-speed (Chapter 3). These memory effects could also be dissociated from an accumulator, as drift occurred even in the absence of new reference interval presentation. Such separation among the various components of the PA has also been supported by pharmacological studies showing a clear dissociation between effects on clock speed and memory (60). On the other hand,

it has been difficult to find a neural instantiation of the accumulator, leading some to question (for this and other reasons) the plausibility of the PA model (155, 234, 235).

Partially to address the shortcomings of the PA model, the Striatal Beat Frequency (SBF) model has been developed. In contrast to the PA model, it makes very concrete assumptions about the neural underpinnings of interval generation and storage. In the SBF model, a bank of cortical oscillators at different frequencies are synchronized (reset) at trial onset by dopaminergic projections from the Ventral Tegmental Area (VTA) and Substantia Nigra Pars Compacta (SNpc), and downstream neurons in the striatum listen to their output (66). These medium spiny neurons of the striatum act as coincidence detectors, comparing the pattern of activity across the cortical oscillators to the pattern they exhibited at the termination of a previously presented interval. (As others have pointed out, however, it is not entirely clear, how the comparison to the remembered pattern is performed (234)). It is biologically plausible that coincidence detection is subserved by medium spiny neurons of the striatum, as cortico-striatal loops are known to be a robust feature of neural processing. In addition, the type of time-related oscillatory activity we observed in V1 (Chapter 2) is more in-line with the SBF model than the PA model, as the SBF model has at its core the assumption that multiple cortical oscillators contribute to timing (7). The fact that we observe this activity at even the earliest stage of visual processing also adds weight to the proposition that time perception is a distributed feature of local circuits rather than the providence of a single, centralized clock.

While aspects of both the PA and SBF models are consistent with the data presented here, neither deals explicitly with interval evaluation—that is, the process by which these

temporal memories are used for atemporal decision-making. For such decision-making, these temporal memories must be translated into a currency of valuation. At a behavioral level, considerable evidence points to the fact humans and animals discount delayed rewards hyperbolically (67); such a discounting model was used to explain foraging patterns of wild animals and humans in Chapter 4. At a neural level, it has been suggested that Orbitofrontal Cortex (OFC) outputs a discounted subjective value signal, as most neurons within it fire more strongly to a reward delivered after a shorter delay (236) and lesions to it can result in less impulsive behavior (237). This region also seems to provide a prospective subjective value signal, as many neurons modulate their firing depending on whether a cue is predictive of a short or long delay (236, 238). (There has even been a popular proposal that the OFC translates a range of parameters into a common value currency (239–241), yet, contrary to this, it has been shown that storage of reward size and delay are dissociable (236)). The Ventral Tegmental Area (VTA) has also been implicated in prospective reporting of subjective value; these dopamine neurons have been found to respond more weakly for learned stimuli associated with more delayed rewards, according to a hyperbolic function (242). In humans, fMRI studies have also implicated the ventral striatum, medial prefrontal cortex, and posterior cingulate cortex in encoding the subjective value of delayed monetary rewards (243). It is important to note that these observations do not explain precisely how this translative computation to subjective value occurs, how it is used, or why it follows a hyperbolic function. Recent work has shed light on the latter question, suggesting that a hyperbolic-like function emerges if an agent is seeking to optimize its reward rate, given some particular constraints (71). This theory—known as TIMERR (for Training-Integrated Maximized Estimation of Reinforcement Rate)—also

accounts for the fundamental observation that the degree of discounting is context-specific and varies across and within individuals.

While this theory deals with the situation in which the agent already has complete information about its environment, it does not address how temporal information factors into decision-making when there is incomplete knowledge of the environment. We deal with such a situation in Chapter 4, and find that the hyperbolic path length distributions exhibited by foragers can be explained by a model which factors in the temporal discounts associated with searching distant regions. But what neural substrates might underlie generation of these path lengths? The answer probably involves a combination of regions, including hippocampal cells representing spatial information (244–246), prefrontal cortical cells involved in movement planning (247), and midbrain, striatal, and prefrontal neurons involved in temporal discounting (236, 242, 243). There has even been a suggestion that evidence for superdiffusive movement paths can be decoded directly from the neural dynamics within CA1 and motor neurons (246). Therefore, interval evaluation involves coordination of various, disparate brain regions.

Understanding the precise mechanistic underpinnings of interval generation, storage, and evaluation is important not only because it sheds light on normal brain function but also because it provides a window into pathological disease. Parkinson's disease, which is characterized by cell death in the Substantia Nigra Pars Compacta (SNpc), leading to a reduction in dopamine levels and concomitant ataxia, is a prime example of this. Indeed, dopamine is considered an important neurotransmitter in both PA and SBF models of timing (7) and depletion of dopamine levels in Parkinson's patients appears to affect interval timing: Parkinson's patients have a hard time keeping the timing associated with

two stimuli separate; in reproducing these intervals, they regress toward the mean of the two intervals (248). Further, these patients fail to exhibit the scalar timing property—the fundamental property in which the coefficient of variation (standard deviation/mean) is constant across the temporal range—when tested off their L-dopa medication. Very recently, a direct connection between dopamine and timing at the seconds range was observed through optogenetic manipulation of midbrain dopamine cells (249). Timing deficits in schizophrenic and severely depressed individuals have added weight to the hypothesis that dopamine depletion adversely impacts time perception (250). Patients with Huntington’s disease, a genetic disorder characterized by a mutation in the Huntington protein which leads to a degeneration of medium spiny neurons in the striatum early on in disease progression, have also exhibited deficits in time perception. For example, patients that are predicted to show imminent onset of the disease show hypoactivation of the putamen, thalamus, pre-SMA, and cingulate areas, and corresponding deficits in timing performance compared to healthy controls and patients where predicted disease onset will not occur for many years (251). This implicates dysfunction in the thalamo-cortico-striatal loop, which is relevant in both PA and SBF timing models, in timing impairments in Huntington’s patients. This connection is bolstered by the finding that there is hypoactivity in the putamen, thalamus, and medial prefrontal cortex of schizophrenic patients exhibiting impaired duration discrimination (252). Finally, diseases which principally affect short-term memory, such as Alzheimer’s disease, have also been linked to impairments in time perception (253). Together, these observations provide insight into the fundamental mechanisms of timing and, simultaneously, help us better understand what goes awry in these pathological illnesses.

In this thesis, we have attempted to relate our findings to cohesive frameworks of timing and time perception. It is important to note, however, that we have neglected several forms of timing. This raises the question: are the myriad forms of timing reconcilable into a single, comprehensive framework? At the macro scale, circadian rhythms govern our biological clocks, and rely heavily on the superchiasmatic nucleus in the hypothalamus. Given that disruptions of circadian rhythms in mice have no observable effect on interval timing, it seems that these processes are orthogonal (254). At the millisecond scale, motor timing guides our behavior (128) and research has suggested that it relies on different mechanisms from interval timing in the seconds range (6). Indeed, whereas lesion studies have strongly implicated the cerebellum in millisecond timing (255) and maintaining balance (256, 257), it appears to not be necessary for interval timing (258, 259). Thus, it seems reasonable to develop distinct models for these different temporal regimes. At some point, however, perhaps in translating a cognitively-timed decision to a split-second subconsciously-timed action, these systems likely interact, and studying their intersection might be a fruitful line of future research.

Appendix

Derivations for optimal foraging under different constraints

As explained in the main text, we assume that animals are mapping out a distribution of subjective reward values across relative space (i.e. distances traveled). To this end, we assume that they maintain a constant speed and are mapping out the distribution of rewards against the time flown on each step length (Figure 16). The aim for such an exploration is to sample each option a given number of times to build a map of the reward distribution across relative space for future exploitation. Since it is known that the subjective value of a delayed reward decays systematically with respect to the delay (e.g. “which do you prefer: \$100 now or \$100 in a year?”), exploration of relative space should also consider the subjective value of a reward for a given flight time. In other words, the exploration of a given flight time must be done under consideration of its utility for future exploitation. We also assume that the search space for exploration is bounded by the forager to be between a minimum (t_{min}) and a maximum flight time (t_{max}). Note that we are using symbols for time here but they can easily be converted to distance as $time=distance/speed$. This conversion obviously applies to the case of constant speed, but also to the case where speed is variable, but independent of distance flown.

If there were no discounts (subjective value of a delayed reward divided by the subjective value of that reward when obtained immediately) associated with time and all flight times are expected to have the same reward distribution, the optimal manner to map out the reward-flight time relationship would be to sample all possible flight times equally and

note the corresponding reward amounts. Such a sampling strategy would lead to a uniform distribution of sample times between t_{min} and t_{max} .

However, when different time intervals have different associated discounts, the problem of optimal sampling becomes non-trivial. We first solve this problem for the simpler case of two possible flight time options (similar to the “two-armed bandit” problem), under the following assumptions:

- 1) As in our behavioral task, the environment is stationary such that the reward distribution associated with any option does not change in time.
- 2) The aim of exploration is to ascertain the optimal option for future exploitation.
- 3) The total number of trials to explore is fixed. The aim of the agent is to calculate how to sample the two different options while keeping the total number of trials fixed. This assumption will be relaxed later to also consider a) the case where the total time for exploration is fixed, and b) a case where the stopping of exploration has to be determined by the forager.
- 4) The agent has access to the standard error of the mean of an option after n samplings.

We first consider the case where total number of trials for exploration is fixed.

Total number of trials for exploration fixed

With the above assumptions, the problem faced by the agent is exactly the same as the problem faced in designing an optimal experiment so as to maximize one’s ability to distinguish between the mean of two distributions. The solution for the optimal experiment

design is to sample each option in such a way that the t-statistic between the two distributions can be maximized. Hence, for the agent trying to solve the optimal exploration problem, the task is to maximize the t-statistic between the subjective value distributions of the two options. Since the variances of the subjective values for the options will not be same owing to the multiplicative discounts, one has to use Welch's t-statistic for unequal variances (260), which is defined as:

$$t = \frac{\langle x_1 \rangle - \langle x_2 \rangle}{\sigma_d}$$

where x_i is the subjective value for option 'i', $\langle x \rangle$ denotes the expected value of x and σ_d refers to the standard error of the difference of means. Since the number of samplings of either option only affects σ_d , maximizing the t-statistic is the same as minimizing σ_d .

If the distributions of rewards for each option are independent and identical, with a standard deviation σ , σ_d —the standard error of the difference of subjective means of the two options—would be:

$$\sigma_d = \sigma \sqrt{\frac{d_1^2}{n_1} + \frac{d_2^2}{n_2}}$$

where d_1 and d_2 are the discounts associated with the two options, and n_1 and n_2 are the number of times the two options were sampled. Given that the total number of trials is constant (N), $n_2 = N - n_1$.

Minimizing σ_d is equivalent to minimizing the square of σ_d . At the minimum of the square of σ_d , the derivative of σ_d^2 with respect to n_1 will be zero. Therefore,

$$\frac{d(\sigma_d^2)}{dn_1} = \sigma^2 \left(-\frac{d_1^2}{n_1^2} + \frac{d_2^2}{(N - n_1)^2} \right) = 0$$

$$\Rightarrow \frac{n_1}{d_1} = \frac{n_2}{d_2}$$

The second derivative can be verified to be positive at this solution, showing that σ_d is indeed at its minimum for the above solution.

Hence, for a binary choice between options with independent and identically distributed (i.i.d) reward distributions but with different discounts, optimal exploration requires sampling in proportion to the discounts.

Next, we extend this analysis to the case of k options (“ k -armed bandits”), each having i.i.d reward distributions with different discounts, d_k . While it is hard to identify a single metric whose optimality can identify the option with the maximum subjective value, one can define the optimality metric as the sum of variances of the difference distributions for each distinct pair of options. Minimizing this metric will lead to maximum discriminability between all options. Hence, for the k -option case, we assume that the aim of the agent is to maximize the ability to distinguish between the subjective rewards of the k options. With this assumption, the agent has to minimize

$$\sigma_{net}^2 = \sum_{i < j} \sigma_d^{ij^2}$$

where σ_d^{ij} is the standard error of the difference of the expected subjective rewards of options i and j .

Expanding the expression on the RHS gives

$$\sigma_{net}^2 = \sigma^2 \left(\frac{d_1^2}{n_1} + \frac{d_2^2}{n_2} + \frac{d_1^2}{n_1} + \frac{d_3^2}{n_3} + \frac{d_1^2}{n_1} + \frac{d_4^2}{n_4} + \dots + \frac{d_1^2}{n_1} + \frac{d_k^2}{n_k} + \frac{d_2^2}{n_2} + \frac{d_3^2}{n_3} + \frac{d_2^2}{n_2} + \frac{d_4^2}{n_4} + \dots + \frac{d_2^2}{n_2} + \frac{d_k^2}{n_k} + \dots \right)$$

Collecting like terms,

$$\sigma_{net}^2 = \sigma^2 (k-1) \left(\sum_i \frac{d_i^2}{n_i} \right)$$

Since the total number of trials is constant, n_k can be written as $n_k = N - \sum_{i \neq k} n_i$.

At the minimum of σ_{net}^2 , its partial derivative with respect to any $n_{i, i < k}$ will be zero.

Therefore,

$$\frac{\partial \sigma_{net}^2}{\partial n_i} = \sigma^2 \left(-\frac{d_i^2}{n_i^2} + \frac{d_k^2}{(N - \sum_{j, j < k} n_j)^2} \right) = 0$$

$$\Rightarrow \frac{n_i}{d_i} = \frac{n_k}{d_k}, i < k$$

Hence, even in the k -option case between options with i.i.d reward distributions but with different discounts, optimal exploration requires sampling in proportion to the discounts.

It is important to point out that the optimal exploration requires sampling in proportion to the discounts only when comparing between options with i.i.d reward distributions. The general solution as we worked out for the case with different variances associated with the *real* values of each option is to sample in proportion to the estimated variance of the mean of the subjective values associated with that option ($n \propto d^2 \sigma^2 / n$). It is interesting to point out that a similar strategy, in which exploration of an option was proportional to uncertainty, was assumed for some previous studies of exploratory behavior in humans (210, 261).

Extending this to the continuous case, if we denote the probability of sampling the flight time t by $p(t)$ and substitute a hyperbolic or a hyperbolic-like (202) discounting function for $D(t)$, we get that for optimal exploration, assuming that flight time is proportional to distance traveled,

$$p(t) \propto \frac{1}{(c+t)^\mu}; t_{\min} < t < t_{\max} \quad (1)$$

where c and μ represent the two constants in the hyperbolic-like function. In other words, an optimal agent samples flight times in proportion to its hyperbolic-like discounting function. Equation (1) has been derived using the assumption that the bins in flight time (or relative spatial location) are linearly spaced. This in turn results from the assumption that the error in perception of time for each flight time is constant. This is an inaccurate assumption as it is known that errors in the representation of longer temporal intervals are larger. For such a case of noisy temporal representation, see Section 0.

Total time for exploration fixed

Now, we solve for optimal exploration when the total time for exploration is fixed. As before, the aim is to minimize σ_d^2 but under the constraint that $n_1 t_1 + n_2 t_2 = T$, where T is the total time available for exploration. Taking the derivative with respect to n_1 , we get

$$\frac{d(\sigma_d^2)}{dn_1} = \sigma^2 \left(-\frac{d_1^2}{n_1} + \frac{d_2^2}{\left(\frac{T - n_1 t_1}{t_2}\right)} \right)$$

Thus,

$$\frac{d(\sigma_d^2)}{dn_1} = \sigma^2 \left(-\frac{d_1^2}{n_1^2} + \frac{t_1 t_2 d_2^2}{(T - n_1 t_1)^2} \right)$$

Thus the minimum of σ_d^2 is when

$$\sigma^2 \left(-\frac{d_1^2}{n_1^2} + \frac{t_1 t_2 d_2^2}{(n_2 t_2)^2} \right) = 0$$

i.e.

$$\frac{n_1}{n_2} = \frac{d_1}{d_2} \sqrt{\frac{t_2}{t_1}}$$

For the case with k options, we have to minimize

$$\sigma_{net}^2 = \sigma^2 (k-1) \left(\sum_i \frac{d_i^2}{n_i} \right)$$

under the constraint $n_k = T - (n_1 t_1 + \dots + n_{k-1} t_{k-1})$. Taking the partial derivative with respect to any $n_{i < k}$, we get

$$\frac{\partial \sigma_{net}^2}{\partial n_i} = \frac{\partial}{\partial n_i} \sigma^2 \left(\frac{d_i^2}{n_i} + \frac{t_k d_k^2}{\left(T - \sum_{j, j < k} n_j t_j \right)} \right)$$

Setting the derivative to zero, we get

$$\sigma^2 \left(-\frac{d_i^2}{n_i^2} + \frac{t_i t_k d_k^2}{(n_k t_k)^2} \right) = 0$$

Thus,

$$\frac{n_i}{n_k} = \frac{d_i}{d_k} \sqrt{\frac{t_k}{t_i}}; i < k$$

Extending this to the continuous case, we get that when the total time for exploration is held constant, the probability of sampling a particular flight time must be

$$p(t) \propto \frac{1}{\sqrt{t}} \frac{1}{(c+t)^\mu}; t_{\min} < t < t_{\max} \quad (2)$$

It is important to mention the caveats associated with the above model for optimality. It is defined as an extension of the optimal experimental design concept wherein the only aim

of the forager is to maximize the ability to discriminate between the means of the subjective values for different flight times. That is, the forager is seeking to purely explore the environment without exploiting its knowledge. The optimality is thus defined by this constraint. The second caveat associated with the above model is that it is only a steady-state solution for optimality. In other words, it only says that *at the steady state*, the probability of sampling a given flight time is as expressed by Equations (1) and (2). It does not provide a dynamical solution and hence, does not predict how the sampling will develop with experience. For a discussion of this point, see Section 5. These equations also assume that every flight time is equally likely to contain the largest fish, i.e. that the prior is uniform.

Self-initiated stopping rule for exploration

With the above caveats in mind, we can now attempt to define a stopping rule for exploration. Such a rule would be useful when the exploration phase is not well-defined, as we assumed previously with fixed total samplings or fixed total time. A reasonable stopping rule can be defined as the moment when the net discriminability ($1/\sigma_{net}^2$) goes above a threshold. This threshold might represent the maximum resolution available to the agent. In other words, sampling beyond this point affords no benefit to the agent in terms of new information about *subjective value*. A caveat of the above statement is that in some cases, there might be no need to exploit even after this threshold has been met. For instance, the total time available for exploration to a forager could be much more than that needed to meet the maximum discriminability threshold. In this case, further exploration can be aimed at gaining more information about the rewards themselves. Under this framework,

if there is infinite time to explore (i.e. no opportunity to exploit any knowledge gained), the forager will start sampling uniformly within the bounded search region.

Mathematically, we can quantify the above mentioned stopping rule of maximum discriminability as the sampling when $\sigma_{net}^2 = \sigma_{stop}^2$. For this calculation, we assume that the forager is sampling each option in proportion to its uncertainty (or discount, assuming uniform prior). To calculate the sampling at the stoppage point, let us represent $n_i^{stop} = \beta d_i$. β can now be calculated as the value that satisfies

$$\sigma_{net}^2 = \sigma^2 (k-1) \left(\sum_i \frac{d_i^2}{n_i^{stop}} \right) = \sigma_{stop}^2$$

Substituting $n_i^{stop} = \beta d_i$, we get

$$\sigma^2 (k-1) \left(\sum_i \frac{d_i^2}{\beta d_i} \right) = \sigma_{stop}^2$$

Therefore,

$$\sigma^2 (k-1) \left(\frac{\sum_i d_i}{\beta} \right) = \sigma_{stop}^2$$

Or,

$$\beta = \frac{\sigma^2}{\sigma_{stop}^2} (k-1) \left(\sum_i d_i \right)$$

Thus,

$$n_i^{stop} = \frac{\sigma^2}{\sigma_{stop}^2} (k-1) d_i (\sum_i d_i) (3)$$

As mentioned previously, if there is no possibility to exploit even after the above threshold has been met, the sampling will then be directed towards gathering more information about the rewards themselves. In this case, the steady-state sampling will be uniform.

Exploration under noisy temporal estimation

In the prior sections, we have assumed that errors in the representation of time are constant for every flight time. This is, however, not true. Hence, the sampling of different flight times will be done linearly with respect to the subjective representation of those intervals (Figure 20), rather than their real time values (as was previously assumed). In a previous theory on intertemporal decision-making and time perception (71, 219), we showed that a decision-making algorithm that considers reward rate maximization over limited temporal interval (including a past interval over which reward rate is estimated as well as the expected interval to future reward) explains well-established observations in intertemporal decision-making and time perception. In our theory, the subjective value of a delayed reward was calculated as

$$SV(r,t) = \frac{r - a_{est}t}{1 + \frac{t}{T_{ime}}} (4)$$

where $SV(r,t)$ is the subjective value of a delayed reward of magnitude r and delay t , a_{est} is the experienced reward rate estimated over the duration T_{ime} (referred to as “past integration interval”). The above equation holds when the average reward rate estimated in the past is

assumed to not be available during the delay to the current reward, resulting in an opportunity cost of the delay. If such an opportunity cost is not present or accounted for, the numerator in Equation (4) will not contain the $a_{est}t$ term. We also showed that the subjective representation of the delay t can be represented by

$$ST(t) = \frac{t}{1 + \frac{t}{T_{ime}}} \quad (5)$$

The above equation represents approximate scalar timing (error in timing grows in proportion to interval being timed (218)) and thus takes into account noisy temporal estimation. It says that the representation of time is non-linear and that this non-linearity is controlled by the past integration interval, T_{ime} .

The subjective value of a delayed reward can be expressed in terms of the subjective representation of the delay as

$$SV(r, t) = r\left(1 - \frac{ST(t)}{T_{ime}}\right) - a_{est} ST(t)$$

Thus, the discounting of a delayed reward is linear with respect to the subjective representation of the delay. It also has two components: one is an explicit cost of time (the first term on the R.H.S) and the second is the opportunity cost of time, expressed in terms of the subjective representation of the delay (second term on the R.H.S).

For exploration, the aim is to sample intervals keeping in mind the explicit cost of time. Thus the subjective value considered during exploration will not include the opportunity cost term. Hence, for exploration,

$$SV(r, t) = r \left(1 - \frac{ST(t)}{T_{ime}} \right)$$

Thus, the discounting function in terms of subjective representation of time is expressed as

$$D(ST(t)) = \frac{SV(r, t)}{r} = \left(1 - \frac{ST(t)}{T_{ime}} \right)$$

As was mentioned previously, the sampling under exploration will be done in subjective time and not real time. Thus, the sampling probability of a flight time t can be expressed (similar to Equation (1)) as

$$p(ST(t)) \propto 1 - \frac{ST(t)}{T_{ime}} \quad (6)$$

The corresponding sampling in real time can then be calculated as

$$p(t) = p(ST(t)) \frac{dST(t)}{dt}$$

From Equation (5), $\frac{dST(t)}{dt} = \frac{1}{\left(1 + \frac{t}{T_{ime}}\right)^2}$ and from Equation (6), $p(ST(t)) \propto \frac{1}{\left(1 + \frac{t}{T_{ime}}\right)}$.

Thus,

$$p(t) \propto \frac{1}{\left(1 + \frac{t}{T_{ime}}\right)^3} \quad (7)$$

Or equivalently,

$$p(t) \propto \frac{1}{(T_{ime} + t)^3} \quad (8)$$

This equation is similar in form to Equation (1) but has a fixed power of 3. When $T_{ime} \rightarrow 0$, equation (8) predicts exploratory sampling with a power law with exponent = 3. When $T_{ime} \rightarrow \infty$, the R.H.S will be dominated by a constant and thus, the sampling will be uniform. Uniform sampling can also be approximated by a power law of exponent = 0. Thus, equation (8) predicts that optimal exploratory sampling of foragers in the wild will depend on their past integration interval—a quantity that measures future tolerance to delay in decision-making, and, the non-linearity of time perception.

For a given value of T_{ime} , the closest power law fit to equation (8) can be calculated by equating the medians of the two distributions. This calculation is worked out below.

From Equation (19), the median for Equation (8) can be expressed as

$$median = \left[(x_{\min} + T_{ime})^{-2} + 0.5 \left\{ (x_{\max} + T_{ime})^{-2} - (x_{\min} + T_{ime})^{-2} \right\} \right]^{-\frac{1}{2}} - T_{ime}$$

From Equation (18), the median for the closest truncated power law can be expressed as

$$median(tp) = \left[x_{\min}^{1-\mu_{opt}} + 0.5(x_{\max}^{1-\mu_{opt}} - x_{\min}^{1-\mu_{opt}}) \right]^{\frac{1}{1-\mu_{opt}}}$$

Equating the two medians, the exponent (μ_{opt}) for the closest power law to Equation (8) is the solution to

$$\left[x_{\min}^{1-\mu_{opt}} + 0.5(x_{\max}^{1-\mu_{opt}} - x_{\min}^{1-\mu_{opt}}) \right]^{\frac{1}{1-\mu_{opt}}} = \left[(x_{\min} + T_{ime})^{-2} + 0.5\{(x_{\max} + T_{ime})^{-2} - (x_{\min} + T_{ime})^{-2}\} \right]^{\frac{-1}{2}} - T_{ime} \quad (9)$$

This can only be calculated numerically and depends on the value of T_{ime} . When $T_{ime}=0$, it is easy enough to see that $\mu_{opt}=3$. When $T_{ime} \rightarrow \infty$, the R.H.S of Equation (9) tends to the limit $0.5(x_{\max}+x_{\min})$. Hence, the solution for $\mu_{opt}=0$ in this case. Thus, in all cases, the exponent of the best fit power law to Equation (8) will be between 0 and 3.

An important caveat needs to be mentioned regarding Equation (8). Its derivation assumes that the discounting function is calculated without any associated model of risk such as those resulting from competition due to other predators. These factors are quite likely important in determining the success of foragers in the wild and hence, would likely be included in their decision-making. However, to preserve simplicity, we have chosen to ignore such factors. Simple models of such risk can be found in the supplement of our prior theoretical work (71). When such factors are included in the discounting function, the resultant path length distribution would be much more complicated. Further, as mentioned in Section 0, the above model assumes a uniform prior. Hence, real life path lengths will certainly be more complicated than the simple model presented here. Nevertheless, our model shows that the resultant path lengths will be heavy-tailed.

Modeling risk due to competition

In section 0, we considered the simple case where animals in the wild only have to account for the passage of time in calculating the temporal discounting. Specifically, we assumed that they do not face explicit risks of losing rewards or at least, that they do not model such risks. However, this assumption is almost definitely incorrect. In the presence of such competition, during the course of a foraging path, the value of a reward might reduce since other animals might consume it. Considering such a risk as a stochastic process with a mean decay proportional to the magnitude of the reward (i.e. larger rewards are more sought after), we showed previously that an appropriate model of risk can be mathematically expressed as

$$r(\text{after path of duration } t) = \frac{r(\text{start of path})}{(1 + k\alpha r(\text{start of path})^\alpha t)^{\frac{1}{\alpha}}}$$

Here, $r(\text{start of path})$ is the reward magnitude at the start of a given path of duration t and k and α represent the degree of competition—the larger their values, the more the competition. In the time t , the mean reward is expected to have decayed to the value $r(\text{after path of duration } t)$ as expressed above. As is clear, this introduces another power law form to the model expressed in Section 0. Thus, a more complete model of path length distribution can be obtained by combining temporal uncertainty (shown in Equation (8)) and competition risk (shown above) as

$$p(t) \propto \frac{1}{(T_{ime} + t)^3 (1 + k\alpha r^\alpha t)^{\frac{1}{\alpha}}} \quad (10)$$

Here, r can be thought of as the mean reward expected in an environment.

Statistical characterization of the hyperbolic distribution in Equation (1)

Rewriting Equation (1) with a proportionality constant k , we get

$$p(t) = k(c+t)^{-\mu}; t_{\min} < t < t_{\max}$$

For this expression to represent a probability distribution, k must have a value such that it is normalized over the domain. We first consider the case of continuous data for which the integral of the probability distribution should be 1, i.e.

$$\int_{t_{\min}}^{t_{\max}} k(c+t)^{-\mu} dt = 1$$

Solving for k , we get

$$k = \frac{1-\mu}{(t_{\max} + c)^{1-\mu} - (t_{\min} + c)^{1-\mu}}$$

Thus,

$$p(t) = \frac{1-\mu}{(t_{\max} + c)^{1-\mu} - (t_{\min} + c)^{1-\mu}} (t+c)^{-\mu} \quad (11)$$

The cumulative distribution function can be calculated as

$$F(t) = \int_{t_{\min}}^t p(t) dt = \int_{t_{\min}}^t \frac{1-\mu}{(t_{\max} + c)^{1-\mu} - (t_{\min} + c)^{1-\mu}} (t+c)^{-\mu} dt$$

Solving and simplifying, we get

$$F(t) = \frac{(t+c)^{1-\mu} - (t_{\min} + c)^{1-\mu}}{(t_{\max} + c)^{1-\mu} - (t_{\min} + c)^{1-\mu}} \quad (12)$$

For testing whether observed data is consistent with the probability distribution shown in Equation (11), it is important to be able to generate random numbers following that distribution. This can be done using inverse transform sampling, provided one has access to a uniform random variate u . Inverse transform sampling states that solving for t in the equation below will require that t is distributed according to the distribution shown in Equation (11).

$$F(t) = u$$

i.e.

$$\frac{(t+c)^{1-\mu} - (t_{\min} + c)^{1-\mu}}{(t_{\max} + c)^{1-\mu} - (t_{\min} + c)^{1-\mu}} = u$$

Solving for t , we get

$$t = \left[(t_{\min} + c)^{1-\mu} + \left\{ (t_{\max} + c)^{1-\mu} - (t_{\min} + c)^{1-\mu} \right\} u \right]^{\frac{1}{1-\mu}} - c \quad (13)$$

Equation (13) describes the random number generator for the distribution shown in Equation (11) with u being a uniform random variate between 0 and 1.

The next question to be addressed is that of parameter estimation for Equation (11) when attempting to fit experimental data. This can be done using maximum likelihood estimation as shown below.

Say that we have n independent observations that are assumed to be from the hyperbolic distribution in Equation (11). Let the i^{th} observation be t_i . Then the likelihood of the data given parameters c and μ is:

$$L = \prod_i p(t_i)$$

The log-likelihood is

$$\log(L) = \sum_i \log(p(t_i))$$

Substituting $p(t_i)$ from Equation (11)

$$\log(L) = \sum_i \log\left(\frac{1-\mu}{(t_{\max} + c)^{1-\mu} - (t_{\min} + c)^{1-\mu}} (t_i + c)^{-\mu}\right)$$

Simplifying,

$$\log(L) = \sum_i \left[\log(1-\mu) - \mu \log(t_i + c) - \log((t_{\max} + c)^{1-\mu} - (t_{\min} + c)^{1-\mu}) \right]$$

Performing the sums, we get

$$\log(L) = n \log(1-\mu) - \mu \sum_i \log(t_i + c) - n \log((t_{\max} + c)^{1-\mu} - (t_{\min} + c)^{1-\mu})$$

At the maximum of the log-likelihood function, its partial derivatives with respect to c and μ will be zero.

Therefore,

$$\frac{\partial \log(\mathbf{L})}{\partial \mu} = \frac{\partial}{\partial \mu} \left[n \log(1 - \mu) - \mu \sum_i \log(t_i + c) - n \log((t_{\max} + c)^{1-\mu} - (t_{\min} + c)^{1-\mu}) \right] = 0$$

Thus, we get

$$\frac{1}{1 - \mu} + \langle \log(x_i + c) \rangle = \frac{(x_{\max} + c)^{1-\mu} \log(x_{\max} + c) - (x_{\min} + c)^{1-\mu} \log(x_{\min} + c)}{(x_{\max} + c)^{1-\mu} - (x_{\min} + c)^{1-\mu}} \quad (14)$$

where $\langle \ \rangle$ signifies the mean.

Similarly,

$$\frac{\partial \log(\mathbf{L})}{\partial c} = \frac{\partial}{\partial c} \left[n \log(1 - \mu) - \mu \sum_i \log(t_i + c) - n \log((t_{\max} + c)^{1-\mu} - (t_{\min} + c)^{1-\mu}) \right] = 0$$

$$-\mu \langle (x_i + c)^{-1} \rangle = (1 - \mu) \frac{(x_{\max} + c)^{-\mu} - (x_{\min} + c)^{-\mu}}{(x_{\max} + c)^{1-\mu} - (x_{\min} + c)^{1-\mu}} \quad (15)$$

Equations (14) and (15) have to be numerically solved simultaneously to calculate the maximum likelihood estimates for parameters c and μ .

In practice, this numerical estimation has to be multi-stepped since typical numerical solvers only provide local solutions. To ensure that the initial values for numerical solution are close to the global solution, we used the following procedure. First, we calculated the

pure power law fit to data using the version of Equation (14) with $c=0$. This is also the ML estimator for a pure power law as calculated previously (262) and is shown below.

$$\frac{1}{1-\mu} + \langle \log(x_i) \rangle = \frac{(x_{\max})^{1-\mu} \log(x_{\max}) - (x_{\min})^{1-\mu} \log(x_{\min})}{(x_{\max})^{1-\mu} - (x_{\min})^{1-\mu}} \quad (16)$$

Equation (16) also needs to be estimated numerically. The initial value for this solution was taken as the ML exponent for a non-truncated power law which has an analytical expression shown below (262). The expression can be obtained as the limit $x_{\max} \rightarrow \infty$ in Equation (16).

$$\mu = 1 - \frac{1}{\log(x_{\min}) - \langle \log(x_i) \rangle} \quad (17)$$

Once the solution to Equation (16) was obtained, the numerical solution for Equations (14) and (15) were calculated using the procedure explained below. Call μ_{mle} for Equation (16) as μ_{tp} since this is the MLE exponent for a pure truncated power law model. The initial values of μ for the numerical solution for Equations (14) and (15) were taken as $[\mu_{tp}, \mu_{tp}+0.05, \mu_{tp}+0.05, \dots, \mu_{tp}+2]$.

The corresponding initial values of c for each of the above mentioned μ was calculated as the value that would produce the same median for the truncated hyperbolic distribution as the median for the best fit truncated power law with exponent μ_{tp} . This is calculated as shown below.

$$median(tp) = \left[x_{\min}^{1-\mu_{mle}} + 0.5(x_{\max}^{1-\mu_{mle}} - x_{\min}^{1-\mu_{mle}}) \right]^{\frac{1}{1-\mu_{mle}}} \quad (18)$$

$$\text{median}(\text{hyp}) = \left[(x_{\min} + c)^{1-\mu} + 0.5 \{ (x_{\max} + c)^{1-\mu} - (x_{\min} + c)^{1-\mu} \} \right]^{\frac{1}{1-\mu}} - c \quad (19)$$

Equating the above two values and solving for c for each value of μ from the list $[\mu_{tp}, \mu_{tp}+0.05, \mu_{tp}+0.05, \dots, \mu_{tp}+2]$ provides the appropriate initial point for the numerical solution for Equations (14) and (15). However, the above equations need to be solved numerically as well. The initial value for this solution was set sequentially. For $\mu = \mu_{tp}$, the initial value for c was taken as zero. The solution to this equation provided the initial value for $\mu = \mu_{tp}+0.05$. The solution for this equation provided the initial value for $\mu = \mu_{tp}+0.1$ and so on.

For each of the above combinations of c and μ as initial values, the corresponding log-likelihood of the data was calculated. The maximum likelihood c and μ for solving Equations (14) and (15) were taken as the pair that maximized the global (against initial values for numerical optimization) log-likelihood calculated above. To appropriately compare the exponential model to truncated hyperbolic and power law models, it is important to use a truncated exponential model. If k is the normalization constant, the exponential distribution can be defined as

$$p(t) = ke^{-\lambda t}; t_{\min} \leq t \leq t_{\max}$$

with

$$\int_{t_{\min}}^{t_{\max}} p(t) dt = 1$$

Solving for k , we get

$$k = \frac{\lambda e^{\lambda t_{\min}}}{1 - e^{-\lambda(t_{\max} - t_{\min})}}$$

Thus the truncated exponential model used for calculating likelihoods is

$$p(t) = \frac{\lambda e^{-\lambda(t - t_{\min})}}{1 - e^{-\lambda(t_{\max} - t_{\min})}}; t_{\min} \leq t \leq t_{\max} \quad (20)$$

It is Equation (20) that must be used to calculate L_{exp} in Equation (5).

The cumulative distribution function over the truncated domain for the exponential distribution can be calculated as

$$F(t) = \int_{t_{\min}}^t p(t) = \int_{t_{\min}}^t \frac{\lambda e^{-\lambda t}}{1 - e^{-\lambda(t_{\max} - t_{\min})}}; t_{\min} \leq t \leq t_{\max}$$

Solving and simplifying, we get

$$F(t) = \frac{1 - e^{-\lambda(t - t_{\min})}}{1 - e^{-\lambda(t_{\max} - t_{\min})}} \quad (21)$$

A random number generator for this distribution can again be obtained using inverse transform sampling by solving for t in the equation below

$$F(t) = u$$

where u is a uniform random variate.

Solving for t , we get

$$t = t_{\min} - \frac{1}{\lambda} \log(1 - u \{1 - e^{-\lambda(t_{\max} - t_{\min})}\}) \quad (22)$$

To get a maximum likelihood estimate of λ , the log likelihood of the data can be expressed as

$$\log(\mathbf{L}) = \sum_i \log\left(\frac{\lambda e^{-\lambda(t_i - t_{\min})}}{1 - e^{-\lambda(t_{\max} - t_{\min})}}\right) \quad (23)$$

We found the MLE λ by numerically maximizing the above equation.

Discrete distributions

Since previously collected data (Table 1) also contained discrete data, we derive the above procedure for discrete data here. For truncated discrete data, the only difference from the above derivation is that the *sum* of the probability distribution should equal 1, rather than the integral. For the truncated hyperbolic model, the appropriate probability distribution function can be written as

$$p(t) = \frac{(c+t)^{-\mu}}{\sum_{t_{\min}}^{t_{\max}} (c+t)^{-\mu}}; t_{\min} \leq t \leq t_{\max}$$

The ML estimates of c and μ were calculated by numerically maximizing the log-likelihood of the data

$$\log() = \langle -\mu \log(c + t_i) \rangle - \log\left(\sum_{t_{\min}}^{t_{\max}} (c + t)^{-\mu}\right)$$

We used the same procedure as described in the above section for global maximization. The same equation above was used to estimate the best fit power law distribution by setting $c=0$.

For a discrete truncated exponential distribution, the probability distribution function can be written as

$$p(t) = (1 - e^{-\lambda}) \frac{e^{-\lambda(t-t_{\min})}}{1 - e^{-\lambda(t_{\max}-t_{\min}+1)}} \quad (24)$$

The ML estimate for λ was calculated by maximizing the log-likelihood. It can be shown that this is equivalent to numerically solving the following equation

$$\frac{e^{-\lambda}}{(1 - e^{-\lambda})} - (t_{\max} - t_{\min} + 1) \frac{e^{-\lambda(t_{\max}-t_{\min}+1)}}{1 - e^{-\lambda(t_{\max}-t_{\min}+1)}} = \langle t_i - t_{\min} \rangle \quad (25)$$

Truncation due to prey encounter

A curious observation regarding forager path lengths is that they tend to become diffusive when food abundance is high (187, 188). While it was previously argued that Brownian walks are sufficiently productive under high food density (187, 188), a recent experimental

finding demonstrated that such path lengths result from truncation of search due to prey encounter (186). A simple theoretical argument provided an explanation for this result. However, their calculation was in one-dimension. Here, we extend their argument to search in 2-D.

We first calculate the probability distribution of truncated path lengths. An easy solution is to assume that foragers are moving in a straight line until they hit a food item and then calculate the resultant path length distribution. We assume that food is homogenously distributed with density (number per unit area) ρ . Denote the diameter of the prey (or a cluster of prey) as d_{prey} , the CDF of path lengths as $F(r)$, path lengths as r , probability density function of path lengths as $p(r)$. Then the infinitesimal change in the CDF, $dF(r)$ over a distance dr from r corresponds to the probability that the path length lies between r and $r+dr$. This is equal to the probability that the forager at least moved r ($= 1-F(r)$) multiplied by the probability that the forager hit a target between r and $r+dr$. The second probability can be calculated as the total angle covered by prey in the ring between r and $r+dr$ divided by 2π . The total number of foragers (on an average) in this ring equals $2\pi r dr \rho$. Thus, we can write

$$dF(r) = (1 - F(r)) \cdot 2\pi r dr \rho \cdot \frac{d_{prey} / r}{2\pi}$$

If the forager had a sensory diameter of d_{perc} , the above equation would remain exactly the same but with the change that d_{prey} would change to $d_{prey} + d_{perc}$.

Solving the above equation, we get

$$F(r) = 1 - e^{-\rho d_{prey} r} \quad (26)$$

Thus the pdf of path lengths is given by

$$p(r) = \frac{dF(r)}{dr} = \rho d_{prey} e^{-\rho d_{prey} r}$$

Hence, the prey-truncated path lengths are exponentially distributed.

If the intended path length distribution (CDF) for exploration was $F_{intended}(r)$, the probability that the path length is at least greater than r is the probability that the intended path length is at least greater than r multiplied by the probability that there was no prey-truncation within r . The latter probability, from Equation (26), is $1-F(r)$. Thus, the observed path lengths would be

$$1 - F_{observed}(r) = (1 - F_{intended}(r)) e^{-\rho d_{prey} r} \quad (27)$$

Thus, as the density of prey increases, path lengths approach the exponential distribution.

Bibliography

1. Levy J, K Namboodiri VM, Hussain Shuler MG (2015) Memory bias in the temporal bisection point . *Front Integr Neurosci* 9. Available at: http://www.frontiersin.org/Journal/Abstract.aspx?s=571&name=integrative_neuroscience&ART_DOI=10.3389/fnint.2015.00044.
2. Namboodiri VMK, Levy JM, Mihalas S, Sims DW, Hussain Shuler MG (2016) Rationalizing spatial exploration patterns of wild animals and humans through a temporal discounting framework. *Proc Natl Acad Sci U S A* 113(31):8747–52.
3. Aschoff J (1981) A Survey on Biological Rhythms. *Biological Rhythms*, ed Aschoff J (Springer, New York), pp 3–10.
4. Richelle M, Lejeune H (1980) *Time in Animal Behavior* (Pergamon, New York).
5. Gallistel CR (1990) *The Organization of Behavior* (MIT Press, Cambridge, Massachusetts).
6. Hinton SC, Meck WH (1997) The “internal clocks” of circadian and interval timing. *Endeavour* 21(1):3–8.
7. Buhusi C V, Meck WH (2005) What makes us tick? Functional and neural mechanisms of interval timing. *Nat Rev Neurosci* 6(10):755–65.
8. Ivry RB, Spencer RMC (2004) The neural representation of time. *Curr Opin Neurobiol* 14:225–232.
9. Gibbon J, Malapani C, Dale CL, Gallistel CR (1997) Toward a neurobiology of

- temporal cognition: Advances and challenges. *Curr Opin Neurobiol* 7(2):170–184.
10. Buonomano D V, Karmarkar UR (2002) How do we tell time? *Neuroscientist* 8(1):42–51.
 11. Walsh V (2003) A theory of magnitude: Common cortical metrics of time, space and quality. *Trends Cogn Sci* 7(11):483–488.
 12. MacInnis MLM, Guilhardi P (2006) Basic temporal discrimination procedures. *Tasks Tech a Sampl Methodol Investig Anim Learn Behav Cogn*:233–244.
 13. Namboodiri VMK, Huertas MA, Monk KJ, Shouval HZ, Hussain Shuler MG (2015) Visually Cued Action Timing in the Primary Visual Cortex. *Neuron* 86:319–330.
 14. Bueti D (2011) The sensory representation of time. *Front Integr Neurosci* 5(34).
 15. Mita A, Mushiake H, Shima K, Matsuzaka Y, Tanji J (2009) Interval time coding by neurons in the presupplementary and supplementary motor areas. *Nat Neurosci* 12(4):502–7.
 16. Akkal D, Escola L, Bioulac B, Burbaud P (2004) Time predictability modulates pre-supplementary motor area neuronal activity. *Neuroreport* 15(8):1283–6.
 17. Lucchetti C, Bon L (2001) Time-modulated neuronal activity in the premotor cortex of macaque monkeys. *Exp Brain Res* 141(2):254–260.
 18. Kim J, Jung AH, Byun J, Jo S, Jung MW (2009) Inactivation of medial prefrontal cortex impairs time interval discrimination in rats. *Front Behav Neurosci* 3(November):38.

19. Narayanan NS, Land BB, Solder JE, Deisseroth K, DiLeone RJ (2012) Prefrontal D1 dopamine signaling is required for temporal control. *Proc Natl Acad Sci* 109(50):20726–20731.
20. Kim J, Ghim J-W, Lee JH, Jung MW (2013) Neural correlates of interval timing in rodent prefrontal cortex. *J Neurosci* 33(34):13834–13847.
21. Xu M, Zhang S, Dan Y, Poo M (2014) Representation of interval timing by temporally scalable firing patterns in rat prefrontal cortex. *Proc Natl Acad Sci U S A* 111(1):480–5.
22. Maimon G, Assad J a (2006) A cognitive signal for the proactive timing of action in macaque LIP. *Nat Neurosci* 9(7):948–55.
23. Janssen P, Shadlen MN (2005) A representation of the hazard rate of elapsed time in macaque area LIP. *Nat Neurosci* 8(2):234–241.
24. Lee IH, Assad JA (2003) Putaminal activity for simple reactions or self-timed movements. *J Neurophysiol* 89(5):2528–37.
25. Tanaka M (2007) Cognitive signals in the primate motor thalamus predict saccade timing. *J Neurosci* 27(44):12109–12118.
26. Matell MS, Meck WH, Nicolelis M a L (2003) Interval timing and the encoding of signal duration by ensembles of cortical and striatal neurons. *Behav Neurosci* 117(4):760–773.
27. Kanai R, Lloyd H, Buetti D, Walsh V (2011) Modality-independent role of the primary auditory cortex in time estimation. *Exp Brain Res* 209(3):465–471.

28. Bueti D, Bahrami B, Walsh V (2008) Sensory and Association Cortex in Time Perception. *J Cogn Neurosci* 20(6):1054–1062.
29. Bueti D, Bahrami B, Walsh V, Rees G (2010) Encoding of temporal probabilities in the human brain. *J Neurosci* 30(12):4343–4352.
30. Sharma J, et al. (2015) Spatial Attention and Temporal Expectation Under Timed Uncertainty Predictably Modulate Neuronal Responses in Monkey V1. *Cereb cortex* (September):2894–2906.
31. Ghose GM, Yang T, Maunsell JHR (2002) Physiological Correlates of Perceptual Learning in Monkey V1 and V2. *J Neurophysiol* 87(4):1867–1888.
32. Poort J, et al. (2015) Learning Enhances Sensory and Multiple Non-sensory Representations in Primary Visual Cortex. *Neuron* 86(6):1478–1490.
33. Shuler MG, Bear MF (2006) Reward timing in the primary visual cortex. *Science* 311:1606–1609.
34. Chubykin AA, Roach EB, Bear MF, Shuler MGH (2013) A Cholinergic Mechanism for Reward Timing within Primary Visual Cortex. *Neuron* 77(4):723–735.
35. Liu CH, Coleman JE, Davoudi H, Zhang K, Hussaina Shuler MG (2015) Selective Activation of a Putative Reinforcement Signal Conditions Cued Interval Timing in Primary Visual Cortex. *Curr Biol* 25(12):1551–1561.
36. Namboodiri VMK, Huertas MA, Monk KJ, Shouval HZ, Shuler MGH (2015) Visually cued action timing in the primary visual cortex. *Neuron* 86(1):319–330.

37. Saleh M, Reimer J, Penn R, Ojakangas CL, Hatsopoulos NG (2010) Fast and Slow Oscillations in Human Primary Motor Cortex Predict Oncoming Behaviorally Relevant Cues. *Neuron* 65(4):461–471.
38. Kulashekhar S, Pekkola J, Palva JM, Palva S (2016) The role of cortical beta oscillations in time estimation. *Hum Brain Mapp* 37(9):3262–3281.
39. Cravo AM, Rohenkohl G, Wyart V, Nobre AC (2011) Endogenous modulation of low frequency oscillations by temporal expectations. *J Neurophysiol* 106(6):2964–72.
40. Bartolo R, Prado L, Merchant H (2014) Information Processing in the Primate Basal Ganglia during Sensory-Guided and Internally Driven Rhythmic Tapping. *J Neurosci* 34(11):3910–3923.
41. Kononowicz TW, van Rijn H (2015) Single trial beta oscillations index time estimation. *Neuropsychologia* 75:381–389.
42. O’Leary B (1936) Components of the electrical response of the optic cortex of the rabbit. *Am J Physiol* 117:292–308.
43. Kimura D (1962) Multiple response of visual cortex of the rat to photic stimulation. *Electroencephalogr Clin Neurophysiol* 14:115–122.
44. Engel AK, Fries P, Singer W (2001) Dynamic predictions: oscillations and synchrony in top-down processing. *Nat Rev Neurosci* 2(10):704–716.
45. Arnal LH, Giraud AL (2012) Cortical oscillations and sensory predictions. *Trends Cogn Sci* 16(7):390–398.

46. Eckhorn R, Reitboeck HJ, Arndt M, Dicke P (1990) Feature Linking via Synchronization among Distributed Assemblies: Simulations of Results from Cat Visual Cortex. *Neural Comput* 2(3):293–307.
47. Eckhorn R, et al. (1988) Coherent oscillations: A mechanism of feature linking in the visual cortex? - Multiple electrode and correlation analyses in the cat. *Biol Cybern* 60(2):121–130.
48. Lima B, Singer W, Neuenschwander S (2011) Gamma Responses Correlate with Temporal Expectation in Monkey Primary Visual Cortex. *J Neurosci* 31(44):15919–15931.
49. Zold CL, Hussain Shuler MG (2015) Theta Oscillations in Visual Cortex Emerge with Experience to Convey Expected Reward Time and Experienced Reward Rate. *J Neurosci* 35(26):9603–9614.
50. Allan LG (2002) The location and interpretation of the bisection point. *Q J Exp Psychol B* 55(1):43–60.
51. Fechner G (1966) *Elements of Psychophysics, Vol 1 (1860)*.
52. Bizo LA, Chu JYM, Sanabria F, Killeen PR (2006) The failure of Weber's law in time perception and production. *Behav Processes* 71(2–3):201–210.
53. Jordan KE, Brannon EM (2006) Weber's Law influences numerical representations in rhesus macaques (*Macaca mulatta*). *Anim Cogn* 9(3):159–172.
54. Kacelnik A, Brito e Abreu F (1998) Risky choice and Weber's Law. *J Theor Biol* 194(2):289–298.

55. Miller JD, Wier CC, Kelly J, Dooling RJ (1978) Discrimination and labeling of noise-buzz sequences with varying noise-lead times: An example of categorical perception*. *J Speech Hear Disord* 60(2):410–417.
56. Grondin S (2001) From physical time to the first and second moments of psychological time. *Psychol Bull* 127(1):22–44.
57. Gibbon J (1977) Scalar expectancy theory and Weber’s law in animal timing. *Psychol Rev* 84:279–325.
58. Treisman M (1963) Temporal discrimination and the indifference interval: Implications for a model of the “internal clock”. *Psychol Monogr Gen Appl* 77(13):1–31.
59. Treisman M, Cook N, Naish PL, MacCrone JK (1994) The internal clock: electroencephalographic evidence for oscillatory processes underlying time perception. *Q J Exp Psychol A* 47(February 2015):241–289.
60. Meck WH (1983) Selective adjustment of the speed of internal clock and memory processes. *J Exp Psychol Anim Behav Process* 9(2):171–201.
61. Kononowicz T, Wassenhove V van (2016) In Search of Oscillatory Traces of the Internal Clock. *Front Psychol* 7(224).
62. Killeen PR, Fetterman JG (1988) A behavioral theory of timing. *Psychol Rev* 95(2):274–295.
63. Machado A (1997) Learning the temporal dynamics of behavior. *Psychol Rev* 104(2):241–265.

64. Staddon JE, Higa JJ (1999) Time and memory: towards a pacemaker-free theory of interval timing. *J Exp Anal Behav* 71(2):215–51.
65. Gibbon J (1999) Multiple time scales is well named. *J Exp Anal Behav* 71(2):272–301.
66. Matell MS, Meck WH (2004) Cortico-striatal circuits and interval timing: Coincidence detection of oscillatory processes. *Cogn Brain Res* 21:139–170.
67. Green L, Myerson J (1996) Exponential versus hyperbolic discounting of delayed outcomes: Risk and waiting time. *Am Zool* 36(January 1995):496–505.
68. Green L, Fristoe N, Myerson J (1994) Temporal discounting and preference reversals in choice between delayed outcomes. *Psychon Bull Rev* 1(3):382–389.
69. Frederick S, Loewenstein G, O’Donoghue T (2002) Time Discounting and Preference : A Critical Review. *J Econ Lit* 40(2):351–401.
70. Kalenscher T, Pennartz CMA (2008) Is a bird in the hand worth two in the future? The neuroeconomics of intertemporal decision-making. *Prog Neurobiol* 84(3):284–315.
71. Namboodiri VMK, Mihalas S, Marton TM, Hussain Shuler MG (2014) A general theory of intertemporal decision-making and the perception of time. *Front Behav Neurosci* 8(February):61.
72. Pozdnyakov V, Meyer T, Wang YB, Yan J, Inouye BD (2014) On modeling animal movements using Brownian motion with measurement error. *Ecology* 95(2):247–253.

73. Bartumeus F, Da Luz MGE, Viswanathan GM, Catalan J (2005) Animal search strategies: A quantitative random-walk analysis. *Ecology* 86(11):3078–3087.
74. Sims DW, et al. (2008) Scaling laws of marine predator search behaviour. *Nature* 451(7182):1098–102.
75. Bouchaud JP, Georges A (1990) Anomalous diffusion in disordered media: Statistical mechanisms, models and physical applications. *Phys Rep* 195(4–5):127–293.
76. Viswanathan GM, et al. (1999) Optimizing the success of random searches. *Nature* 401(6756):911–4.
77. James A, Plank MJ, Edwards AM (2011) Assessing Levy walks as models of animal foraging. *J R Soc Interface* 8(62):1233–47.
78. Hikosaka O, Sakamoto M, Usui S (1989) Functional properties of monkey caudate neurons. III. Activities related to expectation of target and reward. *J Neurophysiol* 61(4):814–832.
79. Shidara M, Aigner TG, Richmond BJ (1998) Neuronal Signals in the Monkey Ventral Striatum Related to Progress through a Predictable Series of Trials. *J Neurosci* 18(7):2613–2625.
80. Apicella P, Scarnati E, Ljungberg T, Schultz W (1992) Neuronal activity in monkey striatum related to the expectation of predictable environmental events. *J Neurophysiol* 68(3):945–960.
81. Schultz W, Apicella P, Scarnati E, Ljungberg T (1992) Neuronal activity in

- monkey ventral striatum related to the expectation of reward. *J Neurosci* 12(12):4595–610.
82. Tremblay L, Hollerman JR, Schultz W (1998) Modifications of reward expectation-related neuronal activity during learning in primate striatum. *J Neurophysiol* 80:964–977.
83. Tremblay L, Schultz W (2000) Reward-related neuronal activity during go-nogo task performance in primate orbitofrontal cortex. *J Neurophysiol* 83(4):1864–76.
84. Tremblay L, Schultz W (1999) Relative reward preference in primate orbitofrontal cortex. *Nature* 398(6729):704–708.
85. Schoenbaum G, Chiba a a, Gallagher M (1998) Orbitofrontal cortex and basolateral amygdala encode expected outcomes during learning. *Nat Neurosci* 1(2):155–159.
86. Hikosaka K, Watanabe M (2000) Delay activity of orbital and lateral prefrontal neurons of the monkey varying with different rewards. *Cereb Cortex* 10(3):263–271.
87. Okano K, Tanji J (1987) Neuronal activities in the primate motor fields of the agranular frontal cortex preceding visually triggered and self-paced movement. *Exp Brain Res* 66(1):155–166.
88. Romo R, Schultz W (1987) Neuronal activity preceding self-initiated or externally timed arm movements in area 6 of monkey cortex. *Exp Brain Res* 67(3):656–662.
89. Kurata K, Wise SP (1988) Premotor and supplementary motor cortex in rhesus

monkeys: neuronal activity during externally- and internally-instructed motor tasks. *Exp Brain Res* 72(2):237–248.

90. Watanabe M (1996) Reward expectancy in primate prefrontal neurons. *Nature* 382:629–632.
91. Schultz W, Romo R (1988) Neuronal activity in the monkey striatum during the initiation of movements. *Exp Brain Res* 71(2):431–436.
92. Hubel DH, Wiesel TN (1962) Receptive fields, binocular interaction and functional architecture in the cat visual cortex. *J Physiol* 160(1):106–154.
93. Hubel DH, Wiesel TN (1965) Receptive Fields and Functional Architecture in Two Nonstriate Visual Areas (18 and 19) of the Cat. *J Neurophysiol* 28:229–289.
94. Gavornik JP, Bear MF (2014) Learned spatiotemporal sequence recognition and prediction in primary visual cortex. *Nat Neurosci* 17(5):732–7.
95. Miall C (1989) The Storage of Time Intervals Using Oscillating Neurons. *Neural Comput* 1(3):359–371.
96. Church RM, Broadbent HA (1990) Alternative representations of time, number, and rate. *Cognition* 37(1–2):55–81.
97. Zold CL, Larramendy C, Riquelme LA, Murer MG (2007) Distinct changes in evoked and resting globus pallidus activity in early and late Parkinson's disease experimental models. *Eur J Neurosci* 26(5):1267–1279.
98. Galiñanes GL, Taravini IRE, Murer MG (2009) Dopamine-dependent periadolescent maturation of corticostriatal functional connectivity in mouse. *J*

Neurosci 29(8):2496–509.

99. Alink A, Schwiedrzik CM, Kohler A, Singer W, Muckli L (2010) Stimulus predictability reduces responses in primary visual cortex. *J Neurosci* 30(8):2960–6.
100. den Ouden HEM, Friston KJ, Daw ND, McIntosh AR, Stephan KE (2009) A dual role for prediction error in associative learning. *Cereb Cortex* 19:1175–1185.
101. Murray SO, Kersten D, Olshausen BA, Schrater P, Woods DL (2002) Shape perception reduces activity in human primary visual cortex. *Proc Natl Acad Sci U S A* 99(23):15164–9.
102. Summerfield C, Trittschuh EH, Monti JM, Mesulam MM, Egnér T (2008) Neural repetition suppression reflects fulfilled perceptual expectations. *Nat Neurosci* 11(9):1004–1006.
103. Kok P, Jehee JFM, de Lange FP (2012) Less Is More: Expectation Sharpens Representations in the Primary Visual Cortex. *Neuron* 75(2):265–270.
104. Somers DC, Dale a M, Seiffert a E, Tootell RB (1999) Functional MRI reveals spatially specific attentional modulation in human primary visual cortex. *Proc Natl Acad Sci U S A* 96(4):1663–8.
105. Gandhi SP, Heeger DJ, Boynton GM (1999) Spatial attention affects brain activity in human primary visual cortex. *Proc Natl Acad Sci U S A* 96(6):3314–9.
106. Ahissar M, Hochstein S (1993) Attentional Control of Early Perceptual Learning. *Proc Nat Acad Sci Usa* 90(June):5718–5722.

107. Fahle M (2004) Perceptual learning: a case for early selection. *J Vis* 4(2004):879–890.
108. Roelfsema PR, Lamme VA, Spekreijse H (1998) Object-based attention in the primary visual cortex of the macaque monkey. *Nature* 395(6700):376–81.
109. Serences JT (2008) Value-Based Modulations in Human Visual Cortex. *Neuron* 60(6):1169–1181.
110. Seitz AR, Kim D, Watanabe T (2009) Rewards evoke learning of unconsciously processed visual stimuli in adult humans. *Neuron* 61(5):700–7.
111. Stănişor L, van der Togt C, Pennartz CMA, Roelfsema PR (2013) A unified selection signal for attention and reward in primary visual cortex. *Proc Natl Acad Sci U S A* 110(22):9136–41.
112. Hasselmo ME (2005) What is the function of hippocampal theta rhythm? - Linking behavioral data to phasic properties of field potential and unit recording data. *Hippocampus* 15(7):936–949.
113. Hyman JM, Zilli EA, Paley AM, Hasselmo ME (2005) Medial prefrontal cortex cells show dynamic modulation with the hippocampal theta rhythm dependent on behavior. *Hippocampus* 15(6):739–749.
114. Siapas AG, Lubenov E V., Wilson MA (2005) Prefrontal phase locking to hippocampal theta oscillations. *Neuron* 46(1):141–151.
115. Fries P (2005) A mechanism for cognitive dynamics: Neuronal communication through neuronal coherence. *Trends Cogn Sci* 9(10):474–480.

116. von Stein a, Chiang C, König P (2000) Top-down processing mediated by interareal synchronization. *Proc Natl Acad Sci U S A* 97(26):14748–14753.
117. Bernasconi C, von Stein a, Chiang C, König P (2000) Bi-directional interactions between visual areas in the awake behaving cat. *Neuroreport* 11(4):689–92.
118. Roelfsema PR, Engel AK, König P, Singer W (1997) Visuomotor integration is associated with zero time-lag synchronization among cortical areas. *Nature* 385(6612):157–61.
119. Siebenhühner F, Wang S., Palva JM, Palva S (2016) Cross-frequency synchronization connects networks of fast and slow oscillations during visual working memory maintenance. *Elife* 5.
120. Fries P, Reynolds JH, Rorie AE, Desimone R (2001) Modulation of oscillatory neuronal synchronization by selective visual attention. *Science* 291(5508):1560–3.
121. Schroeder CE, Lakatos P (2009) Low-frequency neuronal oscillations as instruments of sensory selection. *Trends Neurosci* 32(1):9–18.
122. Fries P, Schröder J-H, Roelfsema PR, Singer W, Engel AK (2002) Oscillatory neuronal synchronization in primary visual cortex as a correlate of stimulus selection. *J Neurosci* 22(9):3739–3754.
123. Cohen JD, McClure SM, Yu AJ (2007) Should I stay or should I go? How the human brain manages the trade-off between exploitation and exploration. *Philos Trans R Soc Lond B Biol Sci* 362(1481):933–942.
124. Arnal LH, Doelling KB, Poeppel D (2014) Delta-Beta Coupled Oscillations

- Underlie Temporal Prediction Accuracy. *Cereb Cortex* (2):1–9.
125. Gavornik JP, Shuler MGH, Loewenstein Y, Bear MF, Shouval HZ (2009) Learning reward timing in cortex through reward dependent expression of synaptic plasticity. *Proc Natl Acad Sci U S A* 106(16):6826–6831.
 126. Niv Y, Daw ND, Joel D, Dayan P (2007) Tonic dopamine: Opportunity costs and the control of response vigor. *Psychopharmacology (Berl)* 191(3):507–520.
 127. Klimesch W, Sauseng P, Hanslmayr S (2007) EEG alpha oscillations: The inhibition-timing hypothesis. *Brain Res Rev* 53(1):63–88.
 128. Edwards CJ, Alder TB, Rose GJ (2002) Auditory midbrain neurons that count. *Nat Neurosci* 5(10):934–6.
 129. Schirmer A (2004) Timing speech: A review of lesion and neuroimaging findings. *Cogn Brain Res* 21:269–287.
 130. Czeisler CA, et al. (1999) Stability, precision, and near-24-hour period of the human circadian pacemaker. *Science* 284:2177–2181.
 131. Kacelnik A, Brunner D (2002) Timing and foraging: Gibbon’s scalar expectancy theory and optimal patch exploitation. *Learn Motiv* 33:177–195.
 132. Sohn MH, Carlson RA (2003) Implicit temporal tuning of working memory strategy during cognitive skill acquisition. *Am J Psychol* 116:239–256.
 133. Wearden JH (1991) Human performance on an analogue of an interval bisection task. *Q J Exp Psychol B* 43:59–81.
 134. Allan LG, Gibbon J (1991) Human bisection at the geometric mean. *Learn Motiv*

22:39–58.

135. Killeen PR, Fetterman JG, Bizo L (1997) Time's causes. *Advances in Psychology: Time and Behavior: Psychological and Neurobehavioral Analyses*, eds Bradshaw CM, Szabadi E (Elsevier, Amsterdam), pp 79–131.
136. Kopec CD, Brody CD (2010) Human performance on the temporal bisection task. *Brain Cogn* 74(3):262–72.
137. Balci F, et al. (2011) Optimal Temporal Risk Assessment. *Front Integr Neurosci* 5. doi:10.3389/fnint.2011.00056.
138. Coskun F, Ceyda Sayali Z, Gurbuz E, Balci F (2015) Optimal time discrimination. *Quarterly J Exp Psychol* 68(2):381–401.
139. Wearden JH, Ferrara A (1996) Stimulus range effects in temporal bisection by humans. *Q J Exp Psychol B* 49:24–44.
140. Brown GDA, McCormack T, Smith M, Stewart N (2005) Identification and bisection of temporal durations and tone frequencies: common models for temporal and nontemporal stimuli. *J Exp Psychol Hum Percept Perform* 31:919–938.
141. Wearden JH, Ferrara A (1995) Stimulus spacing effects in temporal bisection by humans. *Q J Exp Psychol B* 48:289–310.
142. Cheng RK, Dyke AG, McConnell MW, Meck WH (2011) Categorical scaling of duration as a function of temporal context in aged rats. *Brain Res* 1381:175–186.
143. Cheng RK, Scott AC, Penney TB, Williams CL, Meck WH (2008) Prenatal-

- choline supplementation differentially modulates timing of auditory and visual stimuli in aged rats. *Brain Res* 1237:167–175.
144. Penney TB, Allan LG, Meck WH, Gibbon J (1998) Memory Mixing in Duration Bisection. *Timing of Behavior: Neural, Psychological and Computational Perspectives*, eds Rosenbaum DA, Collyer CE (MIT Press, Cambridge), pp 165–193.
145. Penney TB, Tournet S (2005) Modality Effects in Short Interval Timing. *Psychol Fr* 50:131–143.
146. Penney TB, Gibbon J, Meck WH (2000) Differential effects of auditory and visual signals on clock speed and temporal memory. *J Exp Psychol Hum Percept Perform* 26:1770–1787.
147. Fortin C, Rousseau R, Bourque P, Kirouac E (1993) Time estimation and concurrent nontemporal processing: specific interference from short-term-memory demands. *Percept Psychophys* 53:536–548.
148. Fortin C, Breton R (1995) Temporal interval production and processing in working memory. *Percept Psychophys* 57(2):203–215.
149. Gil S, Droit-Volet S (2011) How do emotional facial expressions influence our perception of time? *Attention, Representation, and Human Performance: Integration of Cognition, Emotion, and Motivation*. (London), pp 61–74.
150. Jones L, Wearden JH (2004) *Double standards: memory loading in temporal reference memory*. doi:10.1080/02724990344000088.

151. Lieving LM, Lane SD, Cherek DR, Tcheremissine O V (2006) Effects of delays on human performance on a temporal discrimination procedure: evidence of a choose-short effect. *Behav Processes* 71(2–3):135–43.
152. Spetch ML (1987) Systematic errors in pigeons' memory for event duration: Interaction between training and test delay. *Anim Learn Behav* 15(1):1–5.
153. Meck WH (1996) Neuropharmacology of timing and time perception. *Cogn Brain Res* 3(3–4):227–242.
154. Matell MS, Meck WH (2000) Neuropsychological mechanisms of interval timing behavior. *BioEssays* 22:94–103.
155. Staddon JER (2005) Interval timing: memory, not a clock. *Trends Cogn Sci* 9(7):312–4.
156. Droit-Volet S, Rattat A-C (2007) A further analysis of time bisection behavior in children with and without reference memory: the similarity and the partition task. *Acta Psychol (Amst)* 125(2):240–56.
157. Balci F, Gallistel CR (2006) Cross-domain transfer of quantitative discriminations: is it all a matter of proportion? *Psychon Bull Rev* 13:636–642.
158. Allan LG, Gerhardt K (2001) Temporal bisection with trial referents. *Percept Psychophys* 63(3):524–540.
159. Rodríguez-Gironés MA, Kacelnik A (1995) Interval bisection with and without reference memory. *Time and the Dynamic Control of Behavior*, eds Richelle M, DeKeyser V, D'Ydewalle G, Vandierendonck A (Liege), pp 47–72.

160. Rodríguez-Gironés MA, Kacelnik A (1998) Response latencies in temporal bisection: Implications for timing models. *Time and the Dynamic Control of Behavior*, eds Richelle M, DeKeyser V, D'Ydewalle G, Vandierendonck A (Liege), pp 51–70.
161. Jazayeri M, Shadlen MN (2010) Temporal context calibrates interval timing. *Nat Neurosci* 13:1020–1026.
162. Cicchini GM, Arrighi R, Cecchetti L, Giusti M, Burr DC (2012) Optimal Encoding of Interval Timing in Expert Percussionists. *J Neurosci* 32:1056–1060.
163. Merchant H, Zarco W, Prado L (2008) Do we have a common mechanism for measuring time in the hundreds of millisecond range? Evidence from multiple-interval timing tasks. *J Neurophysiol* 99(2):939–49.
164. Dormal V, Pesenti M (2007) Numerosity-length interference: A stroop experiment. *Exp Psychol* 54:289–297.
165. Xuan B, Zhang D, He S, Chen X (2007) Larger stimuli are judged to last longer. *J Vis* 7:2.1-5.
166. Oliveri M, et al. (2008) Perceiving numbers alters time perception. *Neurosci Lett* 438:308–311.
167. Weber EH (1851) *Annotationes Anatomicae et Physiologicae (Anatomical and Physiological Observations* ed Kohler CF (Lipsiae (Leipzig), Germany).
168. Wearden JH, Lejeune H (2008) Scalar properties in human timing: conformity and violations. *Q J Exp Psychol (Hove)* 61:569–587.

169. Wearden J. (1991) Do humans possess an internal clock with scalar timing properties? *Learn Motiv* 22:59–83.
170. Ivry RB, Hazeltine RE (1995) Perception and production of temporal intervals across a range of durations: evidence for a common timing mechanism. *J Exp Psychol Hum Percept Perform* 21(1):3–18.
171. Wittmann M (2009) The inner experience of time. *Philos Trans R Soc Lond B Biol Sci* 364:1955–1967.
172. Wearden JH, Bray S (2001) Scalar timing without reference memory? Episodic temporal generalization and bisection in humans. *Q J Exp Psychol B* 54:289–309.
173. Allan LG (2002) Are the Referents Remembered in Temporal Bisection? *Learn Motiv* 33(1):10–31.
174. Lewis PA, Miall RC (2003) Brain activation patterns during measurement of sub- and supra-second intervals. *Neuropsychologia* 41:1583–1592.
175. Keele SW, Pokorny RA, Corcos DM, Ivry R (1985) Do perception and motor production share common timing mechanisms: A correlational analysis. *Acta Psychol (Amst)* 60(2–3):173–191.
176. Wing AM (1980) The Long and Short of Timing in Response Sequences. *Tutorials in Motor Behavior*, eds Stelmach G, Requin J (North-Holland Publishing Company, Amsterdam), pp 469–484.
177. Merchant H, et al. (2011) What Can Be Inferred from Multiple-task Psychophysical Studies about the Mechanisms for Temporal Processing? *Time and*

Time Perception, ed Vatakis A et al. (Springer-Verlag, Berlin Heidelberg), pp 207–229.

178. Wing AM, Kristofferson AB (1973) Response delays and the timing of discrete motor responses. *Percept Psychophys* 14:5–12.
179. Lejeune H, Wearden JH (2006) Review article Scalar properties in animal timing : Conformity and violations. *Q J Exp Psychol* 59:1875–1908.
180. Reynolds AM, Rhodes CJ (2009) The Lévy flight paradigm: random search patterns and mechanisms. *Ecology* 90(4):877–887.
181. Viswanathan GM, Raposo EP, da Luz MGE (2008) Lévy flights and superdiffusion in the context of biological encounters and random searches. *Phys Life Rev* 5(3):133–150.
182. Viswanathan G (2011) *The physics of foraging : An introduction to random searches and biological encounters* doi:10.1063/PT.3.1401.
183. Mendez V, Campos D, Batumeus F (2014) *Stochastic Foundations in Movement Ecology: Anomalous Diffusion, Front Propagation and Random Searches* (Springer, Berlin).
184. Sims DW, et al. (2014) Hierarchical random walks in trace fossils and the origin of optimal search behavior. *Proc Natl Acad Sci* (9). doi:10.1073/pnas.1405966111.
185. de Jager M, Weissing FJ, Herman PMJ, Nolet BA, Koppel J Van De (2011) Levy Walks Evolve Through Interaction Between Movement and Environmental Complexity. *Science* 332(December):1551–1553.

186. Jager M De, et al. (2014) How superdiffusion gets arrested : ecological encounters explain shift from Lévy to Brownian movement. *Proc R Soc B* 281(20132605). doi:<http://dx.doi.org/10.1098/rspb.2013.2605>.
187. Humphries NE, et al. (2010) Environmental context explains Lévy and Brownian movement patterns of marine predators. *Nature* 465(7301):1066–9.
188. Humphries NE, Weimerskirch H, Queiroz N, Southall EJ, Sims DW (2012) Foraging success of biological Levy flights recorded in situ. *Proc Natl Acad Sci* 109(19). doi:10.1073/pnas.1121201109.
189. Raichlen DA, Wood BM, Gordon AD, Mabulla AZP, Marlowe FW (2014) Evidence of Lévy walk foraging patterns in human hunter – gatherers. *Proc Natl Acad Sci* 111(2):728–733.
190. Ferreira AS, Raposo EP, Viswanathan GM, Da Luz MGE (2012) The influence of the environment on Levy random search efficiency: Fractality and memory effects. *Phys A Stat Mech its Appl* 391(11):3234–3246.
191. Van Moorter B, et al. (2009) Memory keeps you at home: A mechanistic model for home range emergence. *Oikos* 118(5):641–652.
192. Tabone M, Ermentrout B, Doiron B (2010) Balancing organization and flexibility in foraging dynamics. *J Theor Biol* 266(3):391–400.
193. Boyer D, Walsh PD (2010) Modelling the mobility of living organisms in heterogeneous landscapes: does memory improve foraging success? *Philos Trans A Math Phys Eng Sci* 368(1933):5645–5659.

194. Gautestad AO, Mysterud A (2013) The Lévy flight foraging hypothesis: forgetting about memory may lead to false verification of Brownian motion. *Mov Ecol* 1(1):9.
195. Gautestad AO (2011) Memory matters: Influence from a cognitive map on animal space use. *J Theor Biol* 287(0):26–36.
196. Fagan WF, et al. (2013) Spatial memory and animal movement. *Ecol Lett* 16(10):1316–29.
197. Weimerskirch H, Pinaud D, Pawlowski F, Bost C-A (2007) Does prey capture induce area-restricted search? A fine-scale study using GPS in a marine predator, the wandering albatross. *Am Nat* 170(5):734–43.
198. Weimerskirch H, Gault A, Cherel Y (2005) Prey Distribution and Patchiness : Factors in Foraging Success and Efficiency of Wandering Albatrosses. *Ecology* 86(10):2611–2622.
199. Fauchald P, Erikstad KE, Skarsfjord H (2000) Scale-Dependent Predator–Prey Interactions: the Hierarchical Spatial Distribution of Seabirds and Prey. *Ecology* 81(3):773–783.
200. Fauchald P, Erikstad KE Scale-dependent predator-prey interactions: the aggregative response of seabirds to prey under variable prey abundance and patchiness. *Mar Ecol Prog Ser* 231:279–291.
201. Sims DW, Quayle V a. (1998) Selective foraging behaviour of basking sharks on zooplankton in a small-scale front. *Nature* 393(June):460–464.

202. Green L, Myerson J (2004) A Discounting framework for choice with delayed and probabilistic rewards. *Psychol Bull* 130(5):769–792.
203. Stephens DW, Krebs JR (1986) *Foraging Theory* doi:10.2307/2409049.
204. Kirby & Marakovic, N. N. KN (1995) Modeling myopic decisions: Evidence for hyperbolic delay-discounting within subjects and amounts. *Organ Behav Hum Decis Process* 64(1):22–30.
205. Green & Myerson, J. L (1996) Exponential versus hyperbolic discounting of delayed outcomes: Risk and waiting time. *Am Zool* 36(January 1995):496–505.
206. Vuchinich RE, Simpson C a (1998) Hyperbolic temporal discounting in social drinkers and problem drinkers. *Exp Clin Psychopharmacol* 6(3):292–305.
207. Johnson MW, Bickel WK (2002) Within-subject comparison of real and hypothetical money rewards in delay discounting. *J Exp Anal Behav* 77(2):129–146.
208. Murphy JG, Vuchinich RE, Simpson CA (2001) Delayed reward and cost discounting. *Psychol Rec* 51:571–588.
209. Simpson C a, Vuchinich RE (2000) Reliability of a measure of temporal discounting. *Psychol Rec* 50:3–16.
210. Badre D, Doll BB, Long NM, Frank MJ (2012) Rostrolateral Prefrontal Cortex and Individual Differences in Uncertainty-Driven Exploration. *Neuron* 73(3):595–607.
211. Muller M, Wehner R (1994) The hidden spiral: systematic search and path integration in desert ants, *Cataglyphis fortis*. *J Comp Physiol A* 175:525–530.

212. Cramer AE, Gallistel CR (1997) Vervet monkeys as travelling salesman. *Nature* 387:464.
213. Janson CH (1998) Experimental evidence for spatial memory in foraging wild capuchin monkeys, *Cebus apella*. *Anim Behav* 55(5):1229–43.
214. Valero A, Byrne RW (2007) Spider monkey ranging patterns in Mexican subtropical forest: do travel routes reflect planning? *Anim Cogn* 10(3):305–15.
215. Asensio N, Brockelman WY, Malaivijitnond S, Reichard UH (2011) Gibbon travel paths are goal oriented. *Anim Cogn* 14(3):395–405.
216. Taffe M a, Taffe WJ (2011) Rhesus monkeys employ a procedural strategy to reduce working memory load in a self-ordered spatial search task. *Brain Res* 1413:43–50.
217. Dyer FC (1996) Spatial memory and navigation by honeybees on the scale of the foraging range. *J Exp Biol* 199:147–154.
218. Buhusi C V, Meck WH (2005) What makes us tick? Functional and neural mechanisms of interval timing. *Nat Rev Neurosci* 6(10):755–65.
219. Namboodiri VMK, Mihalas S, Hussain Shuler MG (2014) A temporal basis for Weber's law in value perception. *Front Integr Neurosci* 8(October):1–11.
220. Namboodiri VMK, Mihalas S, Hussain Shuler MG (2014) Rationalizing decision-making: understanding the cost and perception of time. *Timing Time Percept Rev* 1(4):1–40.
221. Namboodiri VMK, Mihalas S, Shuler MGH (2015) Analytical Calculation of

Errors in Time and Value Perception Due to a Subjective Time Accumulator: A Mechanistic Model and the Generation of Weber's Law. *Neural Comput* 28(1):89–117.

222. Reynolds A (2015) Liberating Lévy walk research from the shackles of optimal foraging. *Phys Life Rev* 14:59–83.
223. Bartumeus F (2015) Behavioural ecology cannot turn its back on Lévy walk research. Comment on “Liberating Lévy walk research from the shackles of optimal foraging” by A.M. Reynolds. *Phys Life Rev* 14:84–86.
224. Boyer D (2015) What future for Lévy walks in animal movement research? Comment on “Liberating Lévy walk research from the shackles of optimal foraging” by A.M. Reynolds. *Phys Life Rev* 14:87–89.
225. Cheng K (2015) Answer (in part) blowing in the wind. Comment on “Liberating Lévy walk research from the shackles of optimal foraging” by A.M. Reynolds. *Phys Life Rev* 14:90–93.
226. da Luz MGE, Raposo EP, Viswanathan GM (2015) And yet it optimizes. Comment on “Liberating Lévy walk research from the shackles of optimal foraging” by A.M. Reynolds. *Phys Life Rev* 14:94–98.
227. Focardi S (2015) Do the albatross Lévy fly below the spandrels of St Mark? Comment on “Liberating Lévy walk research from the shackles of optimal foraging” by A.M. Reynolds. *Phys Life Rev* 14:99–101.
228. Humphries NE (2015) Why Lévy foraging does not need to be “unshackled” from

- optimal foraging theory. Comment on “Liberating Lévy walk research from the shackles of optimal foraging” by A.M. Reynolds. *Phys Life Rev* 14:102–104.
229. MacIntosh AJJ (2015) At the edge of chaos – error tolerance and the maintenance of Levy statistics in animal movement. Comment on “Liberating Lévy walk research from the shackles of optimal foraging” by A.M. Reynolds. *Phys Life Rev* 14:105–107.
230. Miramontes O (2015) Divorcing physics from biology? Optimal foraging and Lévy flights. Comment on “Liberating Lévy walk research from the shackles of optimal foraging” by A.M. Reynolds. *Phys Life Rev* 14:108–110.
231. Sims DW (2015) Intrinsic Lévy behaviour in organisms – searching for a mechanism. Comment on “Liberating Lévy walk research from the shackles of optimal foraging” by A.M. Reynolds. *Phys Life Rev* 14:111–114.
232. Reynolds A (2015) Venturing beyond the Lévy flight foraging hypothesis: Reply to comments on “Liberating Lévy walk research from the shackles of optimal foraging.” *Phys Life Rev* 14:115–119.
233. Bartumeus F, Raposo EP, Viswanathan GM, da Luz MGE (2014) Stochastic Optimal Foraging: Tuning Intensive and Extensive Dynamics in Random Searches. *PLoS One* 9(9):e106373.
234. Bhattacharjee Y (2006) A Timely Debate About the Brain. *Science* (80-) 311(5761).
235. Staddon JE, Higa JJ (1999) Time and memory: towards a pacemaker-free theory of

- interval timing. *J Exp Anal Behav* 71(2):215–51.
236. Roesch MR, Taylor AR, Schoenbaum G (2006) Encoding of Time-Discounted Rewards in Orbitofrontal Cortex Is Independent of Value Representation. *Neuron* 51(4):509–520.
237. Winstanley CA (2004) Contrasting Roles of Basolateral Amygdala and Orbitofrontal Cortex in Impulsive Choice. *J Neurosci* 24(20):4718–4722.
238. Roesch MR, Olson CR (2004) Neuronal activity related to reward value and motivation in primate frontal cortex. *Science* 304(5668):307–10.
239. Levy DJ, Glimcher PW (2012) The root of all value: A neural common currency for choice. *Curr Opin Neurobiol* 22(6):1027–1038.
240. Montague PR, Berns GS (2002) Neural economics and the biological substrates of valuation. *Neuron* 36(2):265–284.
241. Kringelbach ML, Radcliffe J (2005) the Human Orbitofrontal Cortex : Linking Reward To Hedonic Experience. *Nat Rev Neurosci* 6(September):691–702.
242. Schultz W (2010) Subjective neuronal coding of reward: Temporal value discounting and risk. *Eur J Neurosci* 31(12):2124–2135.
243. Kable JW, Glimcher PW (2007) The neural correlates of subjective value during intertemporal choice. *Nat Neurosci* 10(12):1625–33.
244. O’Keefe J, Nadel L (1978) *The Hippocampus as a cognitive map* (Oxford University Press, Oxford).
245. Hafting T, Fyhn M, Molden S, Moser M, Moser EI (2005) Microstructure of a

- spatial map in the entorhinal cortex. *Nature* 436(7052):801–806.
246. Gutierrez E, Cabrera JL (2015) A neural coding scheme reproducing foraging trajectories. *Sci Rep* 5(18009).
247. Yoshida W, Ishii S (2006) Resolution of uncertainty in prefrontal cortex. *Neuron* 50(5):781–9.
248. Malapani C, et al. (1998) Coupled Temporal Memories in Parkinson’s Disease: A Dopamine-Related Dysfunction. *J Cogn Neurosci* 10(3):316–331.
249. Soares S, Atallah B V., Paton JJ (2016) Midbrain dopamine neurons control judgment of time. *Science* (80-) 354(6317):1273–1277.
250. Rammsayer T (1990) Temporal discrimination in schizophrenic and affective disorders: evidence for a dopamine-dependent internal clock. *Int J Neurosci* 53(2–4):111–20.
251. Paulsen JS, et al. (2004) fMRI biomarker of early neuronal dysfunction in presymptomatic Huntington’s disease. *Am J Neuroradiol* 25(10):1715–1721.
252. Volz HP, et al. (2001) Time estimation in schizophrenia: an fMRI study at adjusted levels of difficulty. *Neuroreport* 12(2):313–6.
253. El Haj M, Kapogiannis D (2016) Time distortions in Alzheimer’s disease: a systematic review and theoretical integration. *Npj Aging Mech Dis* 2:16016.
254. Lewis PA, Miall RC, Daan S, Kacelnik A (2003) Interval timing in mice does not rely upon the circadian pacemaker. *Neurosci Lett* 348(3):131–134.
255. Koekkoek SKE, et al. (2003) Cerebellar LTD and Learning-Dependent Timing of

- Conditioned Eyelid Responses. *Science* (80-) 301(September):1736–1739.
256. Horak FB, Diener HC (1994) Cerebellar control of postural scaling and central set in stance. *J Neurophysiol* 72(2):479–493.
257. Timmann D, Horak FB (2001) Perturbed step initiation in cerebellar subjects: 2. Modification of anticipatory postural adjustments. *Exp Brain Res* 141(1):110–120.
258. Harrington DL, Lee RR, Boyd LA, Rapcsak SZ, Knight RT (2004) Does the representation of time depend on the cerebellum? Effect of cerebellar stroke. *Brain* 127(3):561–574.
259. Malapani C, Dubois B, Rancurel G, Gibbon J (1998) Cerebellar dysfunctions of temporal processing in the seconds range in humans. *Neuroreport* 9(17):3907.
260. Welch BL (1947) The Generalization of 'Student's' Problem when Several Different Population Variances are Involved. *Biometrika* 34(1–2):28–35.
261. Frank MJ, Doll BB, Oas-Terpstra J, Moreno F (2009) Prefrontal and striatal dopaminergic genes predict individual differences in exploration and exploitation. *Nat Neurosci* 12(8):1062–8.
262. White EP, Enquist BJ, Green JL (2008) On estimating the exponent of power-law frequency distributions. *Ecology* 89(4):905–912.

Curriculum Vitae

Joshua Matthew Levy

The Johns Hopkins University School of Medicine

725 N. Wolfe St., Wood Basic Science Building 914

Baltimore, MD 21205

joshlevy89@gmail.com

Education

2011-present	The Johns Hopkins University School of Medicine Baltimore, MD Predoctoral candidate in Neuroscience; Expected graduation 2017
2007-2011	Princeton University Princeton, NJ A.B., Molecular Biology; Certificate, Neuroscience

Research Experience

2012-present	The Johns Hopkins University School of Medicine Baltimore, MD
--------------	---

Graduate thesis: *“Visually-Guided Timing and its Neural Representation”*

Advisor: Marshall Hussain Shuler

2010-11

Princeton University

Princeton, NJ

Undergraduate thesis: *“Characterizing and Modeling the Motion Onset Response in the Retina”*

Advisor: Michael Berry

2009

Neural Stem Cell Institute

Rensselaer, NY

Summer Intern: *Pluripotent stem cell treatment for macular degeneration in the retina*

Advisor: Sally Temple

2005-2008

Wadsworth Laboratory

Albany, NY

Student, then Summer, Intern: Department of Immunology

Advisor: Dr. David Lawrence

Peer-Reviewed Research Publications

1. **Levy, J.**, Zold, C., K Namboodiri V.M., & Hussain Shuler, M.G. The Timing of Reward-Seeking Action Tracks Visually-Cued Theta Oscillations in Primary Visual Cortex. *In Submission*. (2016).
2. K Namboodiri, V.M., **Levy, J.**, Mihalas, S., Sims., D, & Shuler, M.G. Rationalizing spatial exploration patterns of wild animals and humans through a temporal discounting framework. *PNAS*. (2016).
3. **Levy, J.**, K Namboodiri, V. M. & Hussain Shuler, M. G. Memory bias in the temporal bisection point. *Front. Integr. Neurosci.* 9, (2015).
4. Chen, E. Y., Marre, O., Fisher, C., Schwartz, G. **Levy, J.**, Azeredo da Silveira, R., Berry, Michael. Alert response to motion onset in the retina. *J. Neurosci.* 33, 120–132 (2013).

Published Abstracts

1. **J. Levy**, M. G. Hussain Shuler. Reward timing in primary sensory cortex during multi-model intertemporal decision-making. *Soc. Neurosci.* (2014).

Teaching Experience

- Teaching Assistant, Neuroscience and Cognition I (Graduate course, Fall 2012)

Awards and Honors

- Visual Neuroscience Training Program fellowship, National Eye Institute training grant to the Johns Hopkins University School of Medicine, 2013
- Bausch and Lomb Honorary Science Award, 2006

Skills

- Expertise in multi-electrode recordings from awake, behaving rodents
- Fluency in Matlab, Javascript, Python
- Experience with Java, .NET, PostgreSQL, NHibernate, MongoDB; some C/C++